ROLE OF TRANSPORT DEPENDENT CALCIUM SIGNALING IN NITRIC OXIDE PRODUCTION AND ENDOTHELIAL SHEAR STRESS RESPONSES

A Thesis

Submitted to the Faculty

of

Drexel University

by

Dihui Hong

in partial fulfillment of the

requirements for the degree of

Doctor of Philosophy

August 2007

Acknowledgements

This thesis is the result of three and a half years of work whereby I have been accompanied and inspired by many people. It is a pleasant aspect that I have now the opportunity to express my gratitude for all of them.

First of all, I'd like to give my sincere thanks to my supervisor, Dr. Dov Jaron. Dr. Jaron accepted me as his Ph.D. student without any hesitation when I expressed the desire to pursue my Ph.D. research with him. Thereafter, he offered me so much advice, and has been guiding this work through the years. Without his constant encouragement and support over many years, the thesis would never have been completed.

I also want to extend my deepest gratitude to my thesis advisor Dr. Kenneth Barbee. He was always there to meet and talk about my ideas, to proofread and mark up my papers, to ask me good questions, to help me think thorough my problems. I am truly imbedded to his valuable suggestions in every possible manner, from the experimental design, the initial concept of mathematical model, to the final edition of the thesis. I admire him as a dedicating and knowledgeable researcher, also as an intelligent, humble and kind person. What I have learned from him will also benefit my future career.

I am also very grateful to Dr. Donald Buerk, who is an expert in Nitric Oxide (NO) signaling and transport in physiological system. I thank Dr. Buerk for teaching me NO electrode fabrication, NO measurement techniques and his incredible patience with me. His invaluable technical and editorial advice, suggestions, discussions and guidance were a real support to complete this doctoral thesis.

I sincerely thank Dr. Allen and Dr. Gosh for serving on my doctoral committee. Their constructive feedback and valuable comments at various stages have been significantly useful in shaping the thesis up to completion. I must also thank Dr. lelkes for the help. He kindly provided me the cells and all the valuable suggestion and

discussion during the course of research.

I have been fortunate enough to meet and work with brilliant folks from both Dr. Barbee and Dr. Jaron's groups. I offer my thanks to all the lab members Zach Forbes, Devrim Kilinc, Soonjin Hong, Christin Alejnikov, Allison Andrews, Xuewen Chen, Aiman Fadel, Nina Vukosavljevic who offered friendship which made the experience that much more fulfilling. I want to express my special thanks to Devrim. He was a true friend ever since we began to share the same facilities in a lab and he always gave me the priority. I thank him also because he was always willing to help, discuss some topic, or just remind me to have lunch. I also received a great deal of help from Zach Forbes, who taught me the basic laboratory skills at the beginning of my PhD. I owe special gratitude to Dr. Lelkes's lab members; they were always there to advise my cell culture studies and experimental techniques.

I am really blessed to be able to spend one of the best four years in my life in the School of Biomedical Engineering, Science & Health Systems at Drexel University. All the assistance I received from other faculty and staff members are gratefully acknowledged.

Finally, I would like to say 'thank-you' to: all my friends and family, wherever they are, particularly my Mom and Dad for their continuous and unconditional support. They have always put education as a first priority in my life and let me go far away from them to pursue my dream; My most heartfelt acknowledgement must go to my husband for his enduring patience, understanding, and love; for the motivation he gave me during those tiring times when I had doubts about my research. He's heard so much about shear stress, calcium, nitric oxide and mathematical modeling over the past few years that he really deserves a Ph.D.

List of Tables

List of Figures

Abstract

Role of Transport Dependent Calcium Signaling in Nitric Oxide Pproduction and Endothelial Shear Stress Responses

Dihui Hong

Dov Jaron, Kenneth A. Barbee, Supervisor, Ph.D.

In this study, I compared the calcium response to shear stress between the ECs from large vessels (Bovine Aortic Endothelial Cells: BAECs)and microvessels (Rat AdrenoMedullary Endothelial Cells: RAMECs); characterized the interplay between $[Ca^{2+}]_i$ and endothelial nitric oxide synthase (eNOS) activity in BAECs; and developed a 2-D model of transport-dependent intracellular calcium signaling in endothelial cells to evaluate the effects of spatial colocalization of eNOS and capacitive calcium entry (CCE) channels in caveolae on eNOS activiation in response to shear stress and ATP.

In RAMECs, the calcium response to the onset of shear stress was heterogeneous in time and space. Shear stress induced calcium waves that originated from one or several cells and propagated to neighboring cells. The initiation and the propagation of calcium waves in RAMECs were significantly suppressed under conditions in which either purinergic receptors were blocked by suramin or extracellular ATP was degraded by apyrase. Exogenously applied ATP produced similarly heterogeneous responses.

In BAECs, the onset of shear stress elicited a transient increase in intracellular calcium concentration that was spatially uniform, synchronous, and dose dependent. When BAECs were perfused in PBS containing Ca^{2+}, a step increase in shear stress elilicted a transient increase in $[Ca^{2+}]_i$, followed by a sustained plateau which decayed slowly to near baseline. Elimination of extracellular Ca^{2+} with EGTA did not affect the initial calcium peak, while the $[Ca^{2+}]_i$ plateau was reduced by 20%. Despite the similarity in the calcium responses, nitric oxide (NO) production in the presence of extracellular calcium is more than twice that in the absence of extracellular calcium. Similar results were observed in BAECs in response to stimulation with ATP. To achieve a quantitative understanding the Ca^{2+} and NO signaling mechanism, we developed a mathematical model that incorporates the cell morphology as well as endothelial calcium signaling processes. The model predicts that spatial segregation of calcium channels in endothelial cells can create microdomains where calcium concentration differs significantly from the spatial average calcium concentration.This transport-dependent calcium signaling specificity effect is enhanced in ECs elongated by flow by increasing the spatial segregation of the caveolar signaling domains. Our simulation significantly advances the understanding of how Ca^{2+}, despite its many potential actions, can mediate selective activation of signaling pathways. We show that diffusion limited calcium transport allows functional compartmentalization of signaling pathways based on the spatial arrangements of Ca^{2+} sources and targets.

CHAPTER 1

Background

1.1 Flow-Mediated Endothelial Mechanotransduction

Endothelial cells (ECs) cover the inner surface of blood vessels and are constantly exposed to blood flow. Blood flow imparts physical forces to the ECs and the hemodynamic forces can be resolved into two vectors: shear stress, a frictional force acting at the interface between flowing flow and vessel wall; and second, pressure acting normal to the vessel wall, which imposes circumferential stretch to the vessel. It is well established that shear stress is borne primarily by ECs. Intracellular signals generated in response to flow elicit a cascade of both morphological and functional responses that involve cytoskeletal organization, remodeling of cellular morphology, and changes in gene expression (6, 32).

1.1.1 Significant of Actions of Shear Stress on ECs

Shear stress controls cellular structure and function, including regulation of vascular tone and diameter, vessel wall remodeling, hemostasis, and inflammatory responses. The temporal and spatial variations in shears stress and the flow pattern play important roles in endothelial functions. Impairment of these functions may lead to atherosclerosis and/or thrombosis, which is highlighted by the focal development patterns of atheroscelerosis in hemodynamically defined regions. Straight portions of arteries are exposed to relatively high and uniform well-developed laminar flows and are well protected from atherosclerotic plaque development. In contrast, vessel branch points, bifurcations, and regions of high curvature experience “disturbed” shear stress conditions and the disturbed flow patterns cause endothelial injury and chronic dysfunction, leading to the accumulation of lipids in the vessel wall that eventually form atherosclerotic plaques.

Laminar flow, with a sufficiently high shear stress and a definitive direction, serves a protective role in the following aspects(41):

1. Laminar shear stress causes a dose-related reduction of the rate of EC proliferation by reducing the rate of DNA synthesis.
2. Laminar shear suppress EC apoptosis by up-regulation of eNOS and expression of inhibitors of apoptosis proteins.
3. Laminar shear stress significantly enhances EC migration in wound healing, which is mediated by shear regulation of lamellipodia protrusion and focal adhesions remodeling in the direction of flow.
4. Shear stress inhibits EC turnover, which decreases the endothelium permeability to macromolecules such as low-density lipoprotein (LDL), and the local accumulation of LDL and macrophages is the key element in atherogenesis.

1.1.2 Flow-Mediated Calcium Response

Studies on intracellular signaling events in ECs have shown that shear stress activates multiple signaling molecules. One of the early responses to shear stress is the elevation of intracellular Ca^{2+} concentration ($[Ca^{2+}]_i$). Ca^{2+} is an essential trigger to successive physiological and biochemical reactions such as the production of nitric oxide (NO), the activation of Src tyrosine kinase and C kinase in the cells (32).

ECs act as a sensing interface to transduce hydrodynamic forces. The mechanisms by which ECs sense this mechanical stimulus and transform these signals into intracellular biochemical signals, which further change vessel structure and function have not been resolved. Several putative mechanisms have been proposed among which are: 1) Shear stress is sensed by integrins on the cell surface, transmitting forces through cytoskeleton, thus activating signal transduction through stretch-activated cation channels (32). 2) Shear stress may cause

endothelial cells to synthesize and release ATP. The ATP concentration at the cell surface increases by overcoming the local effects of degradative enzymes, thereby mediating the Ca^{2+} signaling (39, 132, 133). 3) Shear stress induces an efflux of K^+ and membrane hyperpolarization, increasing the driving force for Ca^{2+} entry (98). 4) Flow-sensitive Cl^- currents play a role in modulating Ca^{2+} influx by altering the membrane potential (7, 90). 5) Components of the glycocalyx, of which heparan sulfates are the most abundant, function as signal transduction molecules (44). Shear stress may activate several pathways simultaneously and different mechanosensing mechanisms can interact with on another; however, the relationships and possible interactions among the various pathways have not been determined.

1.1.3 Flow-Mediated Nitric Oxide Production

Endothelial cells can produce at least three kinds of vasodilators in response to shear stress to modulate vascular tone, i.e., nitric oxide (NO), endothelium-derived hyperpolarization factor (EDHF), and prostacyclin (PGI_2). NO, as an endothelium-derived relaxing factor discovered by Furchgott and Zawadzki (48), is of particular interest to researchers as it is an antiantherogenic molecule and an attenuation of NO production in endothelium has been implicated in one of the earliest biochemical markers of endothelial dysfunction found in many cardiovascular diseases such as hypertension, atherosclerosis and diabetes.

In endothelial cells, nitric oxide (NO) is generated via the enzyme endothelial nitric-oxide synthase(eNOS). eNOS is a constitutively expressed enzyme that catalyzes oxidation of L-arginie to L-citrulline and NO. Although it is well known that shear stress stimulates production of NO from eNOS from ECs, the molecular mechanisms by which shear stress regulates NO production have not been clearly elucidated.

The eNOS is composed of two identical monomers, and each monomer contains the amino-terminal oxidase domain and carboxy-terminal reductase domain. For NO to be

produced from substrates O_2 and L-arginin, electron flux has to occur from the reductase domain of one monomer to the oxygenase domain of the other monomer. In basal condition, caveolin-1, being the major coat protein of caveolae, binds to the reductase domain of eNOS. This binding comprises the ability of eNOS to bind Camodulin (CaM) and to donate electrons to the heme subunit, thereby inhibiting NO synthesis. Increase in $[Ca^{2+}]_i$ promote the binding of CaM to the CaM-binding motif which is thought to displace an adjacent autoinhibitory loop on eNOS, thus facilitating NADPH-dependent electron flux from the reductase domain of the protein to the oxygenase domain. The terminal electron acceptor in the oxygenase domain is heme, which can bind oxygen for insertion into the NOS substrate, L-arginine (47).

Exposure of endothelial cells to fluid shear stress results in transient increase in $[Ca^{2+}]_i$, which induces CaM-dependent NO burst. It is now generally accepted that shear stress also induce NO production in a CaM-independent way. Evidences suggest that shear stress activated phosphorylation of eNOS at S1179 by protein kinase B (Akt) pathway, which induce the conformation change of the carboxy terminus; removes the wedge and lowers the calcium requirement, leading to enzyme activation(18). Shear stress also stimulates phosphorylation of eNOS-S635. Once S635 is phosphorylated, eNOS can produces NO in conditions even when intracellular Ca^{2+} is very low(19). Hsp90 is the 90-kDa heat shock protein, which serves as a scaffolding protein, facilitating the organization of additional associated regulatory proteins, positively regulates eNOS activity. Exposure of endothelial cells to fluid shear stress stimulates the association of eNOS and Hsp90; this association increases NO production(43, 52).

NO is involved in many events in normal vascular biology and pathophysiology through autocrine or paracrine action. The autocrine role for NO in regulating endothelial cell function is supported by studies in cultured ECs showing that inhibition of NO production reduces endothelial cell migration, proliferation, and organization into tubelike structures. Important vascular functions such as vessel relaxation and inhibition of platelet aggregation are regulated

by NO paracrine regulation.

1.1.4 Flow-Mediated Endothelial Cytoskeleton Remodeling

The endothelial cell can be viewed as a membrane stretched over a frame composed of microtubules, intermediate filaments and actin fibers which transverse the cells and ends in adhesion complexes. The endothelial cytoskeletal network maintains the shape of the endothelial cell; at the same time, these three principle cytoskeleton groups of proteins participate in flow-mediated mechanotranscution.

Of the three main cytoskeletal polymers, actin filaments are the most abundant and are located in close proximity to the cell membrane. Changes in actin distribution are detectable within minutes of the onset of flow. The remodeling of actin cytoskeleton is primarily by adding and subtracting subunits at free filament ends. Shear also induces intercellular junction disruption, followed by cell movement with the loss of peripheral bands, and an increase of microtubule-organizing centers. Endothelial cells become adjusted to the flow direction with the formation and alignment of thick stress fibers and dense microfilaments and the re-establishement of cell junctions after 12h of shearing(73).

Endothelial cells grown in the absence of flow were polygonal in shape with quite smooth surfaces with no preferential alignment or orientation. Flow induced shear stress lead to stress fibers and microtubules remodeling and cellular elongation and alignment in the direction of flow. Barbee et al. have incorporated data from atomic force microscopy and CFD simulation and showed that after subjected to directional flow, there is a small decrease in the average of surface heights compared with control cells, but a significant decrease in the amplitude of surface undulations(8, 9). Their study predicted that remodeling of cytoskeleton is an important mechanism for the cells to reduce their area and surface exposed to shear stress. By this means, aligned ECs might be less sensitive to shear stress than nonaligned cells by a given flow rate(8, 9). In arteries, endothelial cells in low mean shear stress regions prone to the

development of proatherosclerosis are cuboidal, whereas in athero-resistant regions, they are elongated into torpedo shapes that point into the direction of flow(41). Therefore, there is a need for understanding how the shape of endothelial cells may regulate their function.

1.2 Structure and Function of Endothelial Caveolae

Caveolae were introduced more than 50 years ago to describe 50- to 100-nm (diameter) plasma membrane invaginations identified by electron microscopy in a wide variety of cell types(131). A breakthrough in caveolae research was the discovery of a marker protein caveolin-1 for caveolae. With the use of the caveolae marker protein caveolin, purification techniques established new biochemical criteria for identifying this specialized membrane. These include a light buoyant density, resistance to solubilizaiton by Trion X-100, and enrichment in glycosphingolipids (GSLs), cholesterol, sphingomyelin(SPH) and lipid-anchored membrane proteins.

Two major functions for caveolae have been indetified, which include vesicle trafficking and signal transduction(119). In ECs, caveolae have been implicated in the regulation of many functions including macromolecules transport in the microcirculation through transcytosis. With respect to the latter function, caveolin-1 participates in endothelial signal transduction by ensuring the compartmentation of signal molecules, such as G protein, tyrosine kinase-associated receptors, as well as endothelial nitric oxide synthase. Interestingly, there are strong evidences that a large number of these signaling molecules are involved in flow/shear stress-mediated activation of endothelial cells. Caveolae themselves also have been suspected to serve as flow-activated mechanosensors or transducers of physiological responses in blood vessels. In vitro study shows cholesterol-dependent activation of flow-mediated intracellular signaling pathways(78, 102). In vivo, it has been demonstrated that flow-dependent responses in intact blood vessels required endothelial Cav-1 and caveolae; the endothelium lacking

caveolae was unable to couple changes in blood flow with proportional vascular remodeling, and this abnormality can be correctly partially by reconstituting endothelial Cav-1(138).

Caveolae, either single or in clusters, are present at the surface of the endothelium. Electron microscopy studies indicate that caveolae can exist luminally and abluminally, with the largest number in perijunctional zones between endothelia(22, 50, 57). Isshiki et al. observed that exposing endothelial cells to shear stress also caused polarization of caveolae on cell surface and relocate the caveolin-1 to the upstream edge of the cell(57). Rizzo et al. also reported that exposure to shear stress altered caveolin expression and distribution, and increased caveolae density at luminal cell surface(111).

1.3 CCE: General Concepts

In ECs, vasoactive aognists (ATP, Bradykinin et al..) trigger a biphasic rise in ($[Ca^{2+}]_i$) which consists of an initial transient component followed by a sustained one. The first transient rise by agonists and mechanical stimuli induce $[Ca^{2+}]_i$ elevation results from depletion of Ca^{2+} from the endoplasmic reticulum (ER) through inositol 1,4,5-trisphosphate (IP_3)-sensitive release channels. The depletion of intracellular Ca^{2+} stores is followed by Ca^{2+} influx through plasma membrane calcium channels, referred to as capacitative calcium entry (CCE), and also called store operated calcium entry (SOC).

The key feature of CCE is that it is activated by a signal generated by the decrease calcium concentration in ER. However, the signal transduction mechanism linking changes in intraluminal Ca^{2+} to the opening of plasma membrane Ca^{2+} channels has not been identified. Various factors that regulate CCE have been proposed (94, 101, 107, 124, 125), which include: 1):'CIF' model: Following discharge of the stores, a diffusible and stable, non-protein –like signal - calcium influx factor (CIF) is released from the ER and activates plasma membrane CCE channels; 2)Exocytosis model: Depletion of the stores causes secretion and fusion of

vesicles containing calcium channels with plasma membrane. 3) Conformational coupling model: Discharge of Ca^{2+} stores leads to a communication between the ER and the plasma membrane through conformational change and protein-protein interaction.

CCE calcium entry appears to be the major means of regulated influx of calcium in endothelial cells and has been shown to regulate many of the endothelial functions. Transient receptor potential (TRP) proteins has been proposed to form CCE channels via association either as homomers or heteromers with other Trps(140). CCE channels have been suggested to reside in caveolae(59) and caveolar microdomains provide scaffold for assembly and coordination of CCE signaling proteins (TRPs) into a complex(77).

1.4 Interaction among Calcium, Nitric Oxide Synthase and Caveloae

The activation of eNOS is tightly regulated and mediated by a number of different mechanisms, such as modulation of phosphorylation state by kinases and phosphatases, protein-protein interaction with Ca^{2+}/CaM, caveloin-1 and Hsp90; posttranslational retulations (phosphorylation, acylation); availability of substrates and cofactors (tetrahydrobiopterin (H_4-B), flavin mononucleotide, FAD, NADPH); and subcellular localization (plasma membrane caveolae, Golgi, and cytosolic compartments) (18, 21).

eNOS is predominantly localized to caveloae, a specialized microdomain of the plasma membrane. The basis for eNOS trafficking to microdomain is that eNOS is both N-terminally myristoylated at the glycine residue in position 2 and palmitoylated at the cysteine residues at positions 15 and 26 (117). Studies of caveolae isolated from rat lung suggested that caveolae localization of eNOS occurred in intact endothelial cells and both acylation processes are necessary for optimal targeting of eNOS to caveolae (118).

The localization of eNOS in caveolae is apparently a prerequisite for the effective enzyme activation. Mutant eNOS constructs, in which the glycine at position 2 is mutated to alanine

(G2AeNOS), fail to undergo fatty acylation, and as a consequence remain cytosolic. Both the basal and stimulated NO production by G2AeNOS is markedly reduced compared to wild-type eNOS (WTeNOS). However, no differences are observed in catalytic activity of the isolated WTeNOS and G2AeNOS (28, 116). There is another study suggests the importance of subcellular eNOS localization (61). Jagnandan et al. compared activity of iNOS and eNOS after targeting them to different subcellular locations, and, in contrast to eNOS, no impairment in the ability of iNOS to synthesize NO was found. iNOS, structurally similar enzyme with eNOS, has virtually identical co-factor and substrate affinities with one major exception, calcium-calmodulin. eNOS is highly dependent on increases in intracellular Ca^{2+} for activity, whereas iNOS is already maximally activated by Ca^{2+}/CaM even at basal levels of intracellular calcium and thus is Ca^{2+} independent. iNOS targeted to discrete intracellular regions of the cell behaves similarly to cytosolic iNOS. Since the affinities for L-arginine, and cofactors like BH_4 and NADPH are not different between eNOS and iNOS, with one exception -- calcium dependency. eNOS is highly dependent on increases in intracellular Ca^{2+} for activity, whereas iNOS is Ca^{2+} independent. Therefore, it has been postulated that targeting of eNOS to caveolae domains causes increased localized concentration gradients, which represent a plausible explanation for the caveola localization-dependent activity of eNOS.

There has been a long standing interest in the role of caveolae in intracellular calcium regulation. Caveolae, as subcellular units, have been identified as being involved in calcium signalling in smooth muscle cells(104), as well as endothelial cells(77). Isshiki et al. using modern imaging techniques, have recently shown that spatially organized Ca^{2+} waves originate in subsets of clustered caveolae regions at the edges of endothelial cells in response to ATP(56-58). They also provided evidences to show CCE channels reside in caveolae(59). CCE entry has been indicated the preferential Ca^{2+} source for the activation of the Ca^{2+}-calmodulin depenent endothelial NOS(36, 74). Since both eNOS and CCE channels reside in caveolae, the

spatial proximity of eNOS to the CCE channels has been proposed to explain the significantly different behavior of the wide type eNOS and eNOS with acylation deficient mutants. It also explains the discrepancy of eNOS activity within discrete subcellular locations; however, iNOS activity is not dependent on enzyme localization.

In endothelial cells, NO production is under autoregulatory control. CCE calcium entry has been indicated the as preferential calcium source for eNOS. NO, via the cGMP-dependent inhibition of CCE and acceleration of Ca^{2+} sequestration into the ER, lower $[Ca]_i$ and therefore exert an autoregulatory negative feedback on its own production(36). NO also decreases eNOS expression, disrupt caveolae signaling by distancing elements of the cascade, which lead to terminate eNOS signaling(123)

Plasmalemmal caveolae seem to be well-suited intracellular locale for eNOS and its complex regulation. Caveolin reduces eNOS activity in basal conditions but facilitates its activation upon agonist stimulation. There are two apparently paradoxical tasks that seem to be effectively managed in the context of caveolar/eNOS interaction: Caveolin-1, being the major coat protein of caveolae, interacts with eNOS and represses NO production. Calcium entry from CCE channels, which also reside in caveolae domain, promotes the dissociation of eNOS from caveolin in endothelial cell; Besides CCE channels, caveolae also compartmentalizes many other signal transduction molecules which positively regulate eNOS activity (i.e. heat shock protein 90, protein phosphorylation). Increase in NO will exert an autoregulatory negative feedback on its own production (123).

1.5 Endothelial Cell Heterogeneity

The vascular system is a complex network of vessels connecting the heart with diverse organs and tissues to maintain their homeostasis in response to physiological changes. The endothelial cells that line the lumen of blood vessels play an integral role in the regional

specialization of vascular structure and physiology. They form an active barrier between the blood and the interstitium; fulfill an essential bidirectional signaling role so that the physiochemical environment in blood and tissue and maintained in balance according to demand. Whereas all endothelial cells share certain common properties, they do not behave alike. Given the diversity of the vascular architecture and the associated differences in hemodynamics, structure, and embryonic origins, it is not surprising that the ECs lining different vessels exhibit regional specializations in morphology and functions.

Diversity in endothelial functions between organs has been recognized for decades. In the systemic circulation, blood fluid flux is high variable between organs. Permeability edema is prominent at post-capillary venules; while blood brain barrier is nearly completely fluid impermeable with tight cell-cell junctions; renal glomerular and liver sinusoidal endothelium possess fenestrations that are highly permeable. Chi et al (27), using microarray analysis, studied the mRNA expression profiles in 53 different cultured endothelial populations from 14 distinct locations and revealed that ECs from different anatomical sites have distinct differentiated gene expression pattern. They also performed hierarchical cluster analysis and comparisons to reveal that endothelial cells were reproducibly distinguishable from microvascular endothelial cells and that artery-derived cells also discriminated from vein cells.

Endothelial heterogeneity is not only observed among different anatomic organs. There is also evidence for inherent diversity of phenotype of vascular endothelium within and among arteries in the same tissue. The widespread recognition that environmental conditions critically regulate cell phenotype had lead to some in vitro and in vivo studies about endothelial cells response to different stimuli. Studies have shown differences between the arterial and the venous endothelium in the production of relaxing factors such as nitric oxide and prostaglandin. There are longitudinal differences in endothelial functions between conduit and resistance vessels (51, 65, 128). Kimura et al. report that eNOS expression and eNOS activity

are greater in culture aortic endothelial cells than in cultured microvascular endothelial cells(65). The study of influence of coronary artery diameter on eNOS protein content also reveal eNOS expression is greater in the endothelial cells of conduit arteries, resistance arteries, and large arterioles than in small coronary arterioles(72). Endothelium-derived NO induces a relaxation of vascular smooth muscle cells in large conducting vessels. In contrast, endothelium-derived hyperpolarizing factor (EDHF) has been suggested to play a greater role than NO in microvessels(51).

The microcirculation is the site where many important biological substances are transported between the blood and surrounding tissue. In contrast to transport processes at the organ or whole-body level, transport in the microcirculation is known to be highly heterogeneous, both in space and time. Majno and Palade observed endothelium within post-capillary venules responded to histamine by forming intercellular gaps that increased permeability, whereas immediately adjacent endothelial cells exhibited little or no discernible response(80). The heterogeneous response in capillaries has been shown to account for the distribution of localized leakage sites for macromolecules in microvessels (100). Calcium waves/oscillations have also been observed in arterioles and capillaries (114, 137), which serve to coordinate the heterogeneity and regulate the activities of cell groups.

1.6 Objectives

Endothelial cells are subject to the shear stress generated by blood flowing past their apical surfaces. Changes in fluid shear stress could be sensed directly by cells and elicit a cascade of responses which include the elevation of intracellular Ca^{2+} and production of NO. This study compared the calcium response to shear stress between the ECs from large vessels and microvessels; characterized the interplay between $[Ca^{2+}]_i$ and endothelial nitric oxide synthase (eNOS) activity in bovine aortic endothelial cells (BAECs) in response to shear stress and ATP; and developed a mathematical model quantitatively study the effects of spatial

colocalization of eNOS and capacitive calcium entry (CCE) channels in caveolae on eNOS activiation .

Aim 1: Assess the difference in calcium response to shear stress between macrovascular and microvascular endothelial cells

Hypothesis 1: Given the diversities in hemodynamics and structure, the endothelial cells (ECs) lining different vessels exhibit regional specializations in functions, we hypothesize that the responses of calcium to shear stress of macrovascular endothelial cells are different from the responses of the microvascular endothelial cells.

Aim 2: Characterize the correlation between $[Ca^{2+}]_i$ and NO production in BAECs.

Hypothesis 2: A linear correlation between the magnitude of the free calcium concentration and NO production has been demonstrated in isolated eNOS. However, since the calcium channels and eNOS are not homogeneously distributed in the cells, we hypothesize endothelial NO production is nonlinearly correlated with the spatial average intracellular calcium concentration.

Aim 3: Develop a mathematical model of intracellular calcium signaling in endothelial cells to evaluate the effects of spatial colocalization of eNOS and capacitive calcium entry (CCE) channels in caveolae on eNOS activiation in response to shear stress and ATP.

Hypothesis 3: Microdomain calcium signaling is influenced by calcium channels localization, distribution and cell geometry. The quantitative characterization of the microdomain calcium signaling can only be predicted by mathematical models that incorporate interactions occurring at multiple length and time scales.

1.7 Thesis Organization

This dissertation is presented as three separate chapters with a preceding introduction (Chapter 1) presenting the relative information on the endothelial mechano-transduction, the

role of caveolae in endothelial calcium and nitric oxide signaling and their interaction, and the endothelial heterogeneity. Chapter 2 compares the nature of the response and the mechanisms of mechanotransduction in macro and microvascular endothelial cells. We also investigated the mechanisms of the spatially and temporally heterogeneous calcium changes within cultured monolayers of RAMECs. In Chapter 3, the experimental results of the interplay between $[Ca^{2+}]_i$ and endothelial nitric oxide synthase (eNOS) activity in BAECs in response to shear stress and ATP are presented. In Chapter 4 provides a mathematical model which incorporates endothelial cell morphology as well as endothelial calcium signaling processes to quantitatively evaluate the effects of spatial colocalization of eNOS and capacitive calcium entry (CCE) channels in caveolae on eNOS activiation in response to shear stress and ATP. Chapter 5 summarizes the implications of the results, the primary findings and the recommendations of future work.

CHAPTER 2

Response of Aortic and Microvascular Endothelial Cells to Shear Stress

2.1 Introduction

Endothelial cells (ECs) cover the inner surface of blood vessels and are constantly exposed to shear stress due to blood flow. It is well established that ECs are sensitive to changes in shear stress. Intracellular signals generated in response to flow elicit a cascade of responses that involve cytoskeletal organization, remodeling of cellular morphology, and changes in gene expression (6, 32). One of the early responses to shear stress is the elevation of intracellular Ca^{2+} concentration ($[Ca^{2+}]_i$).

ATP has been shown to be released from large vessel ECs in response to numerous stimuli, such as shear stress and vasoactive agonists, including ATP itself (15, 16, 132, 133). The released ATP can activate purinergic receptors; stimulate the formation of inositol(1,4,5)-trisphosphate (IP_3), which binds to IP_3 receptors and triggers Ca^{2+} release from intracellular stores(37). Thus, endogenously released ATP can act as extracellular messenger, regulating the flow-induced calcium response in large vessels. However the possible role of ATP signaling in the endothelial transduction of shear stress-induced calcium responses in the microvascular ECs is not yet established.

The vascular system is a complex network of vessels connecting the heart with diverse organs and tissues to maintain their homeostasis in response to physiological changes. The endothelial cells that line the vessel lumen play an integral role in the regional specialization of vascular structure and physiology. Whereas all endothelial cells share certain common properties, phenotypic heterogeneity is observed between ECs from large vessels and microvascular ECs (27). Studies have shown longitudinal differences in endothelial functions between conduit and resistance vessels (51, 65, 128). In large vessels, shear stress induced

Ca^{2+} is related to vessel dilation. Either removal of extracellular calcium or chelation of intracellular calcium reduces the shear stress-dependent NO production in aortic endothelial cells (108, 134). However, calcium appears to be less important in shear stress-induced dilations of smaller arteries and arterioles (128). The microcirculation is the site where many important biological substances are transported between the blood and surrounding tissue. In contrast to transport processes at the organ or whole-body level, transport in the microcirculation is known to be highly heterogeneous, both in space and time. The heterogeneous calcium response in capillaries has been shown to account for the distribution of localized leakage sites for macromolecules in microvessels (100). Calcium waves/oscillations have also been observed in arterioles and capillaries (114, 137), which serve to coordinate and regulate the activities of cell groups.

Despite the recognition of regional differences in endothelium, in vitro studies of the responses of endothelial cells to flow have focused almost exclusively on ECs from large vessels. A recent report indicated that NO concentrations in tissues cannot be accurately predicted when blood vessels are considered in isolation (64). NO production from venules and capillaries contribute significantly to the NO concentration in the vicinity of arterioles, which are usually the primary focus of experimental investigations because of their important role in the distribution of blood to tissues. NO release is highly controlled and usually preceded by elevation of intracellular calcium, so it is important to investigate the calcium response to shear stress in microvascular ECs. The typical response to the initiation of shear stress in cultured aortic endothelial cells is a rapid mobilization of intracellular calcium in a dose-dependent fashion (13, 120), although more complex behaviors (e.g. calcium oscillations) have been observed. However, little has been done to investigate whether the nature of the response or the mechanisms of mechanotransduction are similar in microvascular cells. In the present study, we have characterized the responses of microvascular endothelial cells to shear

stress in terms of their calcium signaling. We used ECs isolated from the adrenal medulla, a highly vascularized tissue whose vasculature is composed primarily of microvessels. We compared these cells with cells derived from the aorta and found differences in both the spatial and temporal characteristics of the calcium responses. Shear stress elicited calcium waves that originated from one or several cells and propagated to neighboring cells in RAMECs while the response in BAECs was rapid and synchronous. We further investigated the mechanisms for this novel pattern of response and cell-cell communication in RAMECs.

2.2 Materials and Methods

2.2.1 Cell Culture

BAECs were obtained from Dr. Keith Gooch's lab (University of Pennsylvania) and RAMECs were provided by Dr. Peter Lelkes (Drexel University). RAMECs were isolated from the adrenal medulla. During isolation, large vessels, including any sinusoidal capillaries were carefully removed by dissection. Thus, the isolated cells were primarily continuous capillary endothelium(81). ECs were cultured in Dulbecco's modified Eagle's medium (DMEM, Mediatech Cellgro, VA), supplemented with 10% fetal bovine serum (Sigma), 2 mmol/L L-glutamine (Mediatech CELLGRO). The cultures were studied as confluent monolayer of polygonal cells.

2.2.2 Ca^{2+} measurement

Fluo3 was used as the Ca^{2+}-indicator. Compared with fura-2, the higher Kd value reduces the buffering of the $[Ca^{2+}]_i$ signal. In addition, the longer excitation wavelength avoids the cell damage by exposure to UV, and its large optical signal provides very good signal-to-noise ratio (87). Endothelial cells were loaded in the dark with fluo3 by incubation with 5 μmol/L Fluo3-acetoxymethyl ester (Molecular Probes, Inc.) in Dulbecco's phosphate buffered saline

(DPBS) (Sigma) at pH 7.4, for 40 minutes at room temperature. Cell fluorescence was monitored and recorded.

2.2.3 Device and mechanical stimulation

A custom-built cell-shearing device based on a cone and plate configuration as shown in Fig. 2.1 was mounted on the microscope stage and used to apply precise mechanical loading conditions to the endothelial cells. The principle of the device was described in detail by Blackman et al..(12). Briefly, the device is based on a cone and plate geometry. The rotation of the cone relative to the stationary plate causes motion in the fluid between the two surfaces, thus impose a uniform level of shear stress on the cell surface. The magnitude of shear stress was controlled by the rotation velocity of the motor. ECs were cultured on coverslip and loaded with fluorescence dye fluo3. During experiments, the device was mounted on the microscope and the fluorescence was monitored and recorded. For each experiment, a volume of 1.2 ml DPBS (containing no exogenous ATP or other stimulatory agents) was added to the well to fill the gap between the cone and plate. For the mechanical loading period, endothelial cells were monitored for about 30 s under static conditions prior to the onset of shear stress to establish basal levels of calcium. Then, the shear stress was increased linearly to 5, 10, 20 or 30 dyn/cm^2 over 0.1 seconds and maintained at a steady level for 5 minutes. In addition, RAMECs were exposed to 60 dynes/cm^2 shear stress to account for the fact that shear stress in the microcirculation can be significantly larger than in large vessels (6).

2.2.4 ATP assay:

ATP release from endothelial cells was determined using the luciferin-luciferase assay (Sigma). The samples (100 μl) collected from cells exposed to shear after 5 min. or sham controls were pipetted into the wells of a microplate. The plate was placed in a luminescence

counter (1450 MicroBeta Jet, PerkinElmer) and processed by injection of 50 µl ATP assay mix dilution buffer (20 fold dilution). ATP concentrations were calculated from a calibration curve constructed using ATP standards.

2.2.5 Immunocytochemical staining:

Cells were fixed with 4% paraformaldehyde in DPBS for 20 min. Non-specific binding sites were blocked by incubation with blocking solution (10% normal donkey serum in DPBS) for 30 min. Cells were then incubated at room temperature with primary antibody (anti-P_2Y_2 receptor; Calbiochem) diluted in 1% donkey serum in DPBS to a final concentration of 3 µg/ml for one and a half hours and secondary antibody (anti-rabbit Alexa 488) diluted in 1% donkey serum in DPBS to a final concentration of 1:1000 for 1 hour in the dark. Control experiments were performed identically except for the omission of the primary antibody.

2.2.6 Agonist stimulus protocol

To investigate the mechanism of heterogeneity of RAMECs, agonist stimuli were performed according to the following protocol:

Protocol 1: Cells were exposed to uniform exogenous agonist (ATP, ionophore A23187 or thapsigargin) at their final concentration.

Protocol 2: Cells were first stimulated with an agonist - 1 µM ATP, and after the $[Ca^{2+}]_i$ returned to near basal levels, ATP was washed out and cells were challenged with a second agonist—Bradykinin 1 µM. Then, the cells were stimulated with 100 µM ATP.

2.2.7 Chemicals and reagents:

The non-specific purinergic receptor blocker suramin, apyrase, Dulbecco's phosphate buffered saline (DPBS), nucleotides adenosine triphosphate (ATP), Adenosine 5'-triphosphate

bioluminescent assay kit and 1-heptanol were purchased from Sigma. Suramin, apyrase, heptanol and ATP were directly dissolved at their final concentration in DPBS. Normal donkey serum was purchased from Jackson Immuno Research (West Grove, PA, USA). The Fluo3-acetoxymethyl ester and anti-rabbit Alexa 488 were obtained from Molecular Probes, Inc..

2.2.8 Image Analysis:

To evaluate calcium dynamics, individual cells were outlined manually, and the average fluorescence intensity in each selected cell was calculated using Axon Imaging Workbench. To control for cell-to-cell variations in dye loading, all fluorescence measurements were expressed as a ratio (R) of fluorescence intensity (F) to the basal fluorescence intensity (F0). A fluorescence ratio value greater than 1.2 was selected as the criterion for cell activation because under control conditions, R fluctuated about the control level (R=1) with a standard deviation of 0.19.

The following parameters characterizing the $[Ca^{2+}]_i$ response to the flow or to agonist were analyzed: 1) fraction of activated cells ($R > 1.2$) in the observed field. 2) the amplitude of $[Ca^{2+}]_i$ peak in activated cells as indicated by the peak fluorescence ratio 3) number of calcium waves initiated in the first 5 minutes after the initiation of shear stress 4) number of activated cells in each calcium wave propagation group.

2.2.9 Statistical Analysis:

For each experimental condition, a minimum of 3 runs were analyzed. Relationships between groups were compared using Analysis of variance (ANOVA) followed by Tukey's test for significance between treatment groups. Results were expressed as mean±SEM. $P<0.05$ was considered to be significant.

2.3 Results:

2.3.1 Shear stress induced calcium waves in RAMECs

BAECs were exposed to shear stresses of 5, 10, 20 and 30 dyn/cm^2, and changes in $[Ca^{2+}]_i$ were monitored. Shear stress elicited a rapid and synchronous rise in $[Ca^{2+}]_i$ (more than 90% BAECs were actived when exposed to shear stress of 20 dyn/cm^2). The magnitude of the $[Ca^{2+}]_i$ change increased as a function of shear stress (Fig.2.2 A, Fig. 2.2 B). The calcium rise began 1-3 seconds after shear stress initiation and reached its peak amplitude around 15 seconds. It then decreased to near baseline levels (Fig.2.2 C). These results are consistent with previous reports (13, 120). In contrast, shear stress induced spatially heterogeneous calcium responses in RAMECs, originating from one or several cells and propagating to neighboring cells (Fig 2.3 A.) The propagation radius varied widely in the series of experiments, with activated groups ranging in size from 2 cells to 15 cells. During the propagation, the amplitude of the $[Ca^{2+}]_i$ peak did not decline as a function of the distance away from the initiating cells (Fig.2.3 B, Fig. 2.3 C). In contrast to the synchronous response of BAECs, the calcium waves in RAMECs were initiated at different times and different locations. For example, in the experiment shown in Figure 2.3, 6 seconds after shear stress initiation, calcium waves were observed in cell group 1 and the cells exhibited calcium oscillations (Fig. 2.3 B). Calcium waves were triggered in cells group 2, 158 seconds later. Other small groups of calcium responses were also observed in the interim but not indicated in Fig.2.3. There was no consistent pattern in the calcium wave initiation or propagation.

The calcium response time of BAECs and RAMECs is shown in Fig. 2.4. For BAECs, shear stress induced synchronous calcium responses and the response reached peak amplitude within 15 seconds. In contrast, RAMECs responded to shear stress at different times and the response times occurred mostly in the first 3 minutes. Furthermore, the average magnitude of the response did not depend on the time of the occurrence.

The number of calcium waves initiated and the average number of cells in each activated group under shear stress was significantly greater than in unsheared controls (Fig. 2.5A), but did not depend on the shear stress magnitude. Control cells exhibited occasional spontaneous $[Ca^{2+}]_i$ oscillations, but there was no propagation of $[Ca^{2+}]_i$ waves to neighboring cells. The amplitude of the responses was not dependent on shear stress nor were they statistically different from controls (Fig. 2.5B).

2.3.2 Release of endogenous ATP

Applying the media collected from cells exposed to shear to unsheared cells immediately activated calcium response in a small portion of RAMECs, which suggests release of vasoactive substances from the cells induced by shear stress. In the sham controls, the concentration of ATP in the collected medium was very low. (RAMEC: $16.3 \pm 5 n\,mol/L$, BAEC: $18.9 \pm 4 n\,mol/L$). The stimulation of the cells with a shear stress of 20 dyn/cm2, 5 min. led to an increase in extracellular ATP concentration in both BAECs ($102.3 \pm 23 n\,mol/L$) and RAMECs ($141.2 \pm 40 n\,mol/L$) (Fig. 2.6). It is important to note that these final concentration values depend on the volume of fluid in the experimental chamber. Thus, in order to compare values from different experimental models, the amount of ATP per cell is the relevant datum. Shear stress stimulated BAECs and RAMECs to produce 13.5 and 18.6 picomoles ATP per million cells per minute, respectively.

2.3.3 The effect of suramin, apyrase and 1-heptanol on the shear stress induced calcium waves

To investigate whether the initiation and propagation of calcium waves in response to shear stress was mediated by ATP, cells were pretreated with suramin, a non-specific P2 receptor blocker, for at least 10 minutes before the shear experiments. Suramin treatment

significantly inhibited both the initiation and propagation of calcium waves (Fig. 2.7 A). However, the presence of suramin did not change the magnitude of $[Ca^{2+}]_i$ peak amplitude in the responding cells (Fig. 2.7 B). Suramin pretreatment significantly reduced the magnitude of calcium responses to shear stress in BAECs (Fig 2.12). As a negative control, suramin was added to both BAECs and RAMECs, and it did not lead to calcium mobilization in either of them.

To rule out the non-specific effects of suramin, we also investigated the dependence of the calcium signaling on released ATP by conducting the experiments in the presence of apyrase, which degrades extracellular ATP. Applying of 10 U/ml apyrase resulted in an inhibition similar to the suramin pretreated group (Fig. 2.7 A & B). Administration of apyrase also significantly inhibited the magnitude of calcium response to shear stress in BAECs (Fig. 2.12).

To test the possibility that spreading of the calcium from the initial responding cells to adjacent cells was due to gap junctional communication, we pretreated RAMECs for 15 min. with 3 mmol/L 1-heptanol, which inhibits gap junctions. Inhibition of gap junctional communication had no effect on the shear stress-induced calcium waves (Fig. 2.7 A & B).

2.3.4 The $[Ca^{2+}]_i$ response to ATP in RAMECs

That suramin inhibited calcium wave initiation and propagation suggests that ATP release and autocrine/paracrine signaling is involved in the shear stress-induced $[Ca^{2+}]_i$ response in RAMECs. To further investigate the heterogeneity of the response and the role of ATP, we measured calcium responses of the cells to exogeneous ATP stimulation. The application of ATP to RAMECs elicited a rapid $[Ca^{2+}]_i$ response that was spatially and temporally heterogeneous (Fig.2.8) ATP induced an immediate $[Ca^{2+}]_i$ response in some individual cells. Then, the $[Ca^{2+}]_i$ increase was observed in adjacent cells. The magnitude of the $[Ca^{2+}]_i$ transient did not decline as the $[Ca^{2+}]_i$ changes propagated away from the initial response.

Another characteristic of the RAMEC response to ATP was the large variability in the calcium oscillations even for contiguous cells (Fig. 2.8 B, C). ATP could initiate calcium oscillations which persisted for the full duration of the observation (around 5 minute) (cell 1) or oscillations which had only 1 or 2 transients (cell 2, 3). In some of the cells, $[Ca^{2+}]_i$ decreased to baseline without any oscillations (cell 4). The long lasting oscillations were usually observed in the initially responding cells.

The fraction of activated cells increased as a function of ATP concentration (Fig.2.9). The percentage of responding cells is defined as the number of responding with a detectable increase in Ca^{2+} reported to the total number of cells within the filed (about 200 cells per field). Even 100 μmol/L ATP evoked a response in only around 70% of the cells. Low doses of ATP evoked $[Ca^{2+}]_i$ increases just in individual cells. Higher ATP concentrations induced $[Ca^{2+}]_i$ transients that propagated to adjacent cells. The magnitude of the rise in $[Ca^{2+}]_i$ elicited by ATP was not dependent on the concentration in the range of 0.1 μmol/L to 100 μmol/L (Fig. 2.9 B). The peak amplitude of $[Ca^{2+}]_i$ was reduced only at a level of 0.01 μmol/L ATP. The rise time and return to basal level were not affected by ATP concentration level (Fig. 2.9 C).

When two different doses of ATP (1 μmol/L and 100 μmol/L) were applied sequentially to the same cells, 100 μmol/L ATP activated more cells than 1 μmol/L. The same cells that responded to 1 μmol/L ATP (Fig. 2.10(a)) were also all activated by 100 μmol/L ATP (Fig. 2.10(b)) with similar Ca^{2+} peak amplitude.

2.3.5 The $[Ca^{2+}]_i$ response to ATP in BAEC

Parallel experiments were conducted using BAECs. BAECs responded to ATP in a dose-dependent manner. At the lowest concentrations of ATP (0.01 μmol/L and 0.1 μmol/L), a very small fraction of cells was activated with low $[Ca^{2+}]_i$ amplitude. ATP evoked rapid, simultaneous and homogeneous $[Ca^{2+}]_i$ transients in all the cells (Fig. 2.8A). Higher doses of

ATP evoked higher peak amplitude and longer duration of $[Ca^{2+}]_i$ response elevation (Fig. 2.11).

2.3.6 The effect of suramin pretreatment on the $[Ca^{2+}]_i$ response to ATP

In these experiments, we confirmed that suramin treatment can block the calcium response to ATP in RAMECs. Incubation with 400 μmol/L suramin resulted in a complete inhibition of $[Ca^{2+}]_i$ in response to ATP stimulation up to 1 μmol/L. Higher concentrations of ATP induced increasing percentage of activated cells, but suramin pretreatment caused a 77% inhibition in 10 μmol/L ATP and 22% in 100 μmol/L ATP activation. While suramin significantly reduced the number of responding cells to ATP stimulation, the amplitude of $[Ca^{2+}]_i$ peak in the activated cells was not affected (Fig. 2.9). Suramin significantly reduced the $[Ca^{2+}]_i$ peak amplitude to 1uM ATP in BAECs (Fig. 2.12).

2.3.7 P_2Y_2 receptor staining:

The expression of P_2Y_2 receptors on RAMECs and BAECs was compared by immunofluorescence (Figure 2.13). P_2Y_2 receptor immunoreactivity was clearly present on the BAECs and the mean fluorescence intensity was significantly higher than RAMECs. The immunolabelling of P_2Y_2 receptor in RAMECs also showed a nonuniform pattern of expression. Strong immunoreaction was found in a few cells which had bright fluorescence over the whole cell membrane. Lighter binding was present in some cells which expressed faint fluorescence. Unlabeled or very weak labeled cells were also present with very dim fluorescence (Fig.2.13).

2.3.8 Agonists stimuli experiments

To investigate the mechanisms responsible for the heterogeneity, we stimulated the cells

with other agonists. Calcium ionophore A23187 induced uniform calcium increase in all the RAMECs as shown in Fig. 2.14.A. Similarly, thapsigragin, cell-permeable, IP3-independent intracellular calcium releaser, also increase $[Ca^{2+}]_i$ homogeneously in all the cells (Fig. 2.14. B). Bradykinin in the range of 0.1μM-10μM induced calcium transient in 10%-20% RAMECs. The calcium response magnitude in the activated cells over the entire concentration range varied little. In Fig.2.14 C , the cells were stimulated with a first agonist—1μM ATP, and after the $[Ca^{2+}]_i$ returned to near basal levels, ATP was washed out and cells were challenged with a second agonist—Bradykinin 1μM. Then, the cells were stimulated with 100μM ATP. The results showed few cells responded to both 1μM ATP and 1μM bradykinin, however, for the activated cells, ATP and bradykinin were equipotent in the peak amplitude of the $[Ca^{2+}]_i$. The same cells that responded to 1 μmol/L ATP were also all activated by 100 μmol/L ATP, which is consistent with Fig.2.10.C.

2.4 Discussion:

The results of the present study demonstrate for the first time that BAECs and RAMECs respond differently to shear stress. In BAECs, shear stress elicited a rapid and transient rise in $[Ca^{2+}]_i$ that was synchronous across the monolayer. Furthermore, the magnitude of the $[Ca^{2+}]_i$ change was dependent on the level of shear stress, consistent with previous reports(13, 120). In contrast to the response in aortic ECs, RAMECs responded to shear stress with $[Ca^{2+}]_i$ transients that were spatially heterogeneous and asynchronous. Responding cells initiated a wave-like propagation to neighboring cells of the $[Ca^{2+}]_i$ transients whose magnitude was independent of the shear stress level. Our results with BAECs are also similar to previous results findings using rat aortic ECs (71, 134), suggesting that the characteristics of the response are not species dependent .

We showed that both BAECs and RAMECs release ATP in response to shear stress.

Spatially uniform, exogenously applied ATP produced a similar spatially heterogeneous calcium responses in RAMECs that was similar to the shear stress response. The initiation and the propagation of calcium waves in RAMECs, induced either by shear stress or exogenous ATP, were significantly suppressed by suramin, a purinergic receptor blocker. The Calcium ionophore A23187 and thapsigragin, IP_3-independent intracellular calcium releaser, increase $[Ca^{2+}]_i$ synchronously and homogeneously in all the cells. Furthermore, immunocytochemical staining indicated nonuniform expression of P_2Y_2 receptors in RAMECs. Based on our observations, we propose a mechanism for the spatial heterogeneity of the shear stress response of RAMECs in which shear stress causes the release of ATP, which then elicits calcium responses from a subset of cells that are differentially sensitive to ATP. Then, additional ATP is then released from those cells, creating a locally elevated concentration, sufficient to activate the calcium response in neighboring cells.

It has previously been shown that shear stress induces ATP release from large vessel ECs (17, 132, 133, 135). Our data provides for the first time evidence that ATP is also released from microvascular endothelial cells in response to shear stress. Meanwhile, our data strongly suggest that ATP mediates both the initiation and propagation of calcium waves in response to shear stress via purinergic receptor activation. Preincubation with a purinergic receptor blocker or enzymatic degradation of extracellular ATP significantly inhibited the calcium wave initiation and propagation. Furthermore, when unsheared RAMEC cells were exposed to the media collected from cells that were exposed to shear stress, a calcium response was immediately activated in a small portion of the unsheared cells. It should, however, be mentioned that suramin is relatively nonselective. It may disturb other cellular pathways in addition to its effect on purinergic receptors. Caution is needed in interpreting the data generated from the use of suramin. Nevertheless, the data from the apyrase experiment provide confirmation that ATP release during the shear stress is required for the calcium response.

Our study indicates that ATP released in response to shear stress mediates mechanotransduction in microvascular endothelial cells. The physiological role of ATP release in endothelial cells in vivo has not been thoroughly elucidated but many possibilities exist. One possible physiological effect of ATP release in the microcirculation, that is, regulation of blood vessels vasodilation/vasoconstriction has also been pointed out by other previous studies. Additionally, ATP has been shown to induce the synthesis of nitric oxide in endothelial cells(2), a major modulator of vascular smooth muscle tone. With regard to shear stress, Liu et al. showed a synergistic effect of ATP and flow on dilation that was attenuated by application of purinergic antagonists in isolated rat small mesenteric arteries(76); however, they did not investigate the response to flow in the absence of exogenous ATP.

The potential role of shear stress-stimulated ATP release in the control of microvascular perfusion is further suggested by the following studies. McCullough et al. reported that application of micromolar amounts of ATP into first and second order arterioles resulted in a significant conducted vasodilation in the same arteriole as far as 1750 μm upstream from the site of application (85). Furthermore, Collins et al. showed that intraluminal application of ATP in a collecting venule resulted in an increase in arteriolar diameter and red blood cell flux in capillaries (29). Thus, it appears that ATP is capable of stimulating vasodilatory responses in microvascular networks that propagate well beyond the point of application (upstream and downstream). Therefore, flow induced ATP release by capillary endothelial cells, as observed in our experiments, may serve a role in coordinating the microvascular response to meet the perfusion requirements of the tissue.

Bodine and Burnstock previously quantified the ATP concentration when HUVECs were exposed to 25 dyn/cm^2 shear stress using a luciferin-luciferase assay, and results showed that the highest concentration of ATP (0.1 μmol/L) was seen after 3 minutes of shear (135). In our study, the amount of ATP released from RAMECs exposed to 20 dyn/cm^2 shear stress was very

similar (0.14 μmol/L). This value, however, represents the average concentration in the bulk fluid. As ATP is released from the cell monolayer under flow, the concentration in the diffusive boundary layer adjacent to the cells will be much higher than in the bulk. To estimate the concentration of ATP at the cell surface in our shearing experiments, we can find the exogenously-applied ATP concentration for which suramin treatment inhibited the calcium response to a similar degree. Thus, we estimate the cell surface concentration to be approximately 1-10 μM.

We have proposed that the spatial heterogeneity of the calcium response of RAMECs to shear stress is due to the nonuniform sensitivity to ATP. This is supported by our experiments. There are several possible causes of the response difference among the cells. First, there may be wide variation in the distribution or expression of G protein related receptors or in their binding properties from cell to cell. The alternate mechanisms to explain the heterogeneity are differences in post-receptor coupling signaling mechanisms like the amount of IP_3 generation, the variable number of IP_3 receptors or heterogeneity in intracellular calcium store. If the main source of variation is the IP_3 generation or IP_3 receptors, we predict that the cells responded to 1μM ATP should respond to 1μM bradykinin since both ATP and bradykinin act on G protein-coupled receptors and stimulate phospholiphase C and generation of IP_3, which triggers Ca^{2+} release from intracellular stores. The later application with 100μM ATP showed no reduction in calcium peak amplitude, which demonstrated that cells did not respond to bradykinin was not due to the lack of calcium in the internal stores and vice versa. Calcium ionophore A23187 and thapsigargin induced homogeneous $[Ca^{2+}]_i$ increase in all of the cells, means that the variability in dye concentration and intracellular calcium store are not the mechanisms underlying the heterogeneity. Taken together with the present results, these observations suggest that the main source of variation was the heterogeneous distribution of G protein-coupled receptors in RAMECs. This finding was confirmed by the nonuniform pattern

of expression of P_2Y_2 receptors. The mechanism by which shear stress elicits the release of ATP is unknown, and it is possible that heterogeneity in the sensing mechanism involved in this response also contributes to the heterogeneity of the $[Ca^{2+}]_i$ response. Davies et al. proposed that heterogeneous responses to shear stress could be due to the variations in the detailed distribution of shear stresses acting on the cell surface owing to the specific surface topography of the monolayer (8, 33). While it is possible that this mechanism contributes to the heterogeneity we observed, this explanation seems incomplete in this case. There was no dramatic difference in the morphology of the two cell types, so one would expect similar heterogeneity in the BAEC response if it were determined by surface topography alone.

There are two major families of nucleotide receptors, defined based on molecular structure and signal transduction mechanisms. P_2X receptors are ATP-gated Ca^{2+}-permeable channels, where ATP binding directly causes Ca^{2+} influx from extracellular space. P_2Y receptors are G protein-coupled receptors and are linked to the stimulation of phospholiphase C and the generation of inositol(1,4,5)-trisphosphate (IP_3), which triggers Ca^{2+} release from intracellular stores(109). Even though Yamamoto, et al., demonstrated shear stress activated Ca^{2+} influx into HUVECs via P_2X_4 purinoceptors, there is evidence from several studies that supports the IP_3-mediated release from intracellular stores as the primary source of calcium in response to flow (13, 120). Prasad et al. and Nollert et al. showed that IP_3 production increases in responses to flow with an initial peak at 15 seconds, and the increase is proportional to shear stress magnitude (95, 105). We evaluated the P_2Y_2 receptors in this study because P_2Y_2 are present in endothelial cells from both aorta (88) and adrenal medulla(84). Furthermore, the IP_3 response to ATP appears to be mediated exclusively by P_2Y_2 in the endothelial cells from adrenal medulla (1, 106). However, other purinergic receptors coexist in endothelial cells from both aorta and adrenal medulla, and ATP is able to evoke calcium increases by activating these receptors (30, 84). Thus, it is possible there is similar heterogeneity in other purinergic

receptors, which could also contribute to the calcium response.

Our results suggest that the calcium wave propagation in RAMECs is due to ATP-induced ATP release. 1-heptanol pretreatment did not inhibit the calcium waves, suggesting RAMECs did not require gap junctions to propagate calcium response or that gap junctions were not the main pathway of the intercellular calcium wave. The observation that suramin incubation reduced the spreading of calcium, indicates that the calcium wave operates via ATP release. The spreading of the calcium signal when RAMECs were exposed to spatially-uniform exogenous ATP suggests that a localized peak in ATP concentration due to its release by the initially-responding cell is capable of stimulating neighboring cells. This is consistent with the previous finding that ATP released from endothelial cells stimulates the release of additional ATP(16).

It has been documented that the magnitude of ATP release from large vessel ECs in response to shear stress is dependent on the level of shear stress (17, 135). If in the RAMECs, the ATP is released in proportion to shear stress, then one might expect that the number and size of the responding groups would increase with shear stress. However, as the shear rate is increased, the diffusive boundary layer will be reduced in thickness, facilitating the removal of ATP from the cell surface by convective transport. This situation has been modeled by John and Barakat who found that depending on the relationship between shear stress and ATP release, the surface concentration does not necessarily increase monotonically with increasing shear stress (63). In our study, the number and size of the responding groups were not statistically different over the shear stress range 5-60 dyn/cm^2.

Our study did not directly identify the mechanisms for the heterogeneity in the temporal response in RAMECs. One possible cause for the delay of the response is the time course of ATP accumulation in the medium necessary to reach the threshold of individual cells with different sensitivities to ATP. Our data (Fig 2.4) show that most responses occurred in the first

3 minutes. This is consistent with Burnstock's group's result that the peak concentration of ATP in the collected medium occurred 3 minutes after the application of shear stress(17, 135). Another possible mechanism is the different time course for IP_3 accumulation induced by ATP stimulus in aortic and adrenal medullary endothelial cells(1). In aortic cells, the IP_3 response reaches a maximum within a few seconds, followed by a rapid fall. In adrenal medullary endothelial cells, a substantial response is observed within a few seconds, and then IP_3 concentration continues to rise without reaching a maximum up to 5 minutes after stimulation(1). IP_3 acts as a messenger to link G protein-linked receptors with intracellular calcium activity. The slower time course of IP_3 accumulation to reach its threshold and then induce calcium response in RAMEC may explain the delay in the $[Ca^{2+}]_i$ rise induced by shear stress. One of the characteristics of the response in RAMECs was the large number of responding cells with long duration calcium oscillations in contrast to the very few BAECs with oscillations. It is possible that the incidence of calcium oscillations observed in RAMECs is also due to the slower time course of IP_3 accumulation since sustained concentrations of IP_3 are known to generate intracellular calcium oscillations(92).

Another feature of the calicium signaling in RAMECs was also qualitatively different from BAECs. The RAMECs did not exhibit a graded response either to different levels of shear stress or to different concentrations of exogenous ATP. The following observations support the all-or-none response of RAMECs: 1) Only a fraction of RAMECs responded to ATP. Higher levels of ATP increased the fraction of activated cells but did not increase the calcium peak amplitude, suggesting a threshold in the purinergic signalling in RAMECs. Once the threshold was reached, the transduction system was maximally activated. 2) Suramin pretreatment significantly reduced the fraction of activated cells in response to ATP, but the Ca^{2+} peak amplitude of activated cells remained the same. 3) In the flow experiments, suramin pretreatment inhibited the calcium initiation and propagation but had no effect on the calcium

peak amplitude. 4) When the same culture was exposed sequentially to 1 μmol/L ATP and 100 μmol/L ATP, the high concentration of ATP activated more cells than low concentration, but did not change the Ca^{2+} peak amplitude. Furthermore, the same cells that responded to the low concentration (Fig. 7(a)) were also all activated by the high concentration (Fig. 7(b)) with similar calcium amplitude. The mechanisms of this all-or-none response remains unclear, and additional studies are needed to elucidate them.

The framework we offer for considering the differences between aortic and microvascular endothelial cells in their response to shear stress may be a useful extension of our understanding of the diversity and regional specificity in ECs. It provides insight into the well-recognized regional variations in physiological properties that affect the vascular system. In particular, we have identified two distinct modes of signal modulation. In the aortic endothelium, the strength of the signal is modulated by the dose-dependent amplitude of the response in individual cells. In the microvascular endothelium, taken as a multicellular unit, the strength of the signal is modulated by the number and frequency of responding cells. The ramifications of this novel mode of signaling for the physiological function of microvascular networks are not clear and require further study.

Heterogeneous calcium responses in microvascular endothelial cells have been reported in vivo and in isolated vessels (100, 103). ATP would act on endothelial cell purinergic receptors regulating microvascular permeability via control of intracellular calcium signaling. The transient increases in $[Ca^{2+}]_i$ can remain within localized regions(100), which correlate with sites of macromolecule leakage(86, 100) or can spread to neighboring cells as a calcium wave(137), serving to coordinate vascular functions. Our in vitro model appears to simulate many of these characteristics and has allowed us to propose a mechanism for heterogeneous cell activation and signal transmission to neighboring cells. Our hypothesis suggests that in microvessels, ATP plays a central role in the cell signaling in response to shear stress and

serves to amplify and spread the effects of vasoactive agonists or shear stress beyond their initial sites of action. By this means, ATP acts as an autocrine and paracrine hormone, serving to integrate the heterogeneity of individual cell responses and coordinate vascular functions.

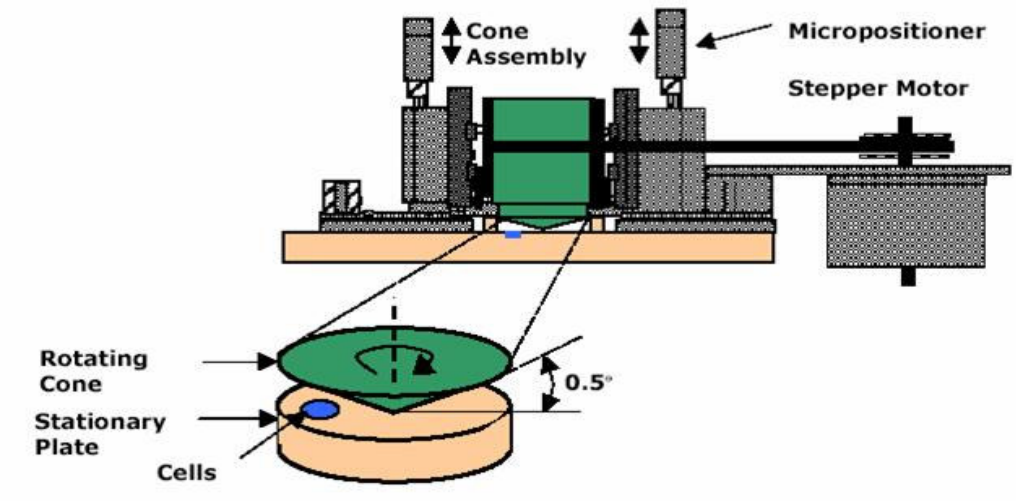

Fig 2.1 Controlled Shear Stress Device –based on cone and plate geometry (Blackman et al, 2000). The rotation of the cone relative to the stationary plate causes motion in the fluid between the two surfaces, thus impose a uniform level of shear stress on the cell surface. The magnitude of shear stress was controlled by the rotation velocity of the motor. ECs were cultured on coverslip and loaded with fluorescence dye fluo3. During experiments, the device was mounted on the microscope and the fluorescence was monitored and recorded.

A:

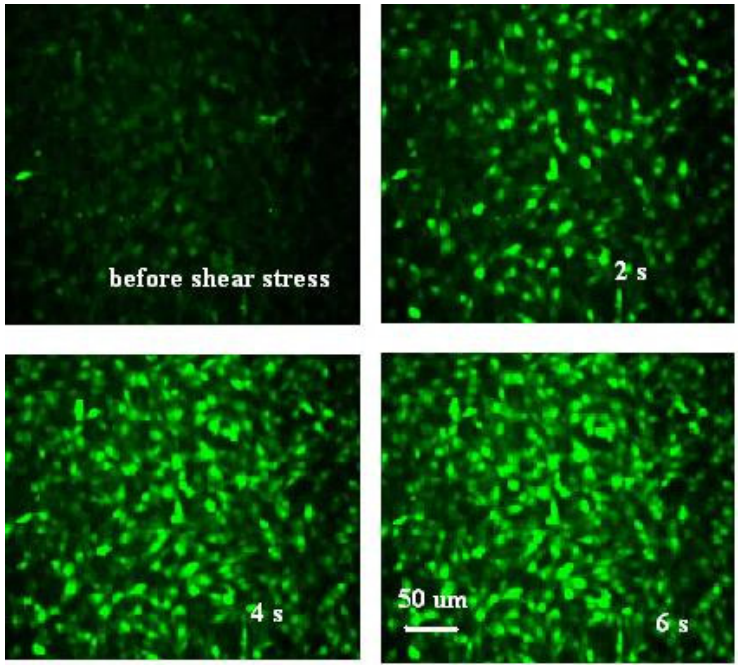

B:

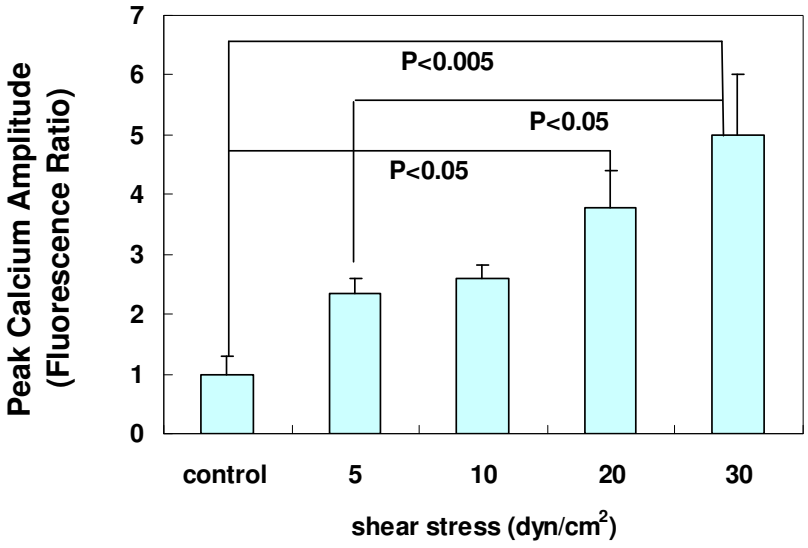

Fig.2.2. The $[Ca^{2+}]_i$ response to shear stress in BAECs. (A) Sequential images of Fluo3 fluorescence taken from BAECs at various times after onset of shear stress (τ=20 dyn/cm^2). Shear stress elicited a rapid, synchronous and relatively homogeneous calcium change in BAECs. The raw data shown here reflects variations in dye concentration, basal $[Ca^{2+}]_i$ level, and cell

morphology. The relative changes in $[Ca^{2+}]_i$ are indicated by the fluorescence ratio, which is insensitive to these variations. (B) Dose dependence of peak calcium amplitude on the magnitude of shear stress ($P<0.01$).

A:

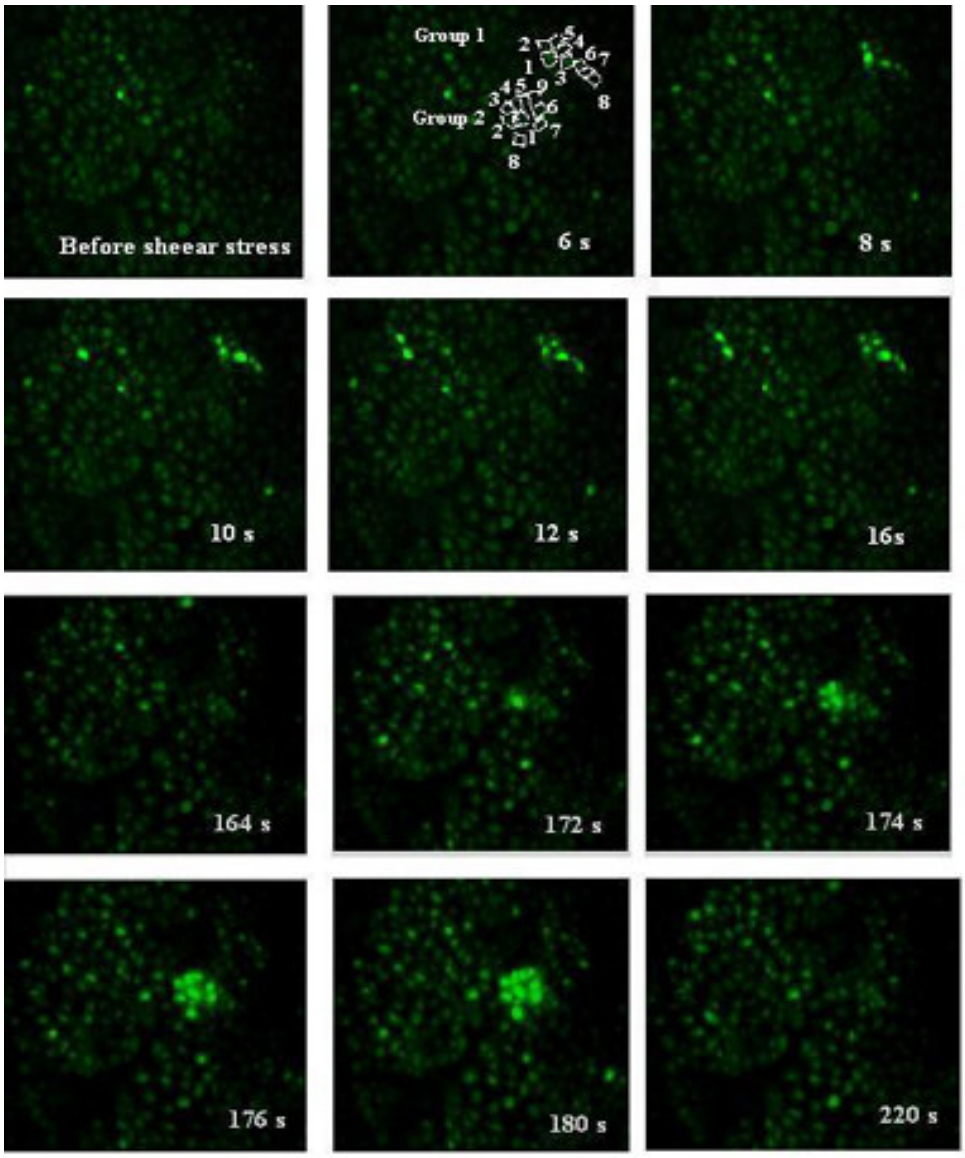
Group 1
Group 2
Before sheear stress
6 s
8 s
10 s
12 s
16s
164 s
172 s
174 s
176 s
180 s
220 s

B:

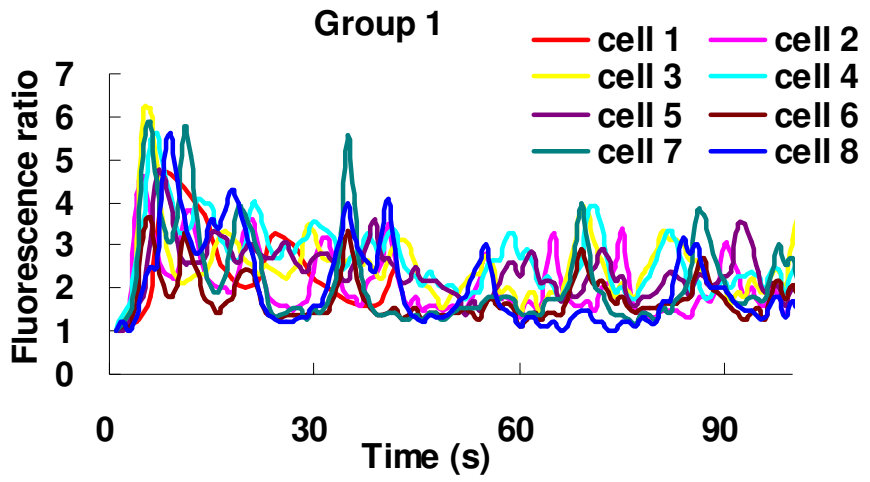

C:

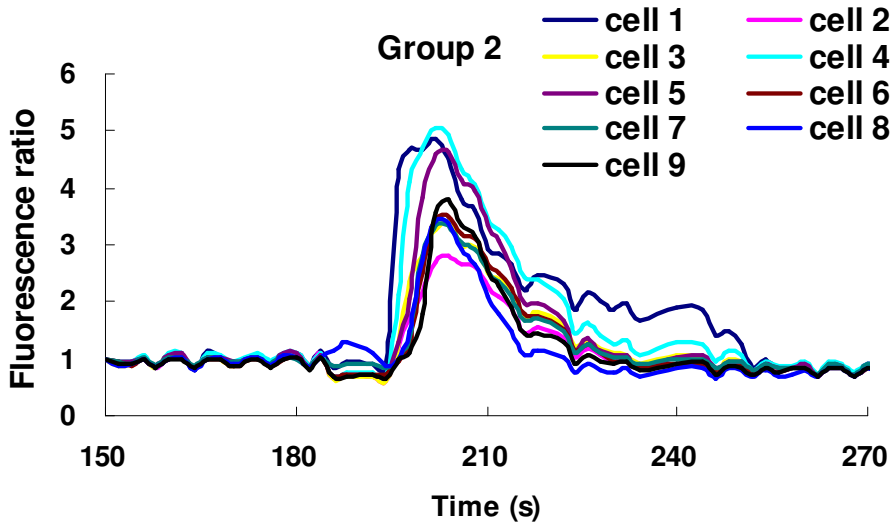

Fig.2.3. Shear stress-induced calcium wave in RAMECs. (A) Single frames of data are shown at various times after the onset of shear stress. The calcium wave was observed at cell group 1 and 2 at 16 s and 172 s respectively after shear stress initiation. In both of the groups, calcium waves started from one or several cells, then propagated to neighboring cells seconds later. (B) The time course of the normalized fluorescence amplitude of the cells indicated in group 1. The Ca^{2+} peak amplitude did not diminish during the calcium wave propagation. (C) The time course of the normalized fluorescence amplitude of the cells indicated in group 2.

A:

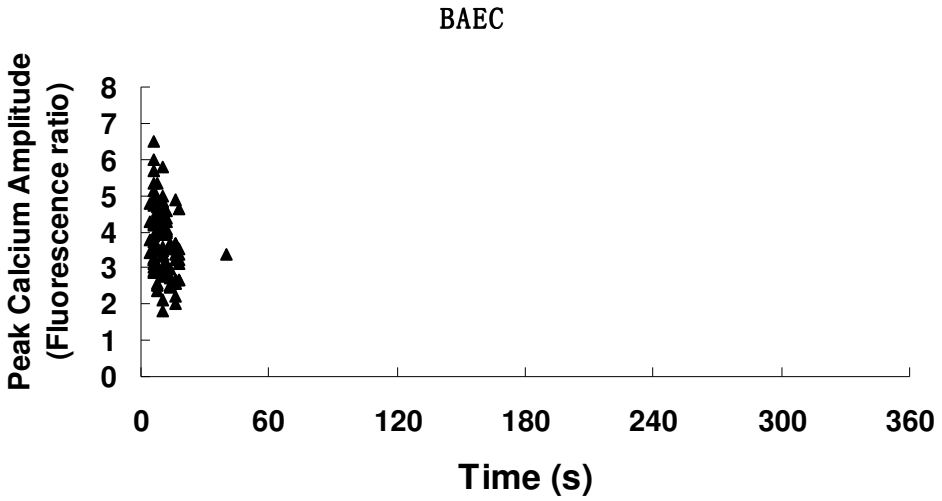

B:

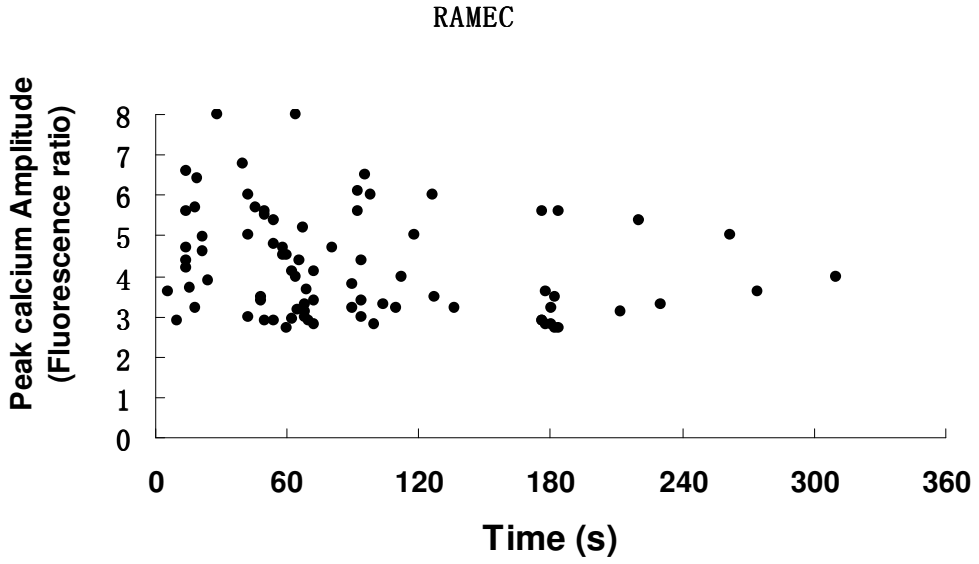

Fig.2.4 Scatter plots of the peak calcium amplitude vs time. (cells were exposed to 20 dyn/cm2 shear stress, 20 responding cells were selected at random from a single experiment, which was representative of 6 similar experiments).

A:

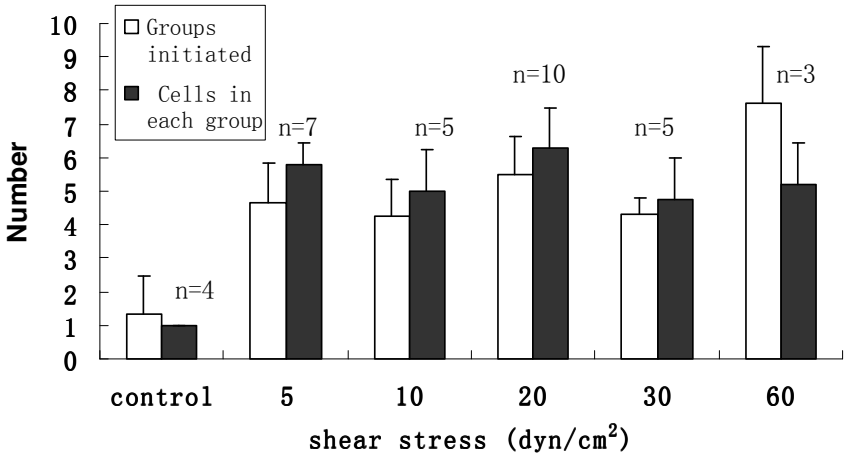

B:

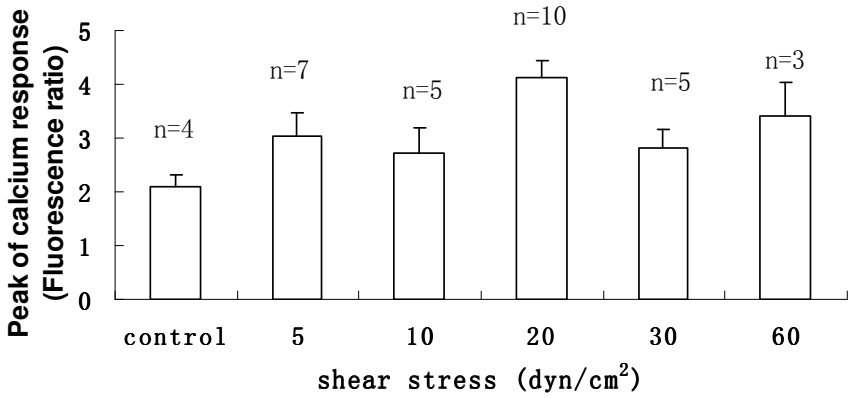

Fig. 2.5 Intercellular calcium wave features of RAMECs subjected to different levels of shear stress: A The number of $[Ca^{2+}]_i$ waves initiated within 5 min of the onset of shear stress and the average number of activated cells in each group were greater than controls ($p<0.05$) but not dependent of the level of shear stress ($p>0.1$). In static controls (no shear stress), occasional spontaneous $[Ca^{2+}]_i$ oscillations were observed. B. The magnitude of the $[Ca^{2+}]_i$ changes was not dependent on the level of shear stress. In controls, the amplitude of spontaneous $[Ca^{2+}]_i$ oscillations was not statistically different from the magnitude of the calcium changes under varying shear stress; however, there was no propagation of $[Ca^{2+}]_i$ waves to neighboring cells, so the variance of the cell group number is zero.

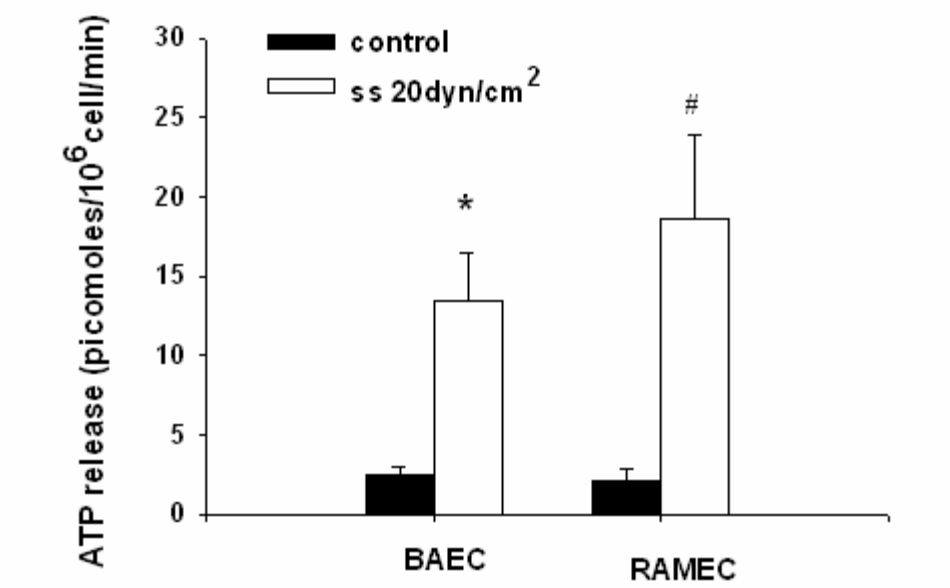

Fig. 2.6 ATP release from from endothelial cells under conditions of shear stress. The cells were subjected to a shear stress 20dyn/cm^2 or sham control for 5 mins and aliquots of bathing buffer were collected and assayed for ATP concentration. (* $p<0.005$, # $p<0.05$ compared with control)

A

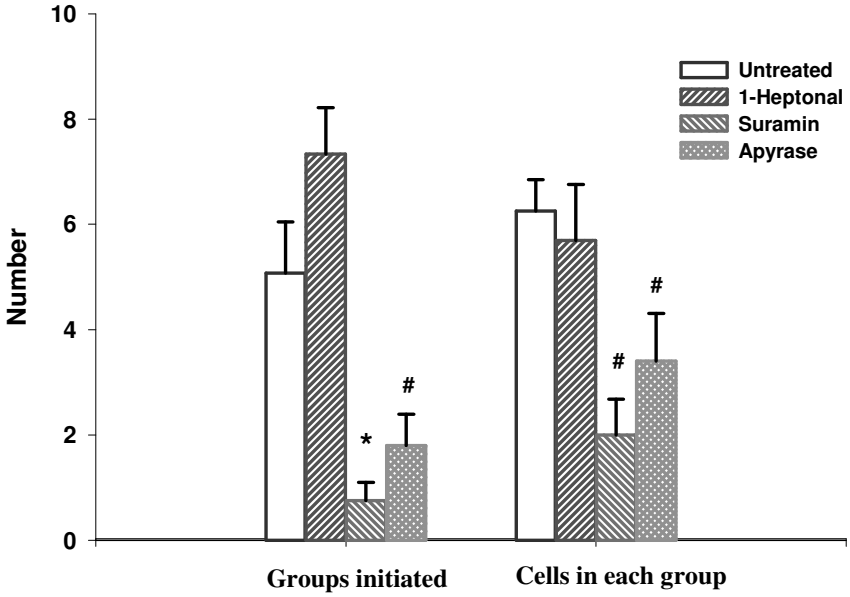

B

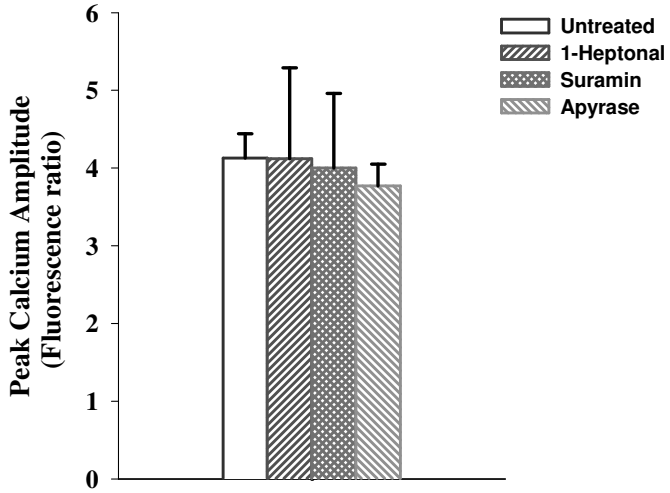

Fig.2.7 Effect of suramin, 1- heptanol and apyrase on flow induced $[Ca^{2+}]_i$ waves in RAMECs. (n=10 for untreated, n=8 for suramin pretreatment, n=10 for apyrase pretreatment, n=3 for 1-heptanol pretreatment, * $p < 0.01$ compared with untreated, # $p<0.01$ compared with untreated) A, Suramin and apyrase pretreatment significantly decreased both the initiation and propagation of shear stress induced Ca^{2+} wave, but 1-heptanol pretreatment did not inhibit the shear stress induced Ca^{2+} wave. B. Neither suramin, apyrase nor 1-heptanol pretreatment affected the peak $[Ca^{2+}]_i$ amplitude in responding cells.

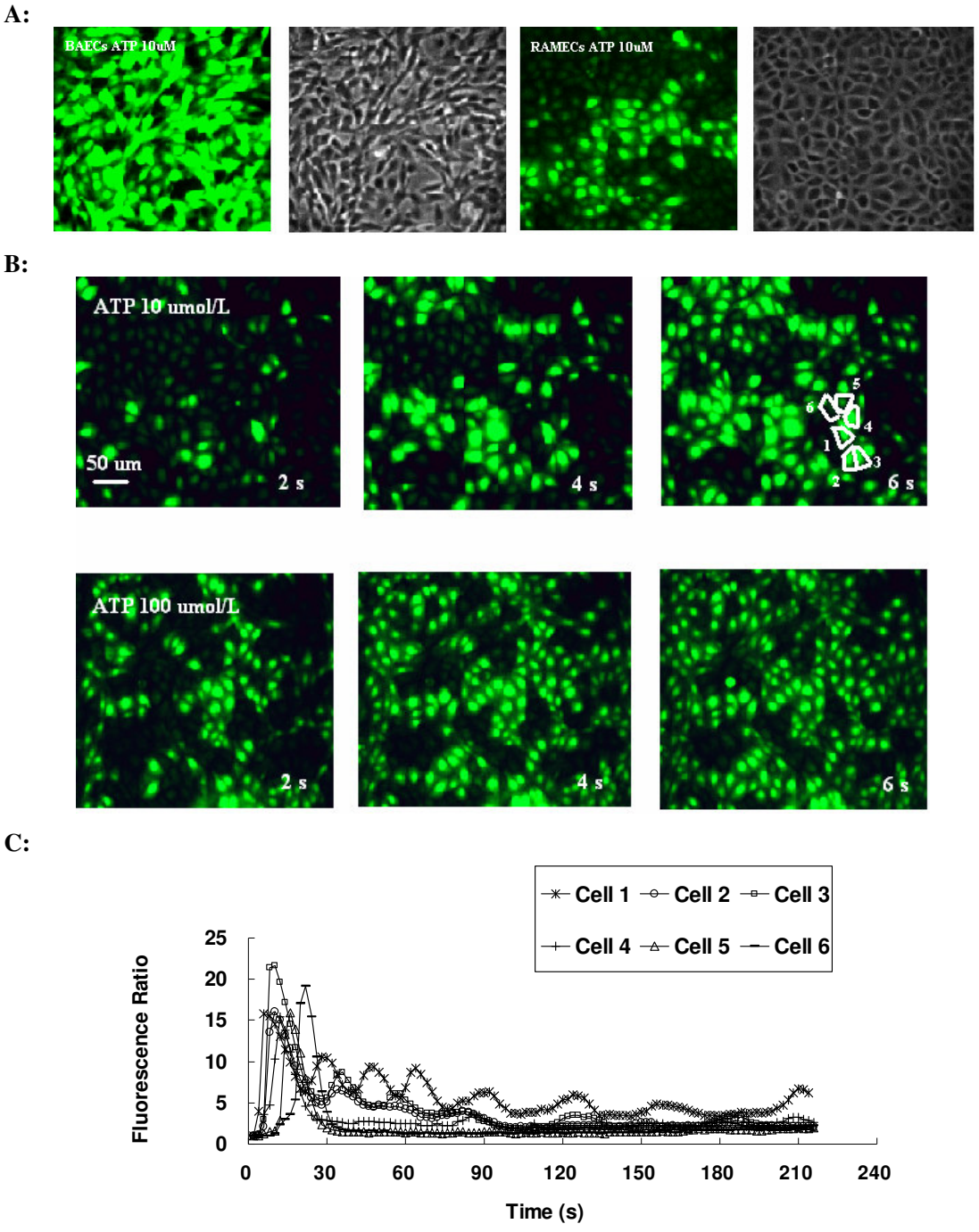

Fig. 2.8 ATP induced calcium response, BAECs vs. RMAECs A. 10μM ATP evoked synchronous $[Ca^{2+}]_i$ transients in BAECs and heterogeneous $[Ca^{2+}]_i$ response in RAMECs. B. The application of ATP to RAMECs elicited a rapid $[Ca^{2+}]_i$ response that was spatially and temporally heterogeneous. The addition of ATP immediately induced a $[Ca^{2+}]_i$ response in a subset of individual cells. The $[Ca^{2+}]_i$ increase then spread to adjacent cells. C. The temporal characteristics of the $[Ca^{2+}]_i$ changes elicited by ATP depended on the cell's position within the group. The initially responding cell exhibited sustained oscillations while more distant cells had a single transient.

A.

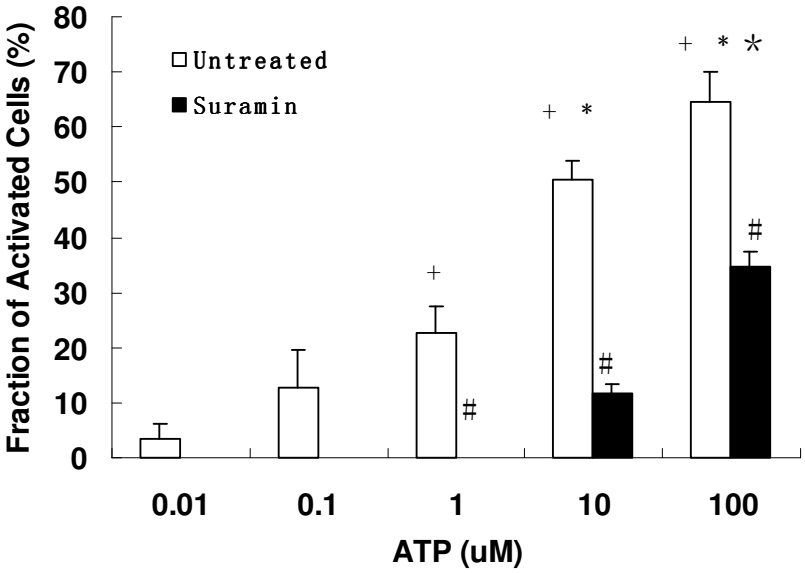
Fraction of Activated Cells (%)
80
70
60
50
40
30
20
10
0
Untreated
Suramin
+
+ *
+ * *
#
#
#
0.01
0.1
1
10
100
ATP (uM)

B.

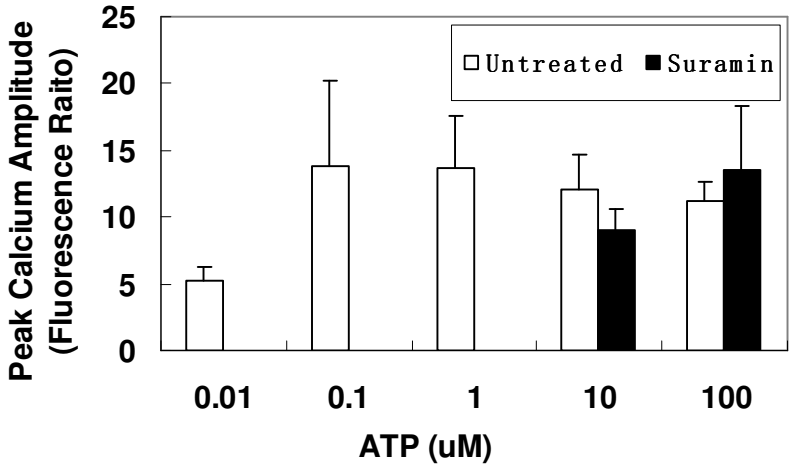
Peak Calcium Amplitude
(Fluorescence Raito)
25
20
15
10
5
0
Untreated
Suramin
0.01
0.1
1
10
100
ATP (uM)

C:

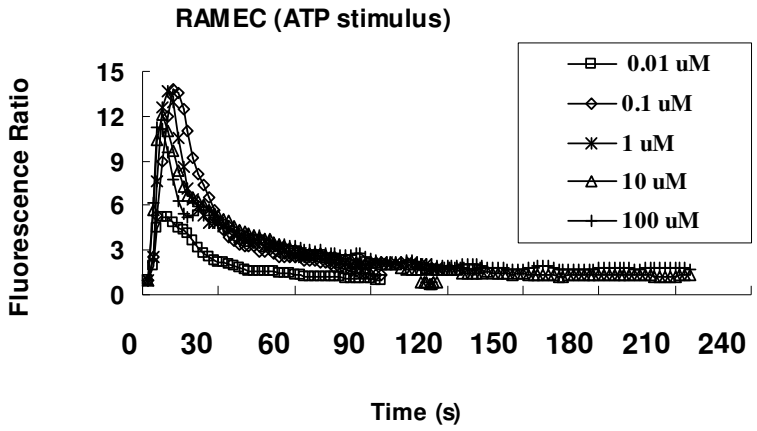

Fig.2.9 Dose-dependent effect of ATP on the $[Ca^{2+}]_i$ response in RAMECs and the effect of suramin pretreatment (n=7-8 for each group). A. The percentage of activated cells increased as a function of the ATP concentration (+ p<0.001 compared with 0.01 μM, * p <0.001 compared with 0.1 μM, ⋆P<0.005 compared with 1μM), and suramin pretreatment significantly reduced the fraction of activated cells (# P<0.01). B. The $[Ca^{2+}]_i$ amplitude was not dependent on ATP concentration in the range of 0.1 μmol/L to 100 μmol/L. Also, suramin pretreatment did not significantly affect the peak $[Ca^{2+}]_i$ amplitude in activated cells. C. The normalized fluorescence amplitude of activated cells over the time. Each trace shown is the average of 7~8 independent experiments. With suramin treatment, there were no activated cells at ATP concentration of 0.01-1 μmol/L.

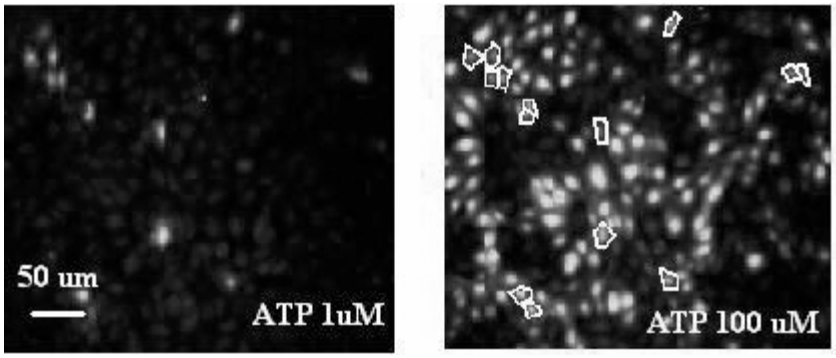

Fig.2.10 The Ca^{2+} response of RAMECs to sequential application of 1 μmol/L and 100 μmol/L ATP separated by 60s. 100 μmol/L ATP activated more cells than 1 μmol/L; however, all the cells that responded to 1 μmol/L ATP also responded to 100 μmol/L with similar Ca^{2+} peak amplitude (indicated by white outline).

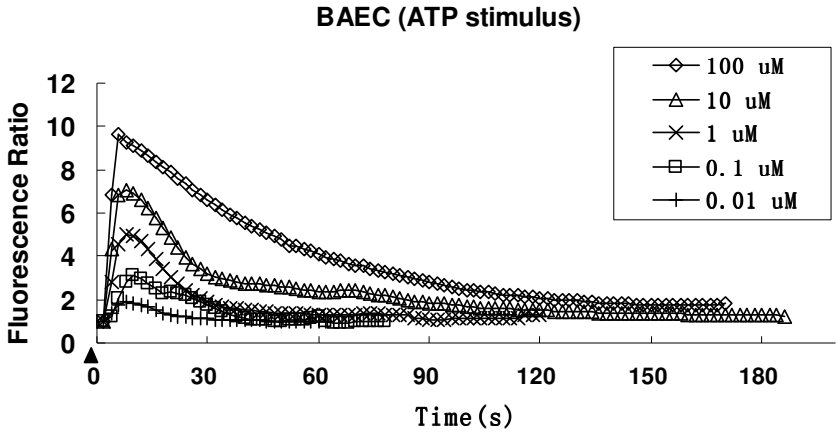

Fig.2.11 The time course of the normalized intracellular $[Ca^{2+}]_i$ response of BAECs subject to different concentrations of ATP. For BAECs, both the magnitude and duration of the response were dependent on ATP concentration. Each trace shown is the average of 6~8 independent experiments. Triangle indicates addition of ATP.

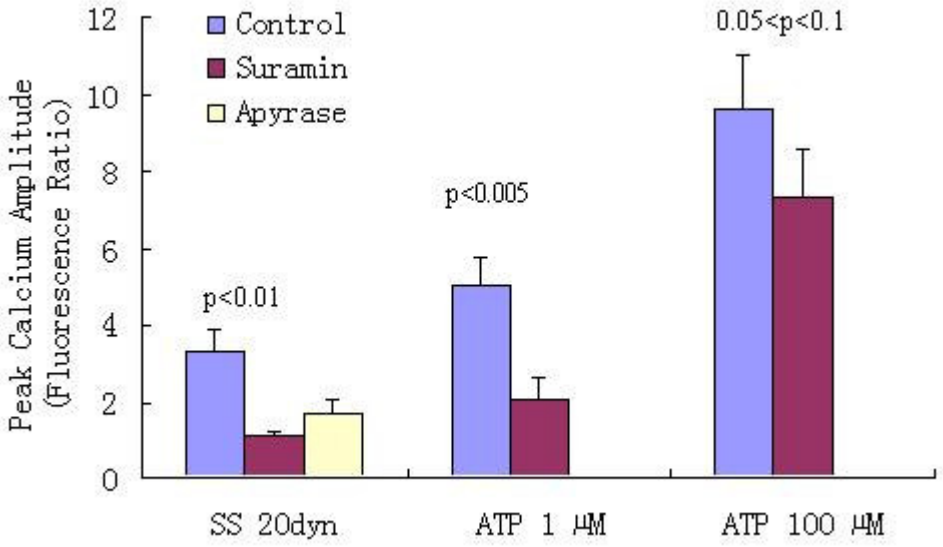

Fig 2.12 Effect of suramin on flow and ATP induced $[Ca^{2+}]_i$ responses in BAECs. (n=10 for shear stress control, n=7 for shear stress, suramin pretreatment, n=12 for ATP 1 μM, n=9 for ATP 1 μM, suramin pretreatment, n=11 for ATP 100μM, n=4 for ATP 100 μM, suramin pretreatment. Suramin pretreatment significantly decreased both the shear stress and ATP induced Ca^{2+} response.

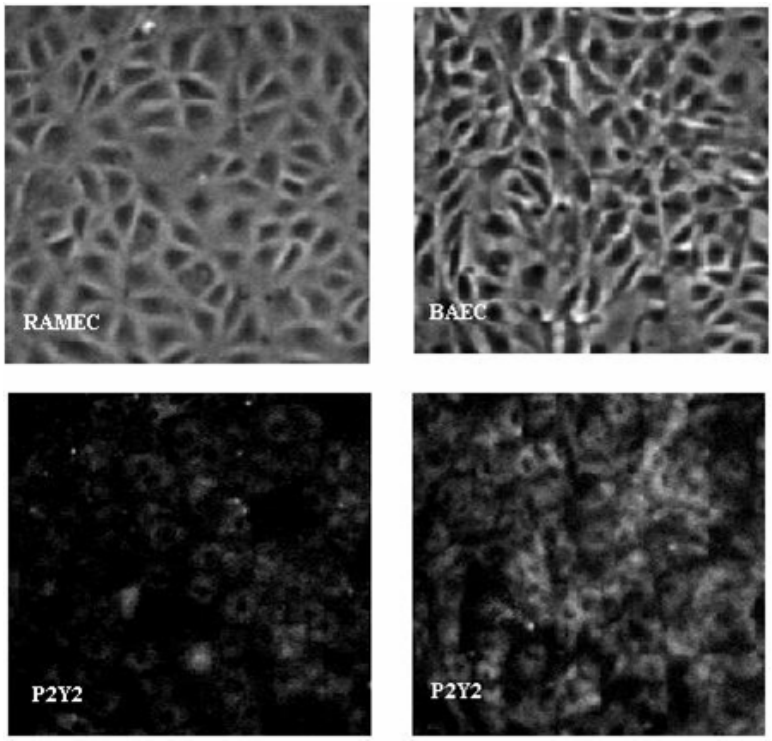

Fig.2.13 Expression of P_2Y_2 receptor on RAMECs and BAECs. P_2Y_2 receptor immunoreactivity was clearly present on the BAECs and the mean fluorescence intensity was significantly higher than RAMECs. Immunoreactivity for P_2Y_2 receptor in RAMECs was heterogeneous, with a few cells staining brightly and little or no staining in surrounding cells.

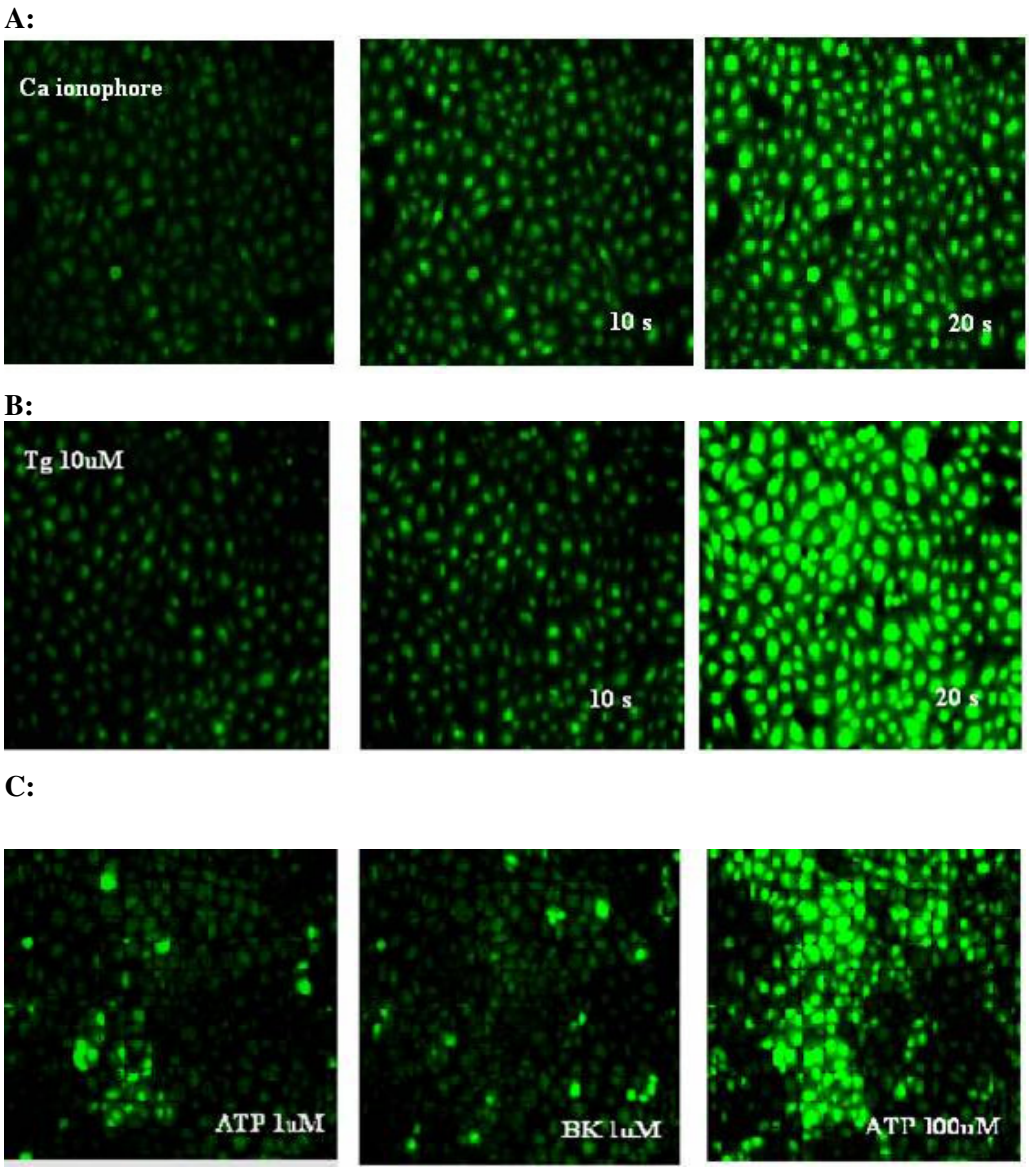

Fig.2.14 The calcium response of RAMECs to Ionphore, Tg, BK. A. Calcium ionophore A23187 induced synchronous and uniform calcium increase in all the RAMECs. B. Thapsigargin, IP3-independent intracellular calcium releaser, also increase $[Ca^{2+}]_i$ homogeneously in all the cells. C. RAMECs were stimulated with a first agonist—1μM ATP, and after the $[Ca^{2+}]_i$ returned to near basal levels, ATP was washed out and cells were challenged with a second agonist—Bradykinin 1μM. Then, the cells were stimulated with 100μM ATP. The results showed few cells responded to both 1μM ATP and 1μM bradykinin, however, for the activated cells, ATP and bradykinin were equipotent in the peak amplitude of the $[Ca^{2+}]_i$.

CHAPTER 3

Nitric Oxide Production Mediated by Endoplasmic Reticulum Liberation and Capacitative Calcium Entry in Response to Shear Stress and ATP stimulus

3.1 Introduction

Lying at the inner surface of blood vessels, the endothelial cells (ECs) are unique for their multi-functional nature. They function to modulate vascular tone, regulate immune responses, control blood coagulation states, adjust vascular permeability, and prompt angiogenesis and vessel repair(125). Most of these endothelial functions depend to various extents on changes in intracellular calcium concentration ($[Ca^{2+}]_i$). In respond to vasoactive aognists (ATP, Bradykinin etc.) and mechanical stimuli, endothelial cells elevate $[Ca^{2+}]_i$ transiently via release of Ca^{2+} from the endoplasmic reticulum through inositol 1,4,5-trisphosphate (IP_3)-sensitive release channels. The depletion of intracellular Ca^{2+} stores is followed by Ca^{2+} influx via calcium channels in the cell membrane. This influx is referred to as capacitative calcium entry (CCE), also called store operated calcium entry (SOC).

eNOS is regulated in a Ca^{2+} --calmodulin – dependent manner. While some reports suggest a correlation between the magnitude of the free calcium concentration and the isolated eNOS activity(20), others could not demonstrate such association in endothelial cells(74). Recent studies provided evidence that the source of calcium appears to be relevant for the efficient activation of eNOS. In the absence of extracellular calcium, NO production is greatly reduced. Several groups have shown that Ca^{2+} entering via CCE is the preferential source for eNOS activation(36, 74). NO also affects the Ca^{2+} signaling, by an autocrine action in ECs themselves(24, 36, 123). The aim of our study was to perform detail study to exam the role of Ca^{2+} in eNOS activity; the relationship between duration and magnitude of $[Ca^{2+}]_i$ load and NO production. We also address the communication between NO production and EC Ca^{2+}.

3.2 Materials and Methods

3.2.1 NO measurement:

Fluorescence Measurement: For direct intracellular nitric oxide (NO) measurement, BAECs were loaded with membrane-permeant DAF-FM diacetate (4-amino-5-methylamino-2'7'-difluorofluorescein diacetate, DAF-FM DA, Molecular Probes, Inc.) (10 μM) in PBS for 30 min at room temperature(134). DAF-FM is in preference to its predecessor DAF-2 since fluorescence from the NO-DAF-FM is influenced less by change in PH. In addition, DAF-FM is more sensitive to NO than that of DAF-2(67, 68). Cells were subsequently washed for three times. DAF-FM fluorescence was excited at 480nm. Emitted cellular fluorescence was recorded at 540nm. Changes in cellular DAF-FM fluorescence are normalized as F/F0, thus representing percentage increases above basal level.

NO electrode Measurement: The real time NO production was measured using carbon fiber electrodes (Carbostar-1, Kation Scientific)(126). The dimension of the electrode is shown in Fig 3.2 A. The tip of the electrode was coated with Nafion (5% wt dissolved in aliphatic alcohols, sigma) to eliminate the interference caused by active anions (e.g., nitrite, nitrate, and ascorbate)(139). The coating consisted of two individual processes. Each coating was applied by immersing the electrode tips into nafion solution for 10 mins and then drying at room temperature for at least 30 mins. After drying, a very thin membrane covered the electrode tips. The microelectrodes were polarized at +0.8V relative to an Ag/AgCl reference electrode. NO will be oxidized at the working electrode surface producing a redox current. This oxidation proceeds via an electrochemical reaction followed by a chemical reaction.(139). The electrochemical reaction is one electron transfer from the NO molecule to the electrode, resulting in a cation formation:

$$NO - e \rightarrow NO^+$$

In the presence of OH^-, NO^+ is further converted into nitrite:

$$NO^+ + OH^- \rightarrow HNO_2 \rightarrow H^+ + NO_2^-$$

Nitrite can then be further oxidized into nitrate. The amount of NO oxidation is thus proportional to the current flow between working and reference electrodes; the current was amplified with a picoammeter (Model 610; Keithley Instruments, Cleveland, OH)

Calibrations are carried out in PBS (PH=7.4) at room temperature. First, the system is bubbled with nitrogen for a period of 10-15 min until a stable zero electrode signal is obtained. NO gas is then bubbled through the deoxygenated solution for 5-10 min until a stable signal is obtained. The system is then purged with nitrogen to get the baseline again, drifts are corrected if necessary (Fig. 3.2 B). The linearity of the electrodes has been proved by Tsai et al..(126). The sensitivity of the electrodes is calculated using NO solubility of 1.876 mM at room temperature (25 °C) as shown in Fig. 3.2 C.

Cellular NO production measurement: BAECs are plated on coverslips and grown on 90% confluence. The cells are then bathed in Tris-HCL buffer. For simultaneous measurement of $[Ca^{2+}]_i$ and NO production in response to ATP, BAECs are loaded with calcium indicator Fluo3. NO electrode is placed as close as possible above the cells (less than 10uM). The total buffer volume in the bath is 2ml. A small bolus (1 ml) of ATP (150 μM, diluted in Tris buffer) is delivered topically in the solution through a tube near the measurement site (the total delivery time is 10 s). The current response is continuously measured after addition of ATP. The response in picoamperes is converted to NO concentration based on the calibration for each microsensor. Between experiments, the electrodes are recalibrated. The tips are cleaned and new Nafion membranes are applied whenever necessary.

3.2.2 Chemicals and reagents:

The Dulbecco's phosphate buffered saline (DPBS), nucleotides adenosine triphosphate (ATP), and EGTA, were purchased from Sigma. Normal donkey serum was purchased from Jackson Immuno Research (West Grove, PA, USA). The Fluo3-acetoxymethyl ester, DAF-FM-DA were obtained from Molecular Probes, Inc.. Tris-HCL buffer contained 25mM Tris/Tris-HCL, 137mM NaCl, 2.7mM KCl, 1mM $MgCl_2$, 4mM $CaCl_2$ was utilized. The Ca^{2+}-free buffer consisted of Tris-HCL buffer solution in which $CaCl_2$ was replaced with EGTA (1mM).

3.3 Results:

3.3.1 Use of DAF-FM to measure NO

Because NO does not dissociate from DAF-FM (D) once this dye reacts with NO, the NO sensitive fluorescence with DAF primarily represents a cumulative amount of NO within the cells. An obvious disadvantage of this method for real time NO measurement is that the fluorescence curve does not represent the actual NO concentration. The formation of the DAF-FM fluorescence complex (NOD) can be described by a process:

$$NOD \Leftrightarrow NO + D$$

The DAF-FM fluorescence intensity will change in response to the binding of and unbinding of NO as described by

$$\frac{d[NOD]}{dt} = k_{on}[NO][D] - k_{off}[NOD]$$

Since NO does not dissociate with DAF-FM once they bind, $k_{off} = 0$ and then

$$\frac{d[NOD]}{dt} = k_{on}[NO][D]$$

Since [D] is much larger than [NO], and thus can be considered as constant. Therefore, the concentration of NO is proportional to the time derivative of the fluorescence intensity ($d(F/F_0)/dt$). To more representatively show the features of NO-DAF fluorescence and to accurately present the NO-DAF-FM fluorescence and cellular NO production, we perform experiments to determine the fluorescence kinetics of DAF-FM. The results are shown in Fig. 3.1 A and B.

To confirm that intracellular DAF-FM indeed sensed NO and determine the fluorescence kinetics, cells loaded with 10 μM DAF-FM were treated with saline equilibrated with NO (3.6 μM). As shown in Fig.3.1 A, exogenous NO led to a robust increase in DAF-FM fluorescence. After exposure to exogenous NO, the DAF-FM F/F_0 signal rate increased significantly in the first 5 min ($d(F/F_0)/dt = 0.156\ min^{-1}$; n=5), then it reduced to 0.096 min^{-1} , which was due to the short life time of NO (the reaction of NO with oxygen explains for the NO decay).

In order to determine the kinetics of DAF-FM, further investigations were carried out with a brief exposure to exogenous NO (less than 1 min), and then, the NO solution was removed and replaced with PBS. When the cells were exposed to NO solution, the DAF-FM signal increased significantly with a rate $d(F/F_0)/dt = 0.196\ min^{-1}$, which is similar with initial fluorescence rise as shown in Fig. 3.1 A . After exogenous NO was removed, the rate of F/F_0 decreased to ($d(F/F_0)/dt = 0.04\ min^{-1}$) (Fig. 3.1 B).

3.3.2 Effect of extracellular calcium on shear stimulated calcium response

As shown in Fig. 3.3 A, when BAECs were perfused in PBS, which contained 0.9mM Ca^{2+} ion, a step increase in shear stress from 0 to 20dyn/cm^2 to cells monolayers resulted in a

transient increase in $[Ca^{2+}]_i$ attaining peak amplitude in 30 s, then followed by a sustained plateau which decayed slowly to near baseline after 5 min. Elimination of extracellular Ca^{2+} with EGTA did not have effect on the initial calcium peak rise time and the peak amplitude. However, the $[Ca^{2+}]_i$ plateau was significantly reduced by the extracellular calcium removal.

3.3.3 Ca^{2+} dependence of shear stress-stimulated NO production

When BAECs were grown on coverslip and subjected to a step increase in flow-mediated shear stress from 0 to 20 dyn/cm^2 in PBS with calcium and without serum, as shown in Fig.3.3 B, the DAF-FM signal increased with an average rate $d(F/F_0)/dt = 0.041$ min^{-1} in the first five min and rise of $d(F/F_0)/dt$ slows down after 10 min, remaining rate of increase at 0.023 min^{-1}, which reflecting a decrease in endogenous NO production. To assess the importance of calcium in shear stress-stimulated NO production, BAECs were exposed to a step increase in flow in calcium free buffer with 1mM EGTA. Fig.3.3 B shows that when cells were perfused in solution containing zero Ca^{2+} and 1mM EGTA, shear stress still elicited a $[Ca^{2+}]_i$ transient of similar amplitude(Fig; compared to Fig.). However, despite the large rise in $[Ca^{2+}]_i$, the increase of DAF-FM signal in the first five min was significantly lower in the absence of extracellular calcium $d(F/F_0)/dt = 0.018$ min^{-1} compared with. $d(F/F_0)/dt = 0.041$ min^{-1} in the presence of calcium. The slight decrease in DAF-FM signal in control trace indicates photo bleaching occurred during the recording periods.

3.3.4 ATP induced increase of $[Ca^{2+}]_i$

To understand the relationships between Ca^{2+} and NO production in endothelial cells, we stimulated BAECs with exogenous ATP. Exposure of BAECs to ATP (50 μM), prepared with Tris-HCL buffer, in the presence of extracellular Ca^{2+} (4 mM) induced a typical biphasic $[Ca^{2+}]_i$ response. ATP elicits Ca^{2+} response consisted of a rapid transient $[Ca^{2+}]_i$ spike,

followed by a subsequent prolonged elevation in $[Ca^{2+}]_i$ that although higher than prestimulus level, is lower than the initial peak, as shown in Fig3. In Ca^{2+} -free PBS supplemented with 1mM EGTA, ATP stimulation induced a calcium spike, the calcium then decreased to below baseline levels. The amplitude of Ca^{2+} increase is similar with or without extracellular Ca^{2+}.

3.3.5 NO electrode measurement of ATP induced NO production

NO release was measured directly from the cell surface by placing an NO electrode close to cell surface. $[Ca^{2+}]_i$ change was measured with fluorescent indicator fluo3 simultaneously. The calcium response to ATP in the presence and absence of extracellular Ca^{2+} has been described above and shown in Fig.3.4 A. A representative NO response is shown in Fig.3.4 B. In the position (< 10μm from the endothelial surface), increase in NO was detected 30 seconds following the addition of ATP to the bath. The NO concentration increased gradually and reached its peak after 90 second. After that, NO decayed slowly and reached the baseline level after 5 mins. Although the amplitude of Ca^{2+} increase is similar with or without extracellular Ca^{2+}, the NO production in Ca^{2+} free medium is significantly lower than in Ca^{2+}rich medium (Fig. 3.4 C). This indicates that the calcium influx (mainly CCE) might be more proficient in activating eNOS than that the Ca^{2+} released from ER. The rise of NO lagged behind the peak of the $[Ca^{2+}]$, which further suggested the capacitative Ca^{2+} could be the preferential source for eNOS activation. After pretreated with L_NAME, the NO production is significantly attenuated.

3.3.6 Effect of NO on capacitative Ca^{2+} entry

We inhibited the endothelial NO production by preincubated the ECs with 1mM L_NAME and measured the effect of endogenous NO on calcium response. Endothelial cells were stimulated with ATP in the presence of Ca^{2+} (4mM) and the change in $[Ca^{2+}]_i$ in single

cell was measured in cells loaded with fluo-3. As shown in Fig.3.4 A, with NO production inhibited, the Ca^{2+} sustained phase mildly potentiated.

3.3.7 ATP induced ER Ca^{2+} release and capacitative Ca^{2+} entry for NO production

The application of ATP to BAECs in the presence of extracellular Ca^{2+} elicits the overlap Ca^{2+} response from ER release and CCE. The following experimental protocol was applied so that we can separate ER Ca^{2+} release from CCE entry. First, cells were exposed to 50μM ATP in the absence of external Ca^{2+} (PBS supplemented with 1mM EGTA). As shown in Fig.3.5A, treatment with ATP lead to a transient increase in $[Ca^{2+}]_i$ due to calcium release from ER, reaching a peak after 5-10 seconds and returning to the basal level within 1-2 mins. Subsequent exposure to 4mM extracellular Ca^{2+} resulted in a rapid and sustained $[Ca^{2+}]_i$ elevation, which under these conditions reflects Ca^{2+} influx through CCE pathway (Fig.3.5A). Compared to the IP_3 mediated ER release, capacitative entry of calcium increases plateau level but has lower magnitude peak. Preincubation with intracellular Ca^{2+} chelator BAPTA-AM (30μM, 30 min) significantly inhibited $[Ca^{2+}]_i$ increase from ER store release as well as CCE entry. BAPTA reduced the $[Ca^{2+}]_i$ amplitude from ER release by 31.4% and from CCE entry by 38.1% (Fig.3.5 A, Fig. 3.5 C).

For BAECs with Ca^{2+} -free medium, ER Ca^{2+} stores was depleted by ATP stimulus. Transient increase in $[Ca^{2+}]_i$ by ER depletion caused only slight increase in NO production ($d(F/F_0)/dt$ = 0.0239 min^{-1} in the first 3 min)as shown in Fig.3.5B. Subsequent addition of 4mM extracellular led to a sustained $[Ca^{2+}]_i$ increase, resulting from CCE pathway. In contrast, there is a large increase in NO production detected during CCE entry ($d(F/F_0)/dt$ = 0.0819 min^{-1} in the first 3 min), even though the calcium magnitude from calcium entry is significantly lower than from calcium liberated from intracellular store. Pre-incubation with BAPTA-AM

significantly decreased NO concentration by both calcium sources, but decreased NO concentration by ER release to a greater extent than that of CCE entry (82% reduction by ER release vs. 46% reduction by CCE entry) (Fig. 3.5 B, Fig. 3.5D).

Endothelial NO production may depend not only on the magnitude of calcium peak, but also the time course of calcium rise. To allow for the fact that NO release is also a function of Ca^{2+} elevation duration, the Ca^{2+} -time-index (CTI), a measure of total Ca^{2+} load over time, was determined. CTI was calculcated by integrating spatial average $[Ca^{2+}]_i$ over time (3 min). Fig. illustrates that the calcium load by CCE entry as determined by CTI in the first 3 min after addition of extracellular calcium is only 1.425 times the ER calcium liberation, nevertheless, the CCE induced NO production indicated by $d(F/F_0)/dt$ is 3.43 times that induced by ER calcium release (Fig. 3.5E).

3.4 Discussion:

NO production in the endothelial cells in response to shear stress or agonists mediated by eNOS is an important vasoactive compound. Loss of endothelial function, particularly impair in NO production, has been implicated in a number of cardiovascular diseases, including hypertension, coronary artery disease, and chronic heart failure(75, 83, 99). The mechanisms of eNOS activity have been intensively investigated. It is generally believed that calcium plays a key role in regulation of eNOS activity and endothelial NO production is usually preceded by increase in $[Ca^{2+}]_i$(45). A close correlation has been shown to exist between the rise in endothelial cell $[Ca^{2+}]_i$ and the cGMP level(69). However, the evidence to support this idea is controversial and the relationship between NO production and measured $[Ca^{2+}]_i$ was uncovered. eNOS can also be activated by certain stimuli like shear stress without a sustained increase in $[Ca^{2+}]_i$.(89)

We showed that application of shear stress to BAEC monolayers resulted in a transient increase in $[Ca^{2+}]_i$, attaining peak amplitude in 15-30 s, then followed by a sustained plateau which decays slowly to near baseline after 5 min. The elimination of extracellular Ca^{2+} with EGTA does not diminish the calcium peak. However, the $[Ca^{2+}]_i$ plateau is significantly reduced by the removal of extracellular calcium. Therefore, the $[Ca^{2+}]_i$ plateau is due to the influx of extracellular calcium. We also use DAF-FM to measure shear stress stimulated NO production by endothelial cells and provide observations about the influence of Ca^{2+} on shear induced NO synthesis. As shown in Fig.3.3 A and B, despite the peak calcium transient remains the same for flow mediated shear stress in calcium containing buffer and calcium free buffer, the initial phase of stress-stimulated NO production is significantly inhibited by extracellular calcium removal. Our results confirmed that NO release stimulated by shear stress exhibits some calcium dependence, which is consist with other's report that shear stress stimulated biophasic NO release. The first phase of NO release is transient and Ca^{2+} dependent (70). We further compare the plateau cytosolic calcium concentration in response to shear stress and observed the spatial average plateau calcium concentration in the presence of calcium concentration is 1.2 times than in the absence of calcium. Nevertheless, the increase in the slope of DAF fluorescence in calcium containing buffer is twice of that in the calcium free solution. Since the calcium plateau is maintained by extracellular calcium influx, which indicates that the Ca^{2+} influx might be more effective in activating eNOS that the Ca^{2+} released from intracellular stores.

Our study demonstrates that exposure of BAECs to fluid flow induces ATP release, and fluid shear stress mediated intracellular calcium concentration increase is via ATP signaling. We want to confirm that our observations in NO production by shear stimulated BAECs were mirrored in ATP mediated NO release. Furthermore, shear stress might also evoke a rise in NO production independently of calcium; however NO generation activated by agonists is highly

calcium dependent(89, 129). Fig.3.4 A shows that exogenously applied ATP produced a pattern of calcium responses in BAECs that was similar to the shear stress response. The simultaneous measurements of $[Ca^{2+}]_i$ and NO concentration in response to ATP indicate the rise of NO lag behind the peak $[Ca^{2+}]_i$(Fig. 3.4 B). The NO concentration rises and reaches the peak during the plateau phase of ATP-induced $[Ca^{2+}]_i$ transient and the $[Ca^{2+}]_i$ plateau is maintained due to extracellular Ca^{2+} influx instead of internal stores release. To further distinguish between the ER release calcium versus extracellular calcium influx to activate NO production, we stimulate ECs with ATP in the absence of extracellular calcium. The transient elevations of $[Ca^{2+}]_i$ in the calcium free buffer are the result of liberation of calcium from intracellular calicum stores, mainly ER. Subsequent exposure to 4 mM extracellular Ca^{2+} resulted in a rapid and sustained $[Ca^{2+}]_i$ elevation, which under these conditions mainly reflects Ca^{2+} influx through CCE pathway since CCE is the predominate source of agonist-regulated Ca^{2+} entry into endothelial cells(55). As shown in Fig.3.5A, fluorescence measurements showed that the Ca^{2+} peak amplitude induced by IP_3-mediated ER store release is significantly higher than CCE entry in the presence of 4mM external calcium. However, the NO production increases dramatically during the CCE entry (Fig.3.5 B). A similar dissociation between peak $[Ca^{2+}]_i$ and NO production also has been observed in shear stress-stimulated endothelial cells. Even we considered the duration of calcium challenge--CTI, the simple linear relationships were inadequate to describe a relationship between $[Ca^{2+}]_i$ measurement and NO generation. This confirms that the greater NO production via CCE compared with others is not due to the ability of CCE to trigger greater elevations in $[Ca^{2+}]_i$. Our data also demonstrate that NO production are not only dependent on a large rise in $[Ca^{2+}]_i$, but also on calcium source; and point to that CCE may be the most significant source for eNOS activity.

The second phase of shear stress induced NO production has been stated to be continuous and Ca^{2+} independent. Our results support this statement by showing that the endothelial NO

production in response to shear stress in the absence of extracellular calcium is significantly higher than control even after intracellular $[Ca^{2+}]_i$ goes below the baseline(Fig.3.3A). This could occur because the C-terminal region of eNOS contains a conserved serine (Ser^{1177}) with a kinase-dependent phosphorylation motif. Although the molecular events that determine eNOS activity in response to fluid shear stress are not fully understood, it has generally believed that eNOS could be phosphorylated in response to shear stress and phosphorylation has been suggested to affect enzyme activity by reducing calcium dependence to eNOS and trigger eNOS activation at a lower Ca^{2+} concentration(25).

Ca^{2+} plays a key role in the regulation of endothelial NO release. This raises the question of whether endothelial NO also influences Ca^{2+} regulation in endothelial cells, thus exerts autocrine regulation of its own synthesis. There are indeed evidences reveal NO has the capability of influencing calcium homeostasis in endothelial cells, however the effects of NO on calcium regulation remain controversial and inconclusive. It was shown that NO release in the form of SNP could stimulate Ca^{2+} influx in porcine aortic endothelial cells by Berkels et al(10). In contrast, it has been shown brief exposure to SNP lowers $[Ca^{2+}]_i$ by inhibition of CCE and acceleration of reuptake of Ca^{2+} into intracellular stores via cGMP-dependent pathway(36). There is also evidence that NO can enhance PMCA extrusion of calcium, however potentiate CCE(24). Our studies show after ATP stimulation, endogenous NO is release. If NO production is inhibited by L_NAME treatment, the Ca^{2+} sustained phase is mildly enhanced (Fig.3.4A). This discrepancy may be due to the concentration dependence of the NO effect on the calcium homeostasis in endothelial cells.

We and others have shown that simple linear relationships were inadequate to describe the regulation of eNOS activity by measured $[Ca^{2+}]_i$ (60, 74). However, Bredt and Snyder demonstrated that within the physiological range of calcium concentration (0.1-5mM), the

isolated eNOS activity increases linearly with Ca concentration(20). Given this controversy, a link between $[Ca^{2+}]_i$ and eNOS activity needs further investigation and one possible reason is calcium channels and calcium sensors are not uniformly distributed in the cell, the calcium comes from different sources has different proportional contributions from critical Ca^{2+} compartements. The possible reason that eNOS is more sensitive to CCE calcium entry than to calcium elevation via ER release has been proposed is that for endothelial cells, eNOS is associated with the plasma membrane caveolae and it has been shown that CCE channels also locate in caveolae domain. The colocalization of CCE channels and eNOS in caveolae microdomains facilitates their interaction. Thus, given equal increase in total measured $[Ca^{2+}]_i$, ER calcium release evoke a less contribution to the calcium concentration in the caveolae domain. Ca^{2+} from ER release diffuses from IP_3 channels reaches the vicinity of caveoloa domain where eNOS resides at insufficient concentrations to trigger eNOS activity, which makes eNOS activity is preferentially associated with CCE. To test this hyothesis, we incubated the cells with intracellular calcium chelator BAPTA-AM. Since BAPTA is unable to immediatedly access and chelate the calcium entering the cytosol through Ca^{2+} influx channels, we expect that CCE stimulated eNOS activity will be relatively less affected by BAPTA compared to that of ER calcium liberation. As shown in Fig.3.5 A and B, pre-incubation with BAPTA-AM decreased NO concentration by both calcium sources, but decreased NO concentration by ER release to a greater extent than that of CCE entry (82% reduction by ER release vs. 46% reduction by CCE entry) even though BAPTA reduced comparable $[Ca^{2+}]_i$ amplitude by ER release and CCE (34.1% vs. 38.1%).

In summary, we show that ATP-mediate NO production in endothelial cells is dependent on the influx of calcium from CCE channels. Shear stress increases endothelial NO production through both calcium dependent and calcium independent way. Our study suggests that calcium influx is an important determinant of NO production stimulated by shear stress and

ATP. Nevertheless, a close correlation does not show that magnitude of the Ca^{2+} elevation, or the measure of total Ca^{2+} load over time - Ca^{2+} -time-index (CTI), determines eNOS activity. eNOS is more sensitive to CCE than any other calcium sources. One explanation is that CCE channels and sensors are strategically distributed on the cell membrane and the localized calcium concentration at the site of eNOS resides rather than the global intracellular calcium concentration $[Ca^{2+}]_i$ regulate endothelial NO production. These results force us to investigate more subtle and quantitative methods to evaluate the effects of spatial colocalization of eNOS and capacitive calcium entry (CCE) channels in caveolae on eNOS activiation in response to shear stress and ATP.

A:

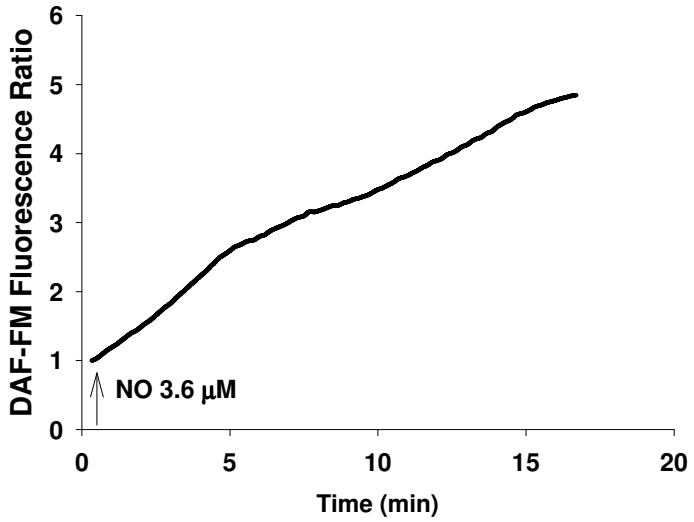

B:

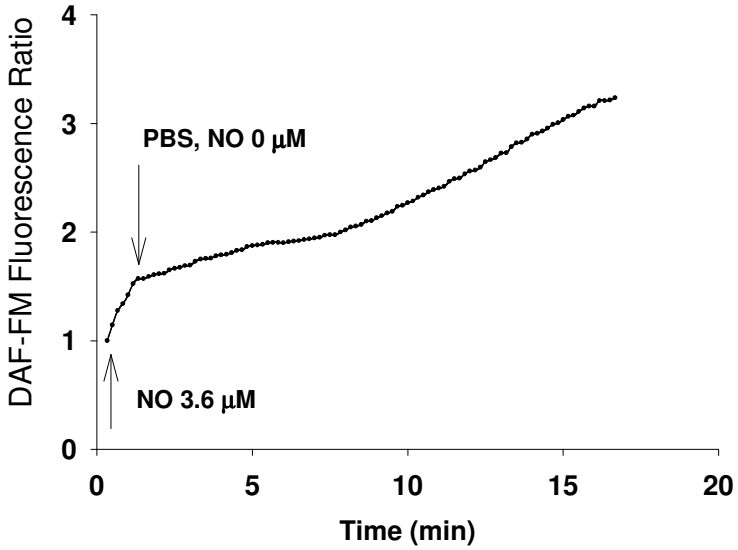

Fig 3.1 Effect of exogenous NO induced DAF-FM fluorescence elevation. A. Cells were loaded with 10uM DAF-FM DA exposed to NO solution (3.6uM) as indicated. B. Cells were exposed to 3.6uM NO solution for 1 min and then NO solution was removed and replaced with fresh PBS.

A.

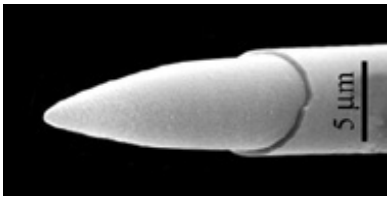

B.

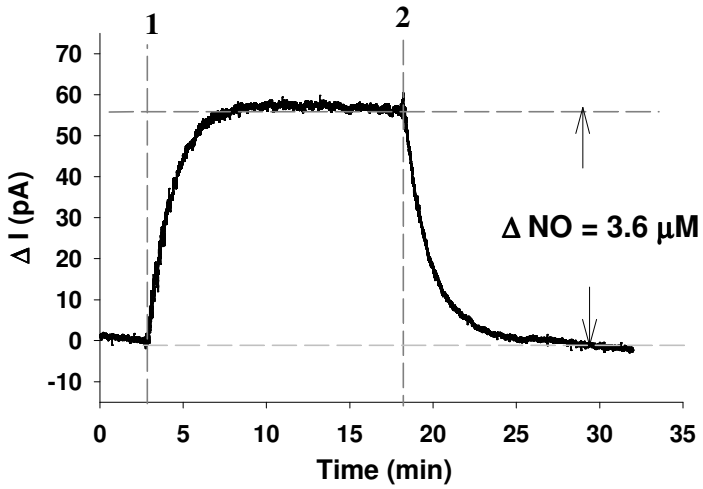

C.

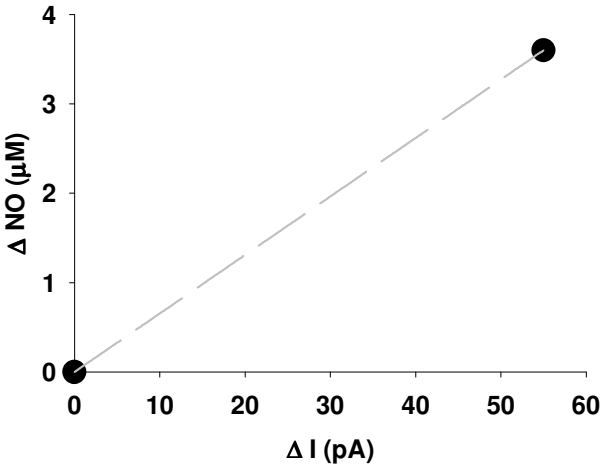

Fig 3.2 Calibration of nitric oxide (NO) electrode. A: Dimensions of the carbon fiber microelectrode. (from http://www.kationscientific.com/fmicroelectrodes.html?cs1) B: Typical

calibration curve for the electrode coated with Nafion. The curve was obtained at nitric oxide concentration 2000PPM at room temperature. The buffer was initially bubbled with N_2 until it saturated (indicated at position **1**). A known NO concentration gas (2000PPM) was then bubbled until saturated (indicated at position **2**). Then, the system was purged with nitrogen to get the baseline again. C: The difference between the two values was then used to calibrate the electrode.

A:

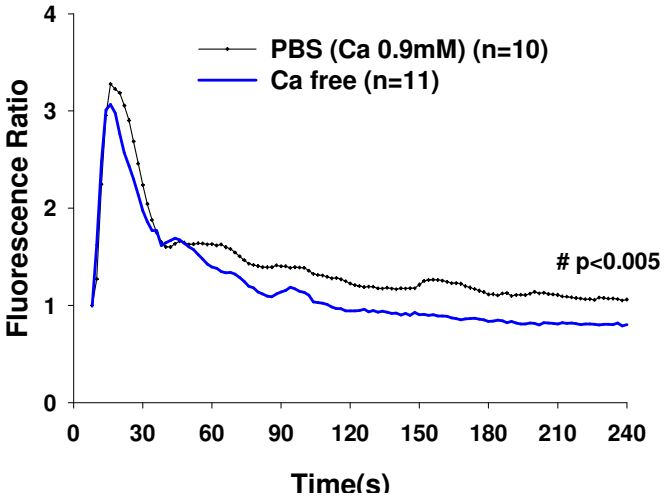

B:

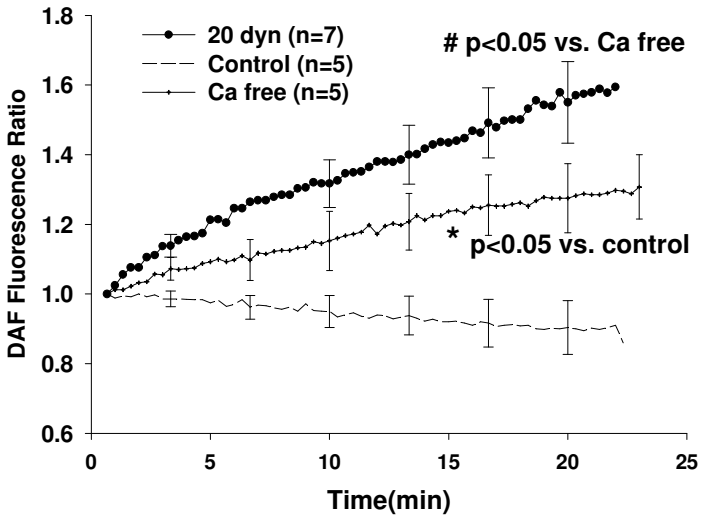

Fig.3.3 Effect of extracellular Ca^{2+} removal (calcium free + 1mM EGTA) on the endothelial calcium and nitric oxide response to shear stress in BAECs. A. Elimination of extracellular Ca^{2+} does not have effect on the initial calcium peak amplitude. However, the $[Ca^{2+}]_i$ plateau is significantly reduced by the extracellular calcium removal. B. Shear stress stimulus (20 dyn/cm^2) significantly increased NO production and the NO production was partly inhibited when calcium was removed from perfusion medium. ($p< 0.05$ vs. Ca^{2+} free)

A:

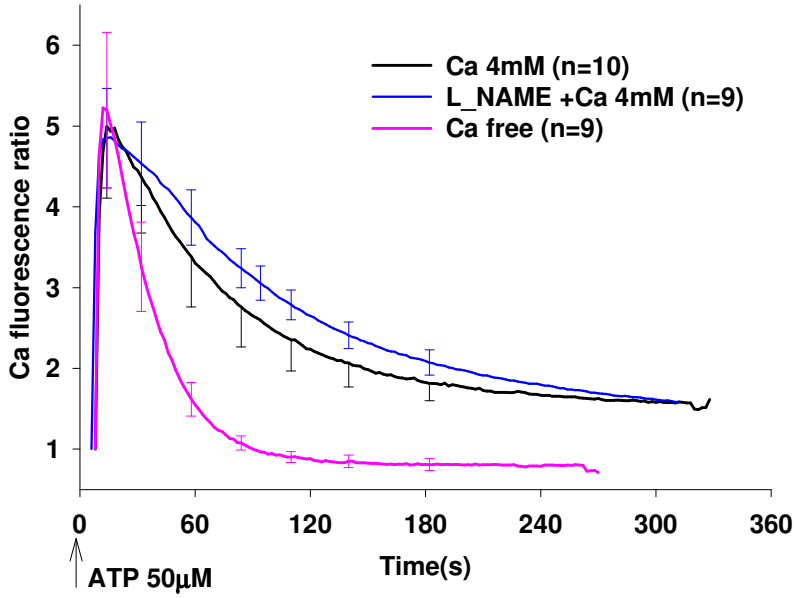
Ca 4mM (n=10)
L_NAME +Ca 4mM (n=9)
Ca free (n=9)
Ca fluorescence ratio
6
5
4
3
2
1
0
60
120
180
240
300
360
Time(s)
ATP 50µM

B:

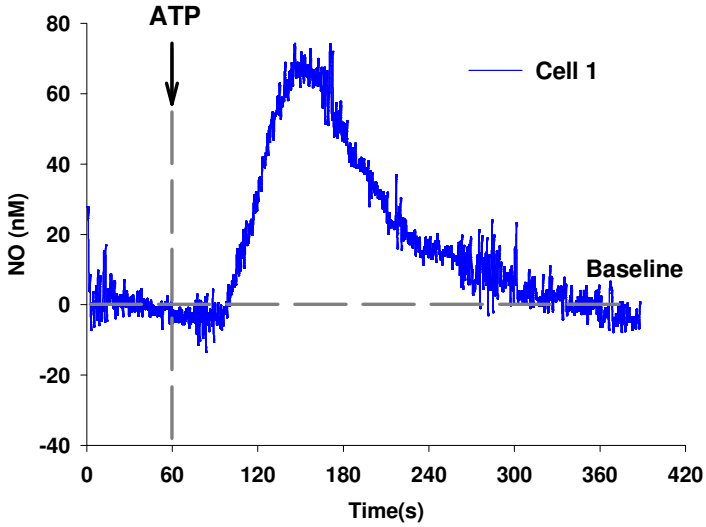
ATP
Cell 1
NO (nM)
80
60
40
20
0
-20
-40
Baseline
0
60
120
180
240
300
360
420
Time(s)

C:

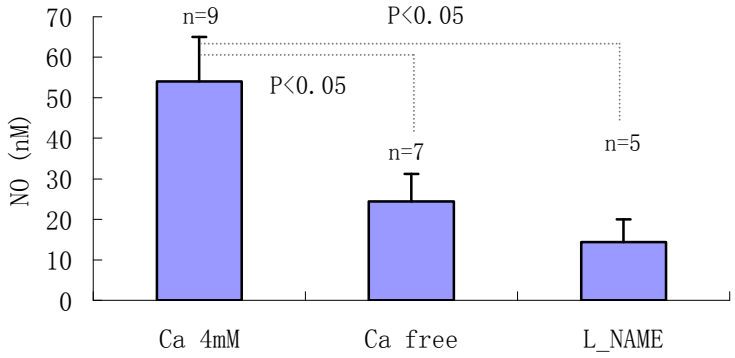

Fig.3.4 Simultaneous measurement of intracellular calcium response with fluorescence dye (A) and cellular NO release with microelectrode (B. C) following addition of ATP to the bath. A. measurement of Ca^{2+} response stimulated by exogenous ATP added at t=0. B. Electrode measurement of NO release from endothelial cells in response to 50μM ATP in the presence of 4mM calcium. Baseline NO is indicated by horizontal dashed lines. C. NO concentration measured in three different mediums after stimulation of cells by ATP.

A:

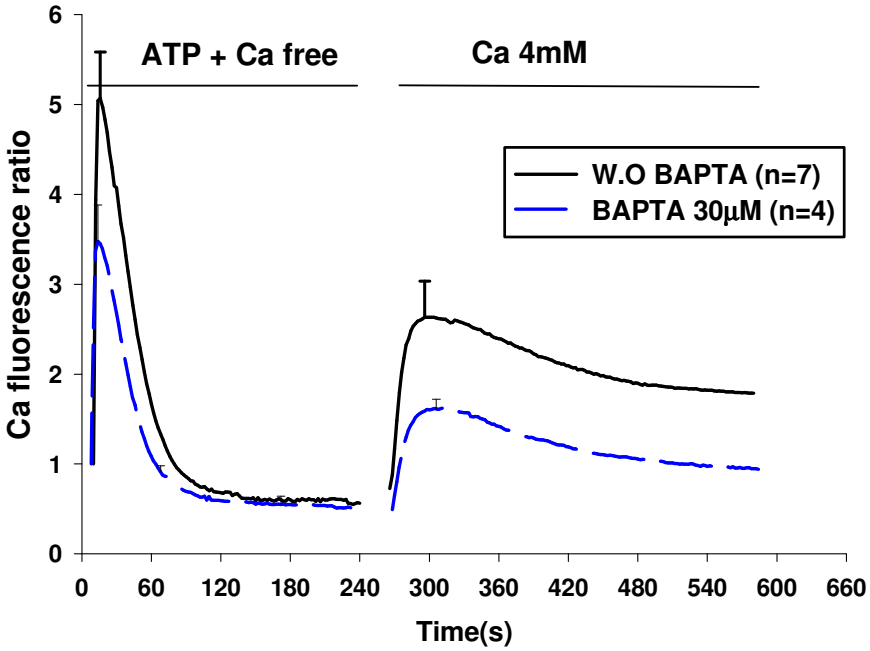
ATP + Ca free
Ca 4mM
W.O BAPTA (n=7)
BAPTA 30µM (n=4)
Ca fluorescence ratio
Time(s)
0
1
2
3
4
5
6
0
60
120
180
240
300
360
420
480
540
600
660

B:

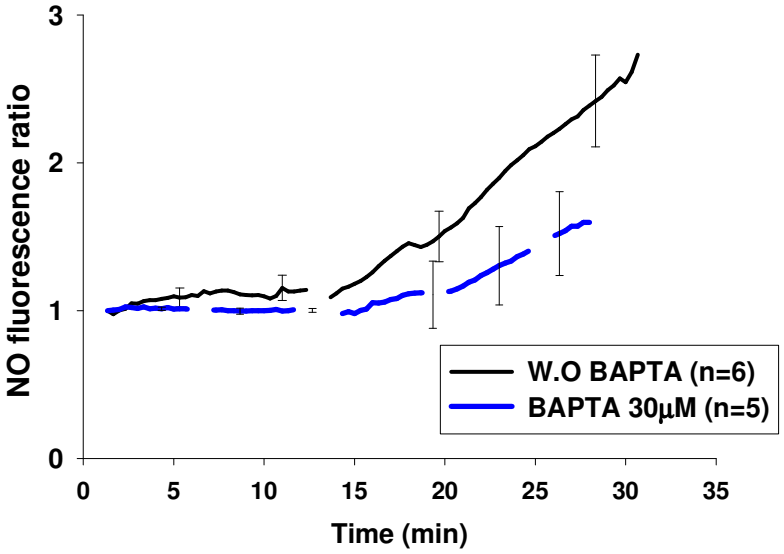
W.O BAPTA (n=6)
BAPTA 30µM (n=5)
NO fluorescence ratio
Time (min)
0
1
2
3
0
5
10
15
20
25
30
35

C:

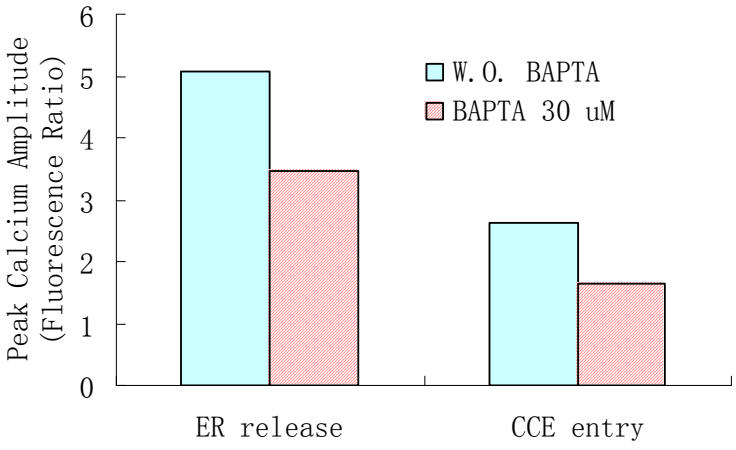
Peak Calcium Amplitude
(Fluorescence Ratio)
6
5
4
3
2
1
0
W.O. BAPTA
BAPTA 30 uM
ER release
CCE entry

D:

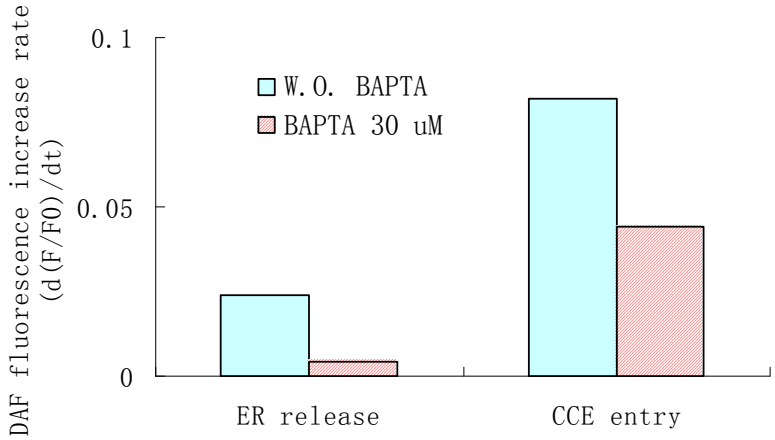
DAF fluorescence increase rate
(d(F/F0)/dt)
0.1
0.05
0
W.O. BAPTA
BAPTA 30 uM
ER release
CCE entry

E:

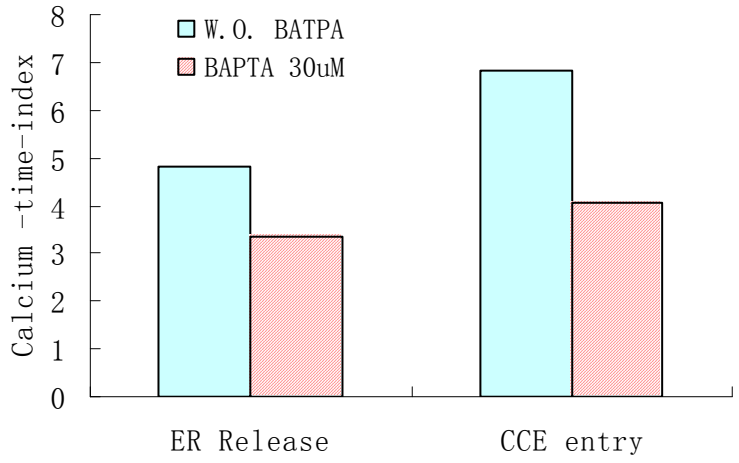

Fig. 3.5 Effect of ATP-induced intracellular Ca^{2+} release and CCE entry in BAECs and Ca^{2+} for NO production. A.Characterization $[Ca^{2+}]_i$ transients elicited by application of 50μM ATP evoked transient elevation of $[Ca^{2+}]_i$ in the absence of extracellular calcium, followed by addition of 4mM calcium. ER calcium depletion induced high peak calcium amplitude and the addition of 4mM external Ca^{2+} resulted in low calcium amplitude but sustained increase in $[Ca^{2+}]_i$. Preincubation with intracellular calcium chelator BAPTA-AM significantly inhibited $[Ca^{2+}]_i$ increase from ER store release as well as CCE entry. B. ER calcium release resulted in slight increase in NO production, and the addition of calcium caused calcium entry via CCE pathway, which resulted large increase in NO production. BAPTA incubation almost completely inhibited NO production by ER calcium store release. However, the NO production mediated by CCE entry is relatively less affected by BAPTA chelation. C. BAPTA pretreatment blocked the $[Ca^{2+}]_i$ amplitude from ER release by 31.4% and from CCE entry by 38.1% D. Effect of BAPTA pretreatment on the rate of DAF fluorescence increase. BAPTA pretreatment attenuated 82% NO concentration by ER calcium liberation and 46% by CCE entry E. The CTI, a measure of total Ca^{2+} load over time for the CCE entry group is 1.425 times the ER calcium liberation.

CHAPTER 4

A Model for Transport-Limited Calcium Signaling in the Endothelial Response to ATP

4.1 Introduction

Calcium is a ubiquitous mediator of intracellular signaling in virtually every cell type. A wide range of stimuli elicit changes in cytoplasmic calcium via influx through channels at the cell membrane or release from the endoplasmic reticulum (ER), and, yet, in many cases, the calcium changes appear to selectively activate different signaling pathways that are associated with the initial stimuli despite the similarity in the calcium changes themselves. Tymianski, et al.(127), provided compelling evidence for this specificity in the case of glutamate excitotoxicity in spinal neurons. They found that when intracellular calcium transients were of similar magnitude in response to a wide variety of stimuli, calcium entering the cytoplasm via the NMDA receptor channels preferentially lead to cell death. More recent work suggests NMDA receptor-mediated Ca^{2+} influx induces excitotoxic death via elevation nuclear C/EBPβ level. Conversely, L channel-dependent Ca^{2+} influx results in decreased C/EBPβ level, and improve neuron survival(49, 82). The identification of such distinct responses raises the question of how the same molecule can differentially activate diverse signaling pathways. The participation of calcium in a large number of physiological and pathological responses makes it an issue of wide reaching importance to understand how cells maintain specificity in calcium signaling despite its participation in many different signaling processes that might be activated in a cell.

One hypothesis is that Ca^{2+} channels and the signaling molecules associated with different pathways are nonuniformly distributed throughout the cell. The non-uniform distribution provides the mechanism by which cells are able to control Ca^{2+} entry at the right place, right

time and right concentration to initiate the appropriate signaling response. Such a mechanism would require spatial arrangement of channels and signaling molecules that permit large spatial gradients of calcium. Tymiansky, et al., proposed that the signaling molecules initiating the pathway leading to cell death were physically linked or colocalized with the NMDA receptor channel. Another striking example of calcium specificity supporting the notion of spatial segregation of signaling pathways is the observation that while bulk average intracellular calcium concentration elevation in smooth muscle cells causes contraction, the local subplasma membrane calcium arising from ryanodine receptor activity promotes K_{ca} opening to hyperpolarize the cell membrane and facilitate relaxation(93)

Numerous specialized domains in cells have been identified and found to contain concentrations of related signaling molecules, e.g., caveolae, lipid rafts, focal adhesions. In domains like focal adhesions, this is clearly a need for spatial colocalization of the molecular constituents related to the organization of cell structure (e.g., to facilitate the assembly of actin bundles). However, one can also appreciate the potential for enhancement of biochemical reactions afforded by the spatial proximity of the myriad signaling molecules located there.

Endothelial cells (ECs) are unique for their multi-functional nature. Most of these endothelial functions depend to various extents on changes in intracellular calcium concentration ($[Ca^{2+}]_i$). In previous chapter, we discussed about the relationship between endothelial calcium response and NO production in response to shear stress and ATP observed in our experiments. When bovine aortic endothelial cells (BAECs) were perfused in PBS containing Ca^{2+}, a step increase in shear stress from 0 to 20 dyn/cm^2 elilicted a transient increase in $[Ca^{2+}]_i$ attaining peak amplitude in 30 s, followed by a sustained plateau which decayed slowly to near baseline after 5 min. Elimination of extracellular Ca^{2+} with EGTA did not affect the initial calcium peak, while the $[Ca^{2+}]_i$ plateau was reduced by 20%. Despite the

similarity in the calcium responses, nitric oxide (NO) production (reflected by the change in relative DAF fluorescence with time ($d(F/F_0)/dt$)) in the presence of extracellular calcium is more than twice that in the absence of extracellular calcium. Similar results were observed in BAECs in response to stimulation with ATP. Other groups also have shown eNOS is more sensitive to CCE calcium entry than to calcium elevation via ER release, and it has been proposed that colocalization of CCE channels and eNOS in caveolae microdomains facilitates their interaction(60, 74) .

Transient receptor potential (TRP) proteins have been proposed to form CCE channels via association either as homomers or heteromers with other TRPs(140). CCE channels have been suggested to reside in caveolae[59] and caveolar microdomains provide scaffold for assembly and coordination of CCE signaling proteins (TRPs) into a complex [77]. Caveolae are distinct flask-shaped invagination of the plasma membrane. They are 50- to 100-nm diameter and can exist individually or in clusters at the surface of the endothelium. Electron microscopy studies indicate that caveolae can exist luminally and abluminally, with the largest number in perijunctional zones between endothelia(122). Caveolae have been suggested to be involved in signal transduction by containing signaling molecules, such as G protein and tyrosine kinase-associated receptors, as well as calcium effector-endothelial nitric oxide synthase (eNOS). Since Ca^{2+}-senstitive molecular effectors and cellular processes are compartmentalized in caveolae microdomain, it is reasonable to assume that the spatial and temporal organization of local calcium concentration in the microdomain are critical for proper cellular function.

The cytosolic calcium diffusion coefficient (D) is 250 $\mu m^2 s^{-1}$. Without calculation, it is difficult to tell how the spatial proximity of CCE channels and eNOS will have influence on the calcium concentration in the endothelial cell membrane since the dimension of endothelial

cells is only $20\,\mu m$. Current experimental techniques are not capable of answering this question quantitatively. The most common technique used to reveal aspects of intracellular calcium signaling is the measurement $[Ca^{2+}]_i$ with a fluorescent calcium indicator. This method, however, has limited spatial and temporal resolution and is usually used to measure the average intracellular calcium changes. Recent advances in imaging techniques, such as confocal microscopy, provide a powerful tool to study the calcium dynamics in the micrometer range and have led to the report of microdomain calcium signals in a variety of excitable and nonexcitable cell types(59, 112). These 'microdomains' have properties that vary in spatial dimensions (from 0.1 to few micrometers). The elementary events of Ca^{2+} signaling (Ca^{2+} blips, Ca^{2+} quarks, Ca^{2+} sparks and Ca^{2+} puffs) appear to have a hierarchical organization that depends on the intensity of stimulus that triggers them. However, the quantitative characterization of the microdomain calcium signaling can only be predicted by mathematical models that incorporate interactions occurring at multiple length and time scales.

To achieve a quantitative understanding the Ca^{2+} signaling mechanism, the purpose of this work was to construct a model incorporating the morphology of the cell to predict the calcium response using our experimental data, as well as data available in the literature. We show that modeling with realistic dimensions and geometry can provide a theoretical framework for analyzing a number of salient functional features that arise in the context of microdomain signaling. The most obvious of these is how the calcium concentration gradient can be affected by changing CCE channel localization and distribution. Linked to this is how and to what extend the calcium signaling is influenced by the cellular geometry. In addressing these issues, we demonstrate how to model calcium transport in a cell and in this way provide new insight into the spatial properties of the Ca^{2+} microdomain signaling.

4.2 Materials and methods

4.2.1 Immunocytochemical staining:

Cells cultured on glass coverslips were washed three times with cold Dulbecco's phosphate buffered saline (DPBS). Then, the cells were fixed with 3% paraformaldehyde for 15 min and permeabilized in DPBS containing 0.1% Triton X-100 for 10 min at room temperature. Nonspecific binding sites were blocked by incubation with blocking solution (10% normal donkey serum in DPBS) for 30 min. Cells were then incubated at room temperature with primary antibody (anti-cav-1; BD transduction labs) diluted 1% donkey serum in DPBS to a final concentration of 1:200 for an hour and secondary antibody (anti-rabbit Alexa 488)diluted in 1% donkey serum in DPBS to a final concentration of 1:1000 for 40 min in the dark.

4.2.2 Mathematical modeling:

We modeled the cell as a 2-Dimensional, disk-shaped object with a radius of 10 μm and a compartment representing the ER located in the center of the cell with a radius of 4.5 μm, as shown in Fig. 4.1. The main parameters used in the simulations are defined in Table 4.1. The following physiological processes were included in the model: 1. Diffusion of free Ca^{2+} in the cytoplasm. 2. Binding of Ca^{2+} ion to immobile buffer in the cytoplasm. 3. Ca^{2+} release from ER through IP_3 pathway. 4. Ca^{2+} re-uptake by the SERCA pump. 5. Calcium extrusion from the cell by the PMCA pump. 6. Ca^{2+} entry through CCE channels.

The release of calcium from intracellular store depends on the ER calcium concentration ($[Ca^{2+}]_{er}$), cytosolic calcium concentration $[Ca^{2+}]_i$, and the cytosolic level of IP_3 ($[IP_3]$).

1. IP_3 dynamics

Under steady state, the level of IP_3 is low. After the cell surface receptors are activated by

agonists, IP_3 is generated by the hydrolysis of PtdIns(4, 5)P_2 to IP_3 and diacylglycerol(DAG). Concurrently, IP_3 in the cytosol is degraded by inositol phosphatases. We implemented De Young and Keizer equation(34) for IP_3 production and degradation:

$$\frac{d[IP_3]}{dt} = v_{IP_3}\left(\frac{[Ca^{2+}]_{avg}}{[Ca^{2+}]_{avg}+k}\right) - I_{er}([IP_3]-[IP_3]^*) \qquad (4.1)$$

where $[IP_3]^*$ is the steady-state concentration,

V_{IP} is a step function $v_{IP} = \begin{cases} 0 & steady\ state \\ 3 & after\ agonists\ bind\ receptors \end{cases}$

and ($[Ca^{2+}]_{avg}$) is defined as the spatially averaged $[Ca^{2+}]_i$,.

$$[Ca^{2+}]_{avg} = \int_{S_{cyt}} [Ca^{2+}]_i \Big/ S_{cyt} \qquad (4.2)$$

where S_{cyt} is the area of the cytosolic space

2. Calcium release model by activation of the IP_3 receptor (IP_3R)

The IP_3R open probability (P_{IP3R}) for IP_3 sensitive calcium channels (P_{IP3R}) in the ER is given by the following equation(5, 34) :

$$P_{IP_3R} = \left[\frac{[Ca^{2+}]_{avg}[IP_3]d_2}{([Ca^{2+}]_{avg}[IP_3]+[IP_3]d_2+d_1d_2+[Ca^{2+}]_{avg}d_3)([Ca^{2+}]_{avg})+d_5}\right]^3 \qquad (4.3)$$

in which, d_1 d_2, d_3 and d_5 are the receptor dissociation constants for IP_3, Ca^{2+} inhibition and IP_3, Ca^{2+} activation respectively.

The outward flux of Ca^{2+} from ER (J_{er}) is determined by Ca^{2+} fluxes from IP_3R and

passive leak, which is given by:

$$J_{er} = (v_{er} P_{IP_3R} + v_{leak,er})([Ca^{2+}]_{er} - [Ca^{2+}]_{avg}) \qquad (4.4)$$

where v_{er} is the maximal Ca^{2+} flux after IP_3R activation and $v_{leak,er}$ is a leak flux constant.

3. Pump uptake

Cytosolic calcium concentration is maintained by a combination of two calcium pumps: sarcoplasmic and endoplasmic reticulum Ca^{2+}-activated ATPase (SERCA) pump and plasma membrane Ca^{2+}-APTase (PMCA) pump. Ca^{2+} extrusion via the PMCA pump (J_{SERCA}) and uptake by SERCA pump (J_{PMCA}) are governed by Hill-type equations[79]:

$$J_{SERCA} = \frac{V_{\max,SERCA}\,[Ca^{2+}]_{avg}^{nSERCA}}{[Ca^{2+}]_{avg}^{nSERCA} + K_{1/2,SERCA}^{nSERCA}} \qquad (4.5)$$

$$J_{PMCA} = \frac{V_{\max,PMCA}\,[Ca^{2+}]_{i}^{nPMCA}}{[Ca^{2+}]_{i}^{nPMCA} + K_{1/2,PMCA}^{nPMCA}} \qquad (4.6)$$

4. Calcium buffering

The rate of change of free cytosolic calcium concentration is due to reversible binding with soluble buffering proteins[130]. The buffering proteins are considered immobile (non-diffusible) and uniform throughout the cytosol. The total concentration of calcium binding sites is denoted by B_T. [B] and [CaB] are the concentration of unbound and bound forms of the buffer present. k_{off} and k_{on}, are respectively, the reverse and forward rate constants of the binding reaction. The rate at which calcium is binds to proteins is proportional to the free calcium concentration and the concentration of free binding sites. Calcium also dissociates from the protein at a rate proportional to the concentration of the complex. Thus, the rate of free calcium change due to

the protein buffering is represented by:

$$\frac{d[CaB]}{dt} = -k_{off}[CaB] + k_{on}[Ca^{2+}]_i([B_T] - [CaB]) \qquad (4.7)$$

The initial condition for buffered calcium CaB can be calculated by setting equation [79] to zero, all the other initial values used are listed in Table 4.2.

5. Capacitative Calcium Entry model

A signal generated by depletion of intracellular calcium stores activates CCE. The signal transduction mechanism linking changes in intraluminal Ca^{2+} to the opening of plasma membrane Ca^{2+} channels is still controversial. A putative calcium influx factor (CIF) was proposed to act as a second messenger(94, 125). When ER concentration of $[Ca^{2+}]$ decreases below a certain level, CIF is rapidly produced and released from ER, activating CCE entry.

$$\frac{d[CIF]_{er}}{dt} = -v_{CIF}([CIF]_{er} - [CIF]_{cyt}) + k_{CIF}([CIF]_{er,0} - [CIF]_{er}) \qquad (4.8)$$

$$\frac{d[CIF]_{cyt}}{dt} = r_{er}v_{CIF}([CIF]_{er} - [CIF]_{cyt}) - k_{soc}[CIF]_{cyt} \qquad (4.9)$$

The flux of calcium through CCE channels (J_{CCE}) is a function of cytosolic CIF concentration and depends on the level of extracellular calcium. The mathematical expression to describe this behavior is given by:

$$J_{CCE} = v_{soc}[CIF]_{cyt}([Ca^{2+}]_{ex} - [Ca^{2+}]_i) \qquad (4.10)$$

where v_{soc} denotes the calcium permeability of CCE channels. CCE channels are non-uniformly distributed on the cell membrane and the CCE influx processes are present only in a segment of the cell membrane where CCE channels are located.

6. Final model:

By combining eqs. 4.1-10, we get the differential equation for cytosolic calcium concentration:

$$\frac{\partial}{\partial t}[Ca]_i = D\nabla^2[Ca^{2+}]_i + k_{off}[CaB] - k_{on}[Ca^{2+}]_i([B_T]-[CaB]) + J_{IP_3R} - J_{SERCA} + J_{CCE} - J_{PMCA}$$

$$J_{er} = (v_{er}P_{IP_3R} + v_{leak,er})([Ca^{2+}]_{er} - [Ca^{2+}]_{avg})$$

$$J_{SERCA} = \frac{V_{\max,SERCA}[Ca^{2+}]_{avg}^{nSERCA}}{[Ca^{2+}]_{avg}^{nSERCA} + K_{1/2,SERCA}^{nSERCA}}$$

$$J_{PMCA} = \frac{V_{\max,PMCA}[Ca^{2+}]_i^{nPMCA}}{[Ca^{2+}]_i^{nPMCA} + K_{1/2,PMCA}^{nPMCA}}$$

$$J_{CCE} = v_{soc}[CIF]_{cyt}([Ca^{2+}]_{ex} - [Ca^{2+}]_i) \quad (4.11)$$

The change over time of the calcium concentration in ER ($[Ca^{2+}]_{er}$) and in the extracellular medium $[Ca^{2+}]_{ex}$ is described by:

$$\frac{\partial}{\partial t}[Ca^{2+}]_{er} = (-J_{IP_3R} + J_{SERCA})/r_{er} \quad (4.12)$$

$$\frac{\partial}{\partial t}[Ca^{2+}]_{ex} = 0 \quad (4.13)$$

The set of coupled non-linear partial differential equations written for the model were solved by finite element method using commercial software (FlexPDE 3, PDESolutions, Antioch, CA). The mesh densities were adaptively refined by the program to insure a relative accuracy of 0.0001 for the numerical solutions.

4.3 Results

4.3.1. Distribution of caveolae on endothelial cell membrane.

BAECs were immunostained with polyclonal antibody to caveolin-1. Caveolin- 1 was distributed heterogeneously in the cells and tended to display a typical clustered pattern at specific parts of the cell, preferentially perijunctional zones between endothelial cells as shown in Fig. 4.2.

4.3.2. Simulation of calcium response to ATP in the absence of external Ca^{2+}

The effect of ATP induced IP_3-mediated calcium release from ER in ECs with calcium-free medium was modeled for a disk-shaped cell. In the absence of external Ca^{2+}, ATP causes a significant depletion of calcium in the ER calcium stores, and there is no calicum influx from CCE channels. Free calcium diffuses in the cytosol, binds with buffering proteins and is extruded via the PMCA pumps and SERCA pumps. The calculated time course of calcium changes for $[Ca^{2+}]_m$ (10nm underneath the cell membrane) and the spatial average of intracellular calcium changes $[Ca^{2+}]_{avg}$ are shown in Fig.4.3 A. We found that the traces of $[Ca^{2+}]_m$ and $[Ca^{2+}]_{avg}$ were almost superimposed. Fig.4.3 B. is the surface plot of spatial intracellular calcium concentration after 10 seconds of ER calcium release. Consistent with Fig. 4.3.A, Fig.4.3.B indicates small calcium gradient exist inside the cell. In Fig.4.3.C. traces of free $[Ca^{2+}]_i$ (located at 10nm, 1 μm, 2 μm, and 3 μm and 4 μm from the membrane) are plotted on an expanded time scale showing that the small spatial gradient only last 5 secs.

4.3.3. Simulation of capacitative calcium entry

The depletion of intracellular Ca^{2+} stores is followed by Ca^{2+} influx through CCE channels. CCE channels have been suggested to reside in caveolae domains and caveolae are

non-uniformly distributed on cell membrane as shown in Fig.4.2 In our model, we assumed two fractions of the membrane (each fraction is 180 nm) in which CCE channels are clustered. Our model predicts a large discrepancy between $[Ca^{2+}]_m$ (calcium concentration at a point in the cytosol,10 nm from the membrane in the center of the cell membrane segment containing the CCE channels domain) and $[Ca^{2+}]_{avg}$ (spatial average of intracellular calcium concentration) (Fig. 4.4 A). A spatial map of intracellular calcium concentration after 30 seconds CCE entry, indicates large calcium gradients near the clustered CCE channels (Fig. 4.4 B). Profiles of $[Ca^{2+}]_i$ at position 10nm, 1 μm, 2 μm, and 3 μm and 4 μm underneath the membrane are shown in Fig.4.4.C. Consistent with Fig.4.4.B, the largest calcium gradient appears in the clustered CCE channels domain close to membrane.

4.3.4. Influence of CCE channels distribution on calcium gradient

To investigate the CCE channels/caveolae clustering on the calcium dynamics, we performed a parametric analysis of the CCE channels density (Fig.4.5). In our simulation, we varied the CCE density by changing the span of the membrane segment occupied by the CCE channels domain. For comparison, the total calcium flux from the CCE channels was kept constant by making the value of CCE permeability v_{soc} inversely proportional to the length of CCE domain. This is equivalent to keeping the number of caveolae constant (each with same CCE channel density), while spreading them over different areas. As the CCE domains become less localized, the cytoplasmic calcium becomes more uniform, and no sharp gradients appear. Increasing the cluster density of CCE channels significantly increased the $[Ca^{2+}]_m$ (Fig.4.5 A) without significantly changing the spatially averaged calcium. $[Ca^{2+}]_{avg}$ (Fig.4.5 B). We also kept the CCE channels density constant, but divided total length of the member segment occupied by the CCE channels constant (180nm x 2) into several small segments and let them homogeneously distribute on the cell membrane. As the number of segments increases,

the calcium gradient significantly decreases and the cytoplasmic calcium becomes more uniform (Fig.).

4.3.5. Effect of cell geometry on calcium gradient

The effects described above are for a round cell. In vivo ECs in straight arterial segments and in vitro monolayers exposed to flow become elongated and aligned with the direction of flow. The width to length ratio of the elongated endothelial cells has been found to be in the range of 0.2 - 0.29 (31). Questions therefore arise as to what is the function of the polarization of cells under flow and if this change in geometry influences the microdomain calcium signaling. To examine the effect of elongation, we simulated the calcium response in elliptically-shaped cells with the same area but varying width to length ratio. The smaller the ratio is, the more elongated the ellipse. The length of the membrane fraction where CCE channels were clustered was 180 nm. The calcium gradients were significantly enhanced when the width to length ratio was decreased to 0.25 (Fig. 4.6), but at an intermediate aspect ratio, there was little effect. The elliptical shape increases the diffusion distance, resulting in a higher gradient of calcium distribution.

4.3.6. Effect of ER location on calcium gradient

Besides the CIF model, another theory -- conformational coupling model - has been proposed to explain the signaling mechanism between intracellular Ca^{2+} stores and CCE. This model suggests ER and CCE may be physically close to each other and that there is a direct protein – protein interaction between the ER and CCE channel in the membrane. The IP_3R are hypothesized to play a role in this signaling by using their large cytoplasmic heads to transmit the information. Because this mechanism requires the ER to be in close proximity to the plasma membrane, we performed simulations to examine the effect of the separation distance

between the ER and CCE channels (Fig.4.7). When the ER membrane is 500 nm from the portion of cell membrane where CCE channels reside, there is an even greater enhancement of the local calcium concentration near the CCE domain. (Fig. 4.7 A). As the separation distance between the ER and the CCE domain increases, the calcium concentration near the CCE channels decreases dramatically (Fig. 4.7 B).

4.4 Discussion

Calcium is a ubiquitous second messenger linking a variety of external stimuli to cellular responses. Ca^{2+} enters the cell through several kinds of calcium channels and has the ability to selectively couple to different physiological processes. Ca^{2+} signaling inherently involves three factors: time, space and amplitude. The correct spatial and temporal control of calcium signaling is essential for this targeted signaling(11).

A number of mathematical models for calcium transients have been published for different cell types including endothelial cells. These models of cellular calcium dynamics have traditionally been of a lumped-parameter type i.e. systems of ordinary differential equations(5, 34, 130) The use of such formalism assumes no spatial gradients in the calcium concentration. There are some studies that explore calcium distribution throughout a model cell. These studies mainly focus on the impact of pulse duration, buffer diffusion rates, buffer affinity and kinetics on the shape of the calcium transients(62, 66, 91, 96, 113) . Modern imaging techniques have recently shown that spatially organized Ca^{2+} waves originate in subsets of clustered caveolae regions at the edges of endothelial cells in response to IP_3-mobilizing agonist ATP(56-58). In the research reported here, we have highlighted the importance of the spatial segregation of CCE channels – leading to different concentration gradients within the cell - in determining the targeted calcium signaling, especially NO signaling.

eNOS, a calcium-dependent enzyme, is dually acylated by the fatty acids myristate and

palmitate, and these modifications target eNOS to plasma membrane caveolae domains(46, 50). The proper targeting of eNOS to caveolae has been suggested as a prerequisite for effective enzyme activation. Mislocalization of eNOS in the cytoplasm by oxLDL treatment, cholesterol depletion, or acylation deficient mutation reduces both the basal and the stimulated NO production (14, 28, 60, 116). Furthermore, Jagnandan et al.(60) compared the activity of iNOS and eNOS after targeting them to different subcellular locations, and, in contrast to eNOS, no impairment in the ability of iNOS to synthesize NO was found. iNOS is structurally similar to eNOS and has virtually identical co-factor and substrate affinities with one exception -- calcium dependency. eNOS is highly dependent on increases in intracellular Ca^{2+} for activity, whereas iNOS is Ca^{2+} independent. Therefore, it has been postulated that targeting of eNOS to caveolae domains causes increased localized concentration gradients, which represent a plausible explanation for the caveola localization-dependent activity of eNOS (22).

Several recent studies suggest that CCE is more effective in the activation of eNOS, while other means of elevating $[Ca^{2+}]_i$ are ineffective(60, 74). Our results are consistent with those studies. As shown in Fig.3.4 and Fig.3.5, fluorescence measurements showed that the Ca^{2+} peak amplitude induced by IP_3-mediated ER store release is significantly higher than CCE in the presence of 4mM external calcium. However, NO production increases dramatically during CCE. Since both CCE channels and eNOS reside in caveolae domains, the colocalization of these two signaling elements suggests that the preferential sensitivity of eNOS to CCE is due to the spatial proximity of eNOS and CCE channels.

The results of our simulation indicate the spatio-temporal profile of intracellular calcium signals depends heavily on the spatial arrangement of calcium channels. If Ca^{2+} is assumed to be released uniformly from ER, which is located in the center of the cell, the cytosolic calcium gradient is very small (Fig.4.3). Similarly, if CCE channels were distributed uniformly over the cell membrane, there would be insignificant differences between the average calcium

concentration and the locally elevated concentration in the subplasmalemma domain (Fig.4.5.). Thus, the differential sensitivity of eNOS to CCE calcium requires both the clustering of CCE channels and the colocalization of eNOS. The study by Lin et al(74) provides evidence to support our simulation results. They observed that ionomycin, which elevates $[Ca^{2+}]_i$ by facilitating uniform, non-localized transmembrane calcium influxes, produces a comparable increase in average intracellular concentration to thapsigargin (TG) in the presence of extracellular calcium. However, the increase in NO production is much lower than that produced by TG-stimulated CCE.

The cav-1 immunostaining result (Fig.4.2) shows the heterogeneous distribution of caveolae domain in the endothelial cells. The picture clearly indicates that caveolae tend to accumulate at the edge of endothelial cells, an observation consistent with previous reports(22, 50, 57, 122). Quantified by electron microscopy, the caveolae number in endothelium in vivo is observed to be much higher than ECs in culture(122). Although caveolae are abundantly present in endothelial cells, ATP induced CCE does not involve the entire cavolin-1 rich region; only a small subpopulation of the caveolae is involved(57). However, whether the highly clustered CCE channels can help create the spatial gradients of Ca^{2+} to explain the preferential activation of eNOS remained to be elucidated. Our model was used to investigate this question. As shown in Fig. 4.4, clusters of CCE channels can contribute to the buildup of high calcium concentration gradients and these gradients are determined by channel cluster density. Higher cluster density allowed for higher microdomain calcium concentrations. We also examined the effect of close proximity of ER to CCE domains on the localized calcium concentration. Despite the close proximity of the calcium pumping activity of the ER membrane, the decreased volume of cytoplasm created by the presence of this organelle hinders the dissipation of the calcium gradient by diffusion into the cytoplasm. The calcium buffer in the vicinity of CCE channels gets locally saturated, resulting in the buildup of a high

calcium concentration domain. We have modeled the cell as having a single large organelle surrounded by a large cytoplasmic volume. The inclusion of other organelles would further reduce the cytoplasmic volume available for diffusive transport of calcium. As with the effect of moving the ER compartment close to the plasma membrane, the incorporation of the additional excluded volume of organelles distributed through the cytoplasm would tend to enhance the gradients in calcium possible.

Under shear stress, endothelial cells become elongated and polarized. Isshiki etc. observed that exposing endothelial cells to shear stress caused polarization of caveolae on cell surface and relocated the caveolin-1 to the upstream edge of the cell(57). At the same time, CCE channels also were repositioned at the upstream edge of the cells. Isshiki's work suggests that the caveolae are mobile, and the migration of caveolae can carry signaling molecules to different locations in response to different stimuli. Our results suggest that polarization of the CCE channels, concomitant with relocation of the caveolae, increases the calcium gradient in the microdomain. Our results (Fig.4.6) also suggest a novel mechanism by which the well-known flow-induced elongation of ECs can affect their behavior. By increasing the spatial segregation of the caveolar signaling domains, the effect of the transport-dependent calcium signaling specificity is enhanced. In such a manner, the ubiquitous second messenger, Ca^{2+}, can be used in a highly controlled way by a cell, achieving a specific pattern of response to a specific stimulus.

Barbee et al. have combined data from atomic force microscopy and CFD simulation and showed there is a significant decrease in the amplitude of endothelial surface undulations(8, 9) as a result of the realignment process. By this means, the peak shear stress and shear stress gradients are reduced, suggesting the aligned cells might be less sensitive to shear stress than nonaligned cells at a given flow rate. However, Rizzo et al., demonstrated that flow-conditioned ECs appear more mechanosensitive(111). They showed that, in

flow-conditioned ECs, a step increase in shear stress for 2 minutes significantly enhanced tyrosine phosphorylation of luminal surface proteins, including caveolin-1 and Ser^{1179} phosphorylation of eNOS compared to static culture cells. Although they did not show whether the phosphorylation is mediated by calcium signaling, the shear stress-mediated Cas tyrosine phosphorylation is known to be calcium-dependent(97). The phosphorylation of eNOS at Ser^{1179} increases eNOS activity at low Ca^{2+} concentrations and has been referred to as the "Ca^{2+}-independent activation of eNOS"; however, the eNOS activity was completely inhibited by the calcium chelator EGTA, suggesting eNOS is still, stricitly speaking, Ca^{2+} dependent(42). Therefore, it is possible that the elongated shape of ECs enhance their ability to respond to shear stress by exaggerating the transport-dependent calcium signaling effects described by our model. Our simulations indicate that in elongated ECs, high calcium concentrations in the caveolae domains can be achieved even when the spatial average concentration is relatively low. This is may explain why, in intact vessels, NO-mediated dilation is observed in response to increases in shear stress despite only minor calcium changes(129). In contrast, in cultured cells, increases in shear stress elicit significant increases in endothelial cell Ca^{2+} concentration and release of NO (4, 134).

In our experimental results, the integrated calcium load ($[Ca]_{avg}$) of CCE is 1.42 times that due to ER release. However, the CCE induced NO production indicated by $d(F/F_0)/dt$ is 3.43 times that induced by ER calcium release. Assuming NO production is proportional to the calcium concentration as suggested by Bredt and Snyder(20) , we can predict the NO production based on the calcium concentration at the caveolar domain (where eNOS resides). Our simulation results showed that integrated calcium concentration in the caveolar domain can be up to 3 times the average cytoplasmic calcium concentration, (depending on channel density, cell shape etc.), consistent with the observed NO production due to CCE.

This illustrates an important implication of our study in that the spatial average of calcium

concentration, which is typically measured experimentally, may be significantly different from the highly localized calcium concentration near caveolae. Fig.4.5B indicates that with similar spatially averaged calcium concentration ($[Ca^{2+}]_{avg}$), the localized calcium concentration can be significantly different, depending on the calcium channels cluster density (Fig 4.5A). Our results illustrate that the conventional fluorescent measurement of $[Ca^{2+}]_{avg}$, may not accurately report local calcium concentrations.

The results of our model are generally in good agreement with experimental data. However, as with all models, ours is limited by certain assumptions. Some of our assumptions have minor effects on the predictions of our model; others will have to be examined in future models. First, in this model, it is assumed that the calcium diffusion coefficient is homogeneous through the whole cell. Naraghi et.al.(91) revealed the inhomogeneity of calcium diffusion coefficient in chromaffin cells. Their data indicated that the Ca^{2+} diffusivity is lowest under the plasma membrane. Nevertheless, the inhomogeneity of calcium diffusivity will not affect our conclusions since intuitively, in this case, the restricted diffusion at the cell membrane should enhance the calcium gradient in the caveolae clustered microdomain.

Second, we assumed the buffering protein concentration to be homogeneous. Naraghi etc(91) performed photolysis experiments and did not observe significant variation of calcium buffer distribution on a micrometer spatial scale in bovine chromaffin cells. We only considered the fixed buffer and ignored the mobile buffer. We reasoned that mobile buffer concentration is relatively low, and even when mobile buffers are considered, the diffusion coefficient of mobile buffer will be much lower than calcium diffusion coefficient. Sala and Hernandez-Cruz(113) showed that the mobility of the buffers has little influence on the calcium transients in the outermost shells of the cells. We also ignored the calcium extrusion by the Na^+/Ca^{2+} exchanger (NCX) on the cell membrane and only considered the PMCA pump since there is evidence that PMCA is important for Ca_i^{2+} extrusion while NCX plays a minor

role(115). We did not simulate the mitochondrial sequestering mechanism because it possesses a much lower affinity and is too slow to influence the results for the transient response we examined(54, 113).

Finally, in this study, we did not consider the IP_3 and CIF diffusion, and the impact on the calcium signaling. We used disk-shaped cell rather than real cell geometry to calculate the spatial and temporal distribution of calcium. These have to be included in future models as the cell geometry also affects IP_3 and CIF diffusion, and thus influences calcium signaling. We assumed the CCE channels to be distributed uniformly across the whole caveolae-clustered domain and ignored the spatial arrangement of each caveola. If the calcium channel properties in a single caveola are known, our model can be further extended to calculate the calcium profile in neighborhood of a single caveola and accordingly to be scaled up to determine how much separation between caveolae would be necessary to produce even smaller scale gradients in calcium and whether the calcium concentration in the isolated caveolae domain could be high enough to trigger calcium dependent eNOS activation.

In spite of these limitations, our model adequately reproduces the experimental results and provides important insights into the role of the spatial arrangement of CCE channels in shaping the calcium gradient and to what extent this gradient is influenced by the cluster density of CCE channels and the cell geometry. Our results indicate that the spatial clustering of calcium channels allows for steeper microdomain calcium gradient. Our simulations support that cells can achieve intimate associations between Ca^{2+} channels and Ca^{2+} regulated targets by spatially arranging their calcium channels to fulfill the targeted signaling. We provide a specific example of transport-dependent signaling that provides functional compartmentalization of a signaling pathway that could be generalized to model other signaling molecules and pathways.

Table 4.1: General Parameters

Parameter	Value	Description:
R_{ec}	$10\mu m$	Radius of EC
R_{er}	$4.5\mu m$	Radius of EC
$r_{er}=V_{ER}/V_{cyt}$	0.185	Volume ratio of ER to cytosol
k	$0.7\mu M$	Dissociation constant for Ca^{2+} stimulation of IP_3 production
D	$250\mu m^2 s^{-1}$	Diffusion coefficient of free Ca^{2+}
d_1	$0.5\mu M$	IP_3 dissociation
d_2	$0.9\mu M$	Ca^{2+} inhibition
d_3	$0.94\mu M$	IP_3 dissociation
d_5	$0.082\mu M$	Ca^{2+} activation
v_{IP_3}	$3\mu M / s$	Maximum rate of IP_3 production rate
I_{er}	$2.5s^{-1}$	IP_3 degradation constant
v_{er}	$30\mu M / s$	Maximum Ca^{2+} permeability to ER membrane
$v_{leak,er}$	$11/s$	Ca^{2+} leak permeability across the ER membrane
$v_{max,SERCA}$	$0.175\mu M / s$	Maximum flux across SERCA
$v_{max,PMCA}$	$0.75\mu M / s$	Maximum flux across PMCA
$K_{1/2,SERCA}$	$0.4\mu M$	SERCA activation constant
$K_{1/2,PMCA}$	$0.2\mu M$	PMCA activation constant
n_{SERCA}	2	SERCA Hill coefficient

n_{PMCA}	2	PMCA Hill coefficient
k_{on}	$100\mu M^{-1}.s^{-1}$	On-rate of non-diffusible protein buffers
k_{off}	$500\ s^{-1}$	Off-rate of non-diffusible protein buffers
I_{SOC}	$0.11\ s^{-1}$	CIF degradation constant
v_{CIF}	$0.078/s$	CIF permeability across the ER membrane
k_{CIF}	$0.018s^{-1}$	CIF production rate
v_{SOC}	$0.035/(s\mu M)$	CCE permeability, per μM

Table 4.2. Initial Concentration

Parameter	value	Description
$[Ca^{2+}]_i$	0.1	Cytosolic calcium concentration (μM)
$[Ca^{2+}]_{avg}$	0.1	Spatial average cytosolic calcium concentration (μM)
$[Ca^{2+}]_{er}$	350	Calcium concentration in ER (μM)
$[Ca^{2+}]_{ex}$	4	Extracellular calcium concentration (mM)
$[IP_3]$	0.03	Cytosolic IP_3 concentration (μM)
$[CIF]_{er}$	20	ER CIF concentration (μM)
$[CIF]_{cyt}$	0	Cytosolic CIF concentration (μM)

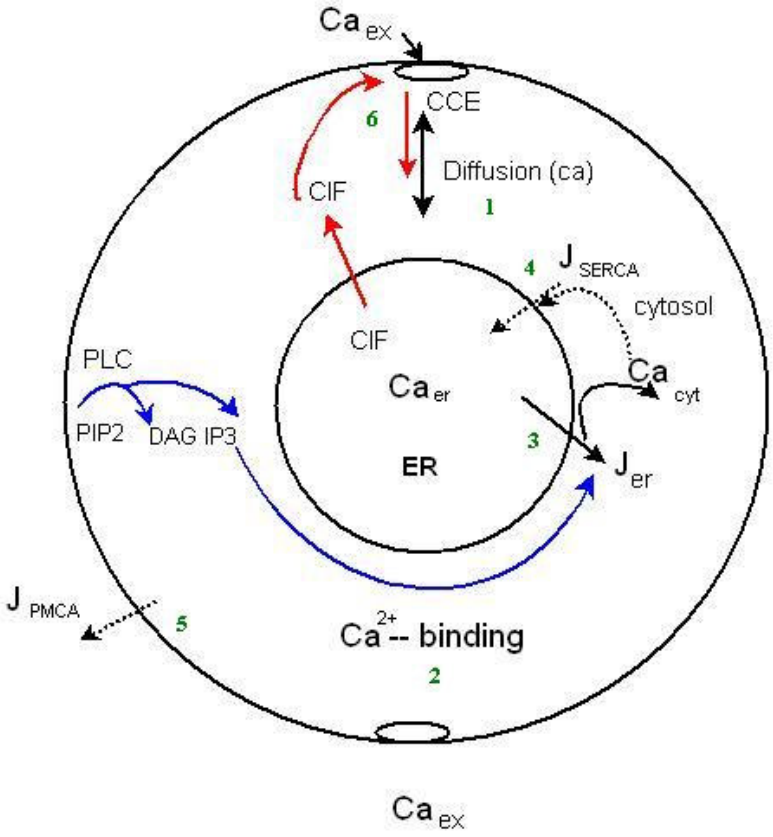

Figure 4.1: Model geometry and the processes included in the model

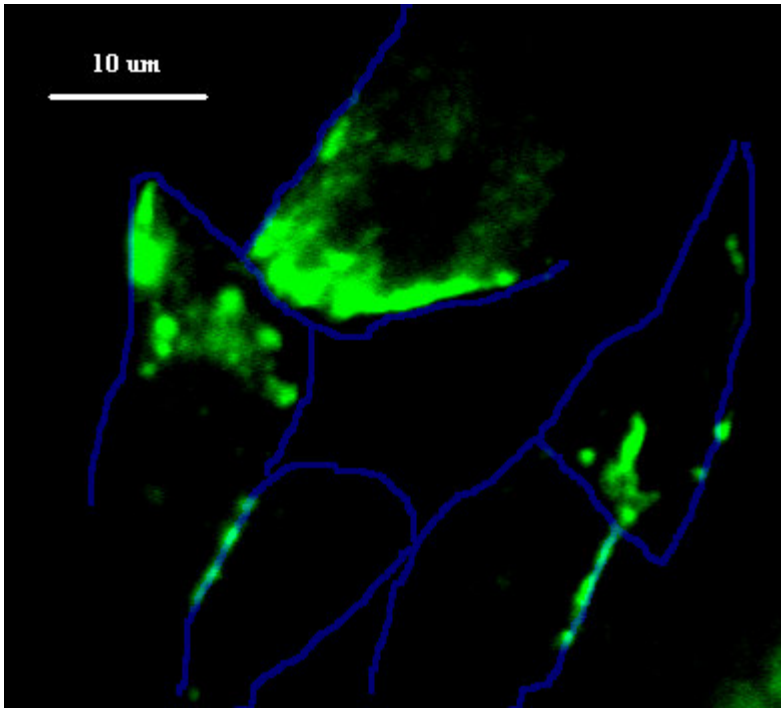

Figure 4.2: Immumolocalizaton of Cav-1 in BAECs. Immunofluorescence demonstrated the heterogeneous distribution of caveolin-1 with clustering near cell boundaries.

A:

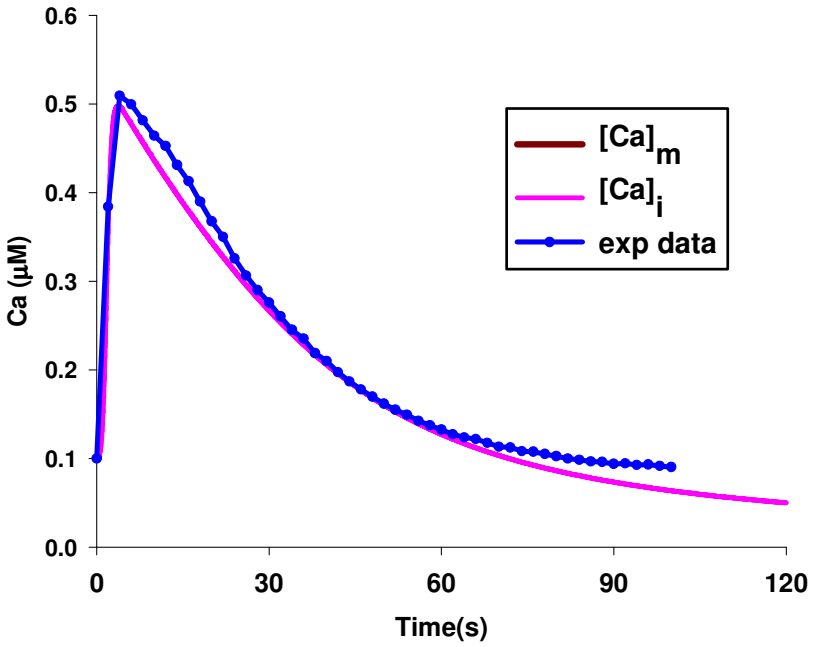
0.6
0.5
0.4
0.3
0.2
0.1
0.0
Ca (μM)
0
30
60
90
120
Time(s)
[Ca]m
[Ca]i
exp data

B:

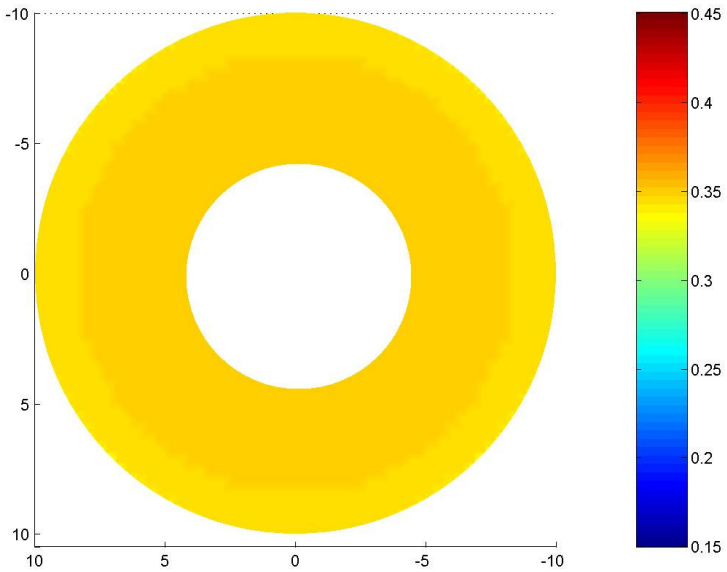
-10
-5
0
5
10
10
5
0
-5
-10
0.45
0.4
0.35
0.3
0.25
0.2
0.15

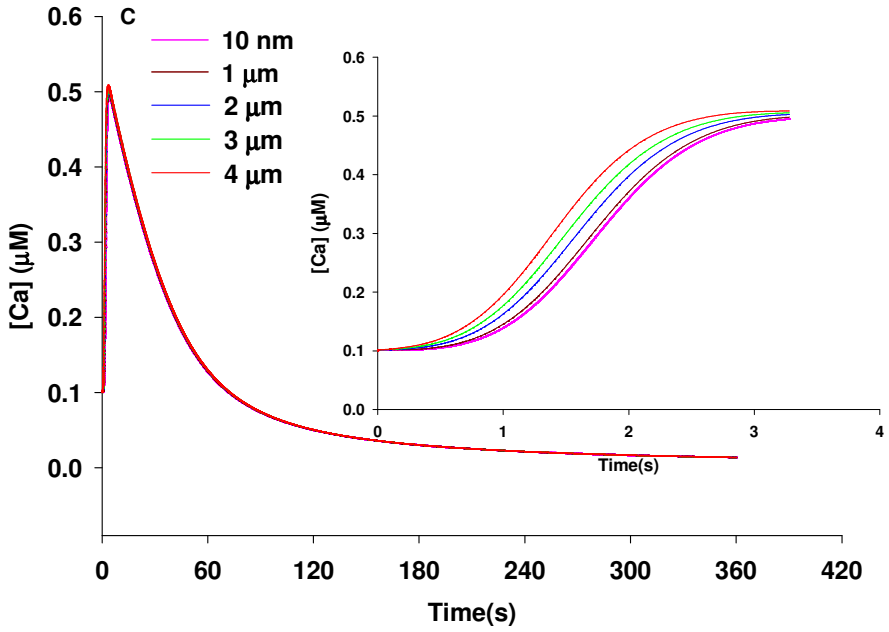

Figure 4.3: Simulation of IP_3-mediated calcium release from ER. A. Comparison of localized calcium concentration 10nm from cell membrane ($[Ca^{2+}]_m$) and the spatial average of intracellular calcium concentration ($[Ca^{2+}]_{avg}$). Also plotted for comparison is an experimental calcium transient. B. Surface plot shows spatial variation of $[Ca^{2+}]_i$ after 10 seconds ER calcium release. C. Traces of free $[Ca^{2+}]$ (located at 10nm, 1 μm, 2 μm, and 3 μm and 4 μm underneath the membrane) versus time. For spatially uniform release of calcium from the ER, gradients are dissipated by diffusion in less than 5 seconds (See insert).

A:

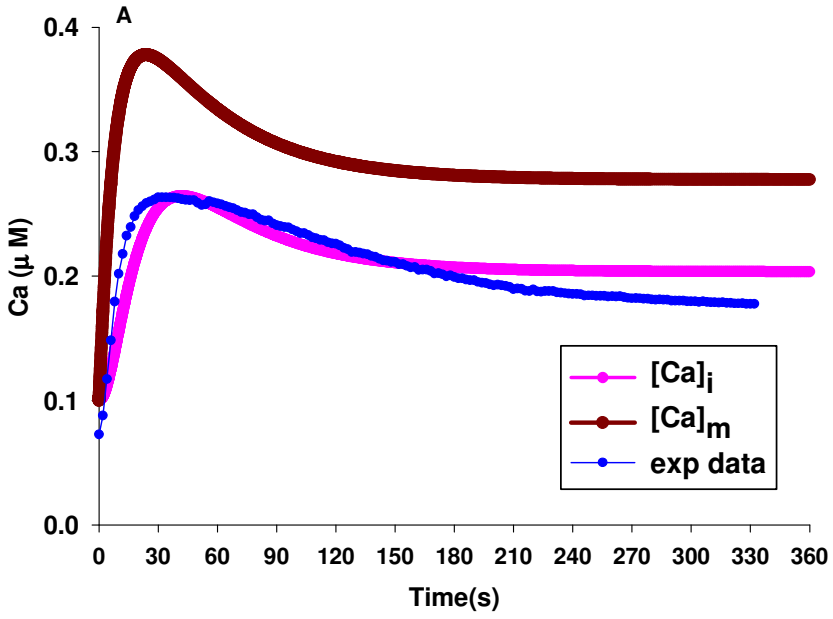
A
0.4
0.3
0.2
0.1
0.0
Ca (μ M)
0
30
60
90
120
150
180
210
240
270
300
330
360
Time(s)
[Ca]i
[Ca]m
exp data

B.

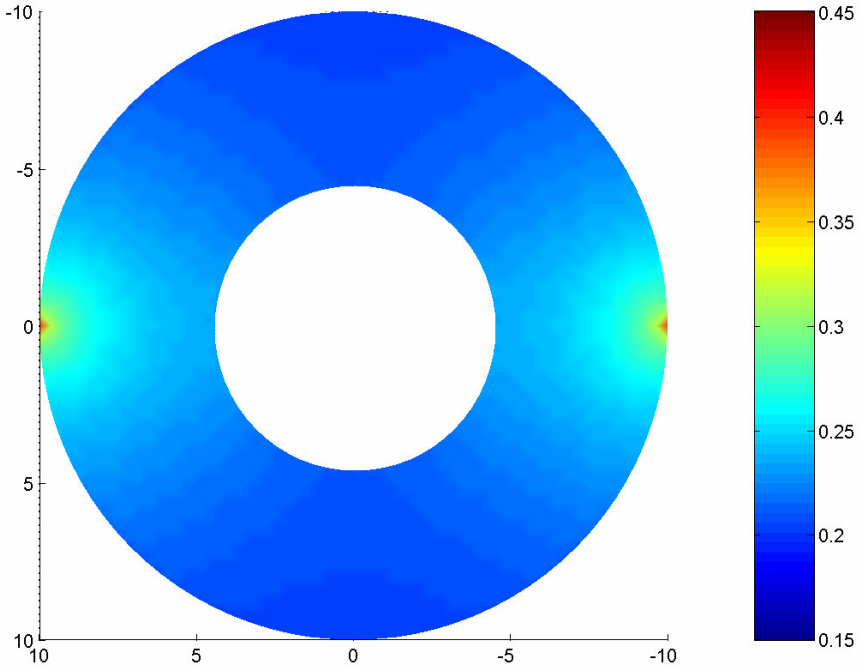
-10
-5
0
5
10
10
5
0
-5
-10
0.45
0.4
0.35
0.3
0.25
0.2
0.15

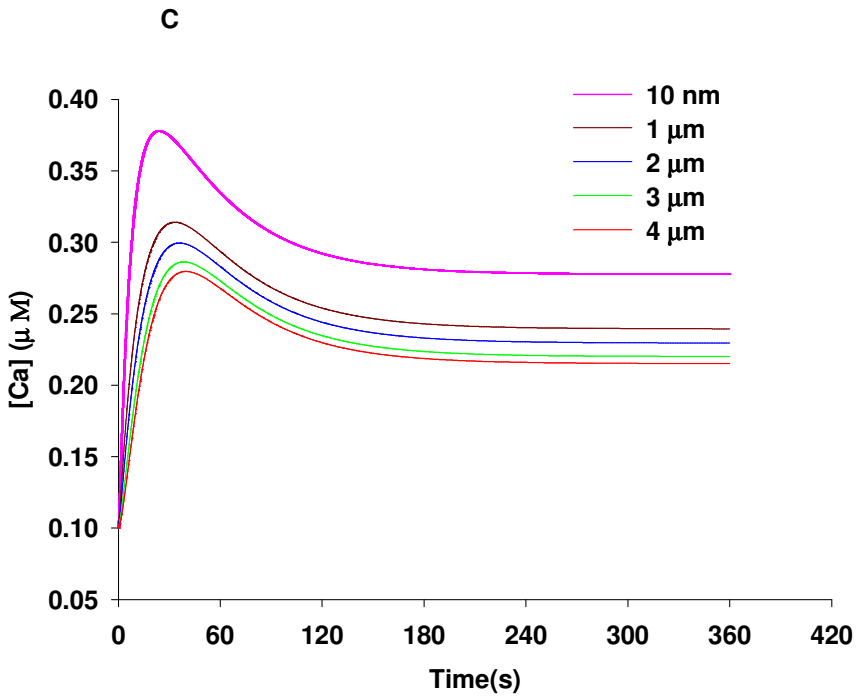

Figure 4.4: Simulation of CCE entry. A. Large discrepancy between submembranous calcium levels in caveolae microdomain ($[Ca^{2+}]_m$) and spatial average of intracellular calcium concentration ($[Ca^{2+}]_{avg}$) is predicted by simulation. B. Spatial map of intracellular calcium concentration after 30 seconds CCE entry. C. Profile of $[Ca^{2+}]_i$ at depth of 10nm, 1μm, 2μm, and 3μm and 4μm from cell membrane. Peak calcium concentration at membrane is significantly higher than in the bulk cytoplasm.

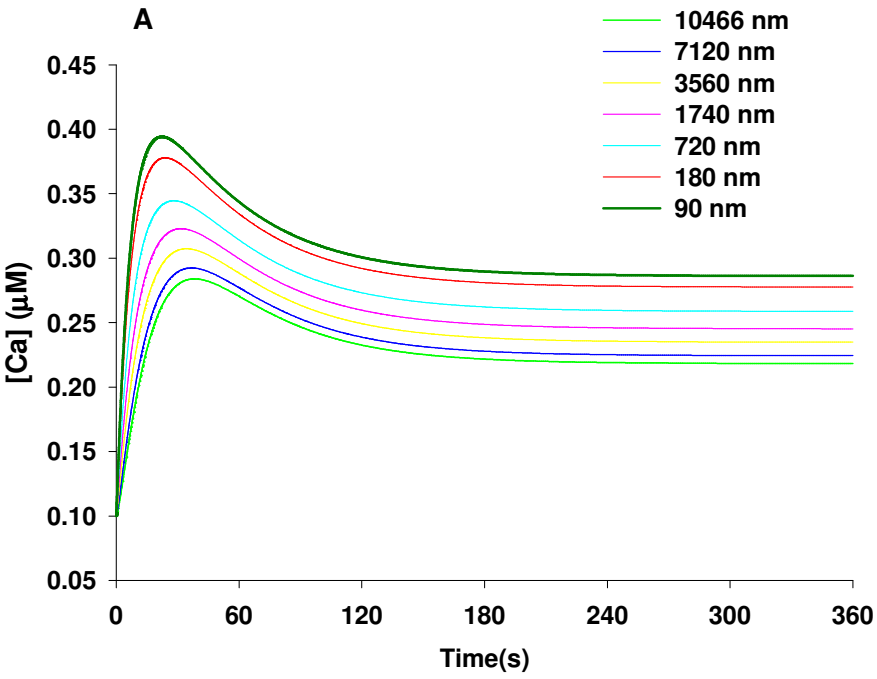
A
10466 nm
7120 nm
3560 nm
1740 nm
720 nm
180 nm
90 nm
0.45
0.40
0.35
0.30
0.25
0.20
0.15
0.10
0.05
[Ca] (µM)
0
60
120
180
240
300
360
Time(s)

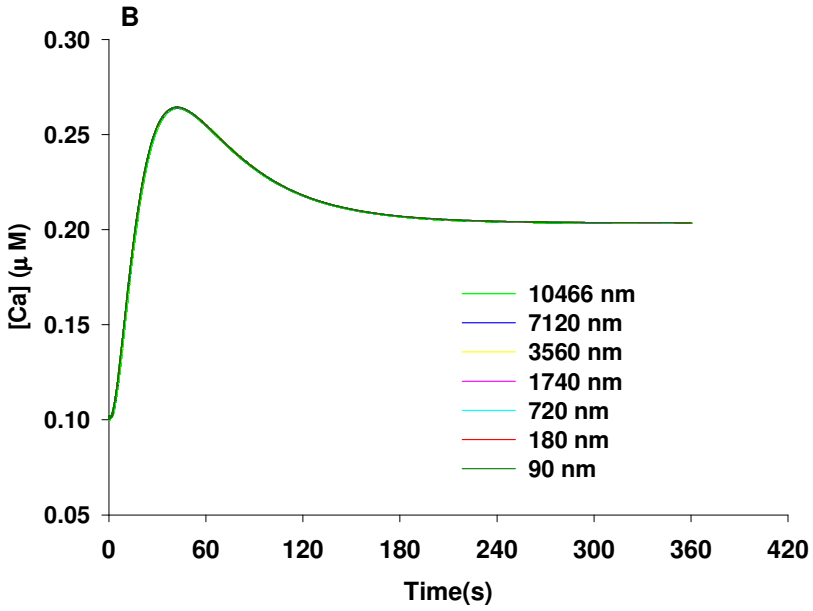
B
0.30
0.25
0.20
0.15
0.10
0.05
[Ca] (µ M)
10466 nm
7120 nm
3560 nm
1740 nm
720 nm
180 nm
90 nm
0
60
120
180
240
300
360
420
Time(s)

C:

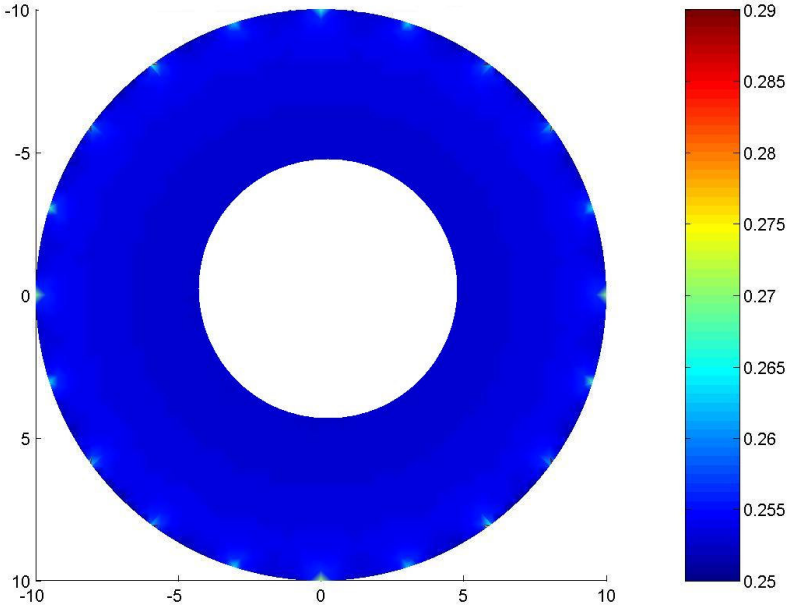
-10
-5
0
5
10
-10
-5
0
5
10
0.29
0.285
0.28
0.275
0.27
0.265
0.26
0.255
0.25

D:

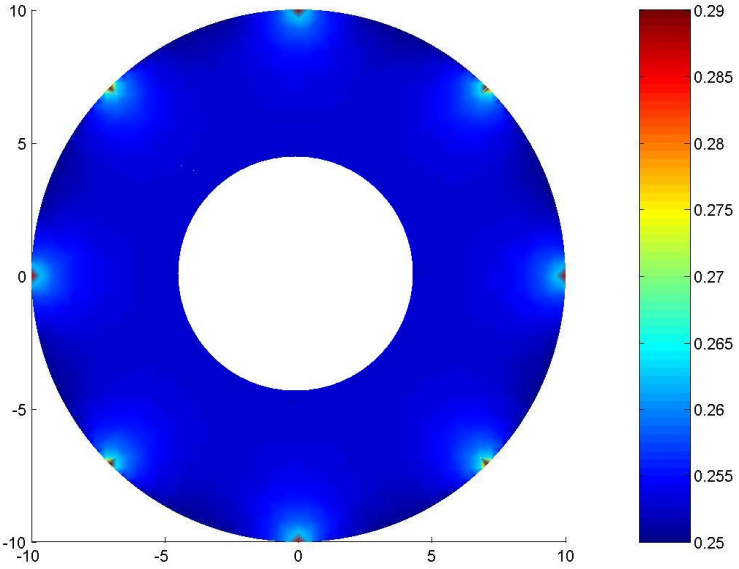
10
5
0
-5
-10
-10
-5
0
5
10
0.29
0.285
0.28
0.275
0.27
0.265
0.26
0.255
0.25

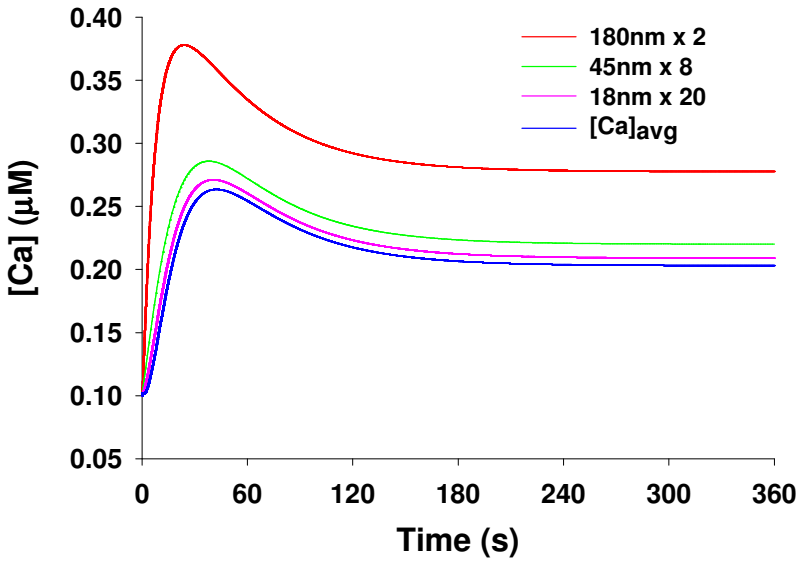

Figure 4.5: Effect of CCE channels cluster density and distribution on calcium kinetics. Peak and plateau values of calcium transient in CCE channels domain are significantly affected by CCE channels cluster density and distribution. A. The effect of CCE channels density on the free calcium concentration in CCE channels cluster domain: as the channels are spread over a larger area, the concentration enhancement at the membrane disappear. B. Changing the CCE channels density had no effect on the spatial average calcium concentration. C.Split each membrane segment (180nm) occupied by the CCE channels domain into ten small segments (18nm x 10) and distribute them uniformly on cell membrane. Spatial map of intracellular calcium concentration in the cell after 30 seconds CCE entry. D. Split each membrane segment (180nm) occupied by the CCE channels domain into ten small segments (45nm x 4) and distribute them uniformly on cell membrane.Spatial map of intracellular calcium concentration in the cell after 30 seconds CCE entry. E. The impact of CCE channels distribution on the spatial average calcium concentration.

A:

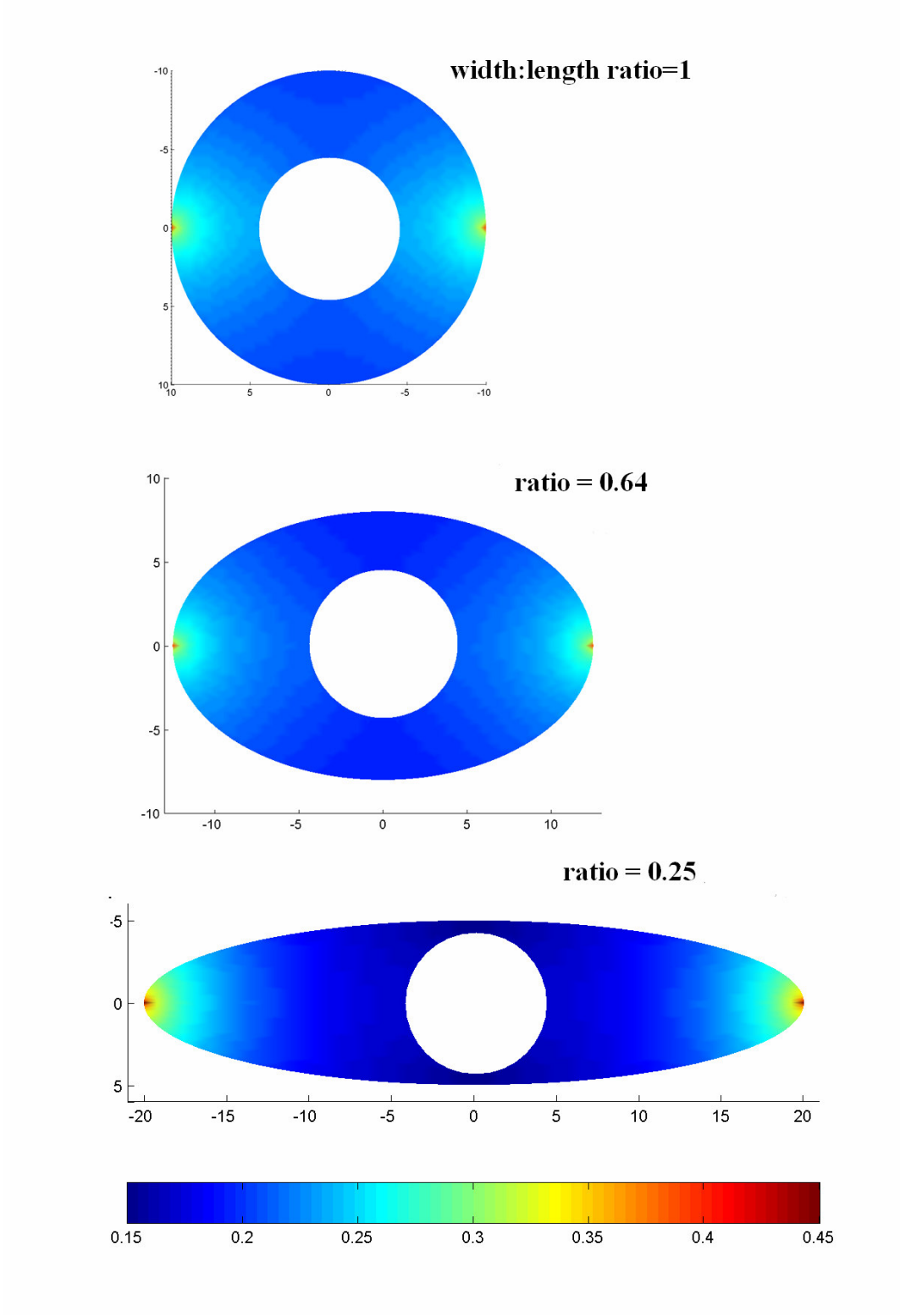
width:length ratio=1
ratio = 0.64
ratio = 0.25
0.15
0.2
0.25
0.3
0.35
0.4
0.45

B:

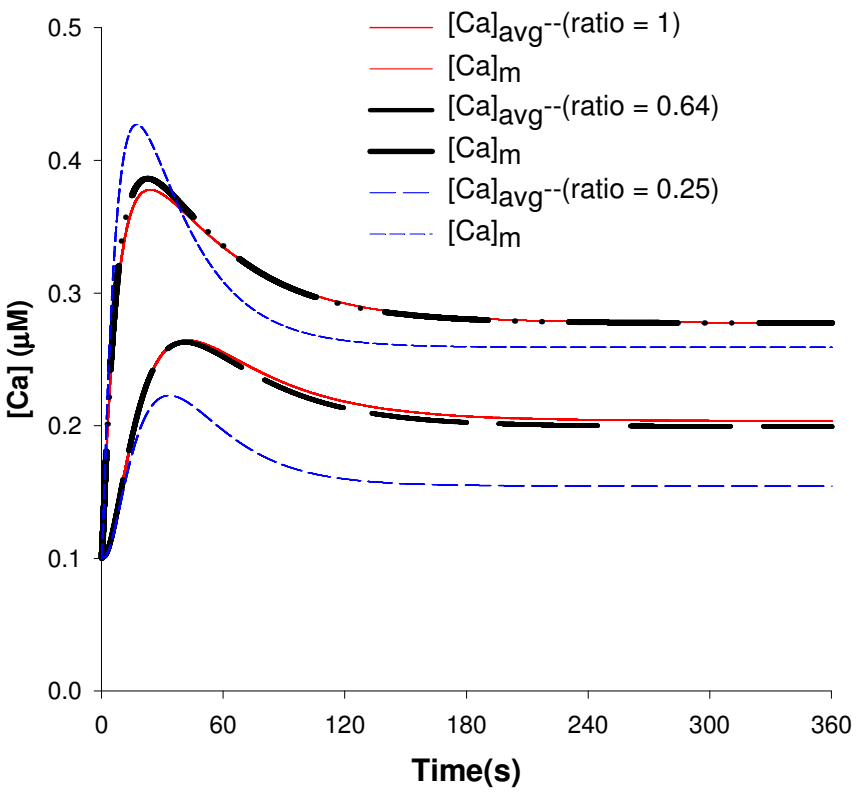

Figure 4.6. Comparison of ellipses with different eccentricity. A: Spatial map of intracellular calcium concentration in elliptical cells with different eccentricity after 30 seconds CCE. All ellipses have been set to have the same area. B: The profiles of $[Ca]_{avg}$ correspond to spatial average of calcium concentration changes, and profiles of $[Ca]_{m}$ correspond to calcium transients positioned 10nm underneath the membrane in the caveolae microdomain.

A:

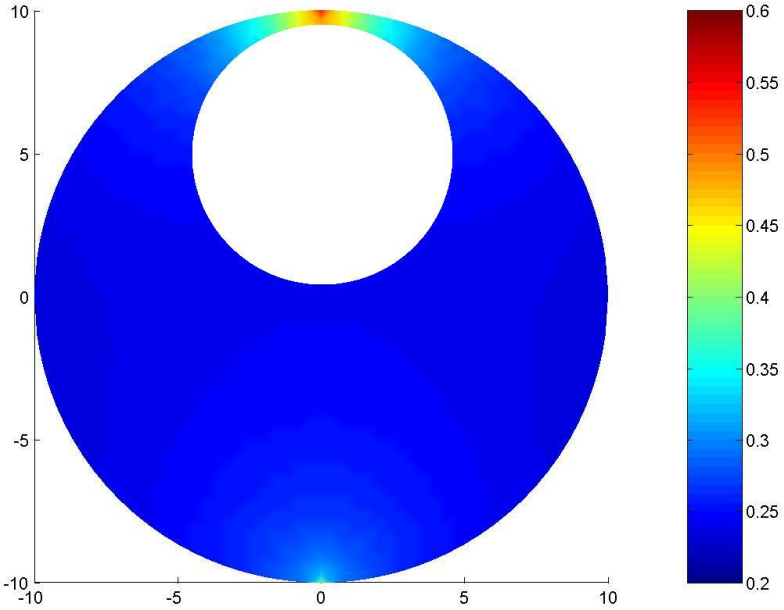

B:

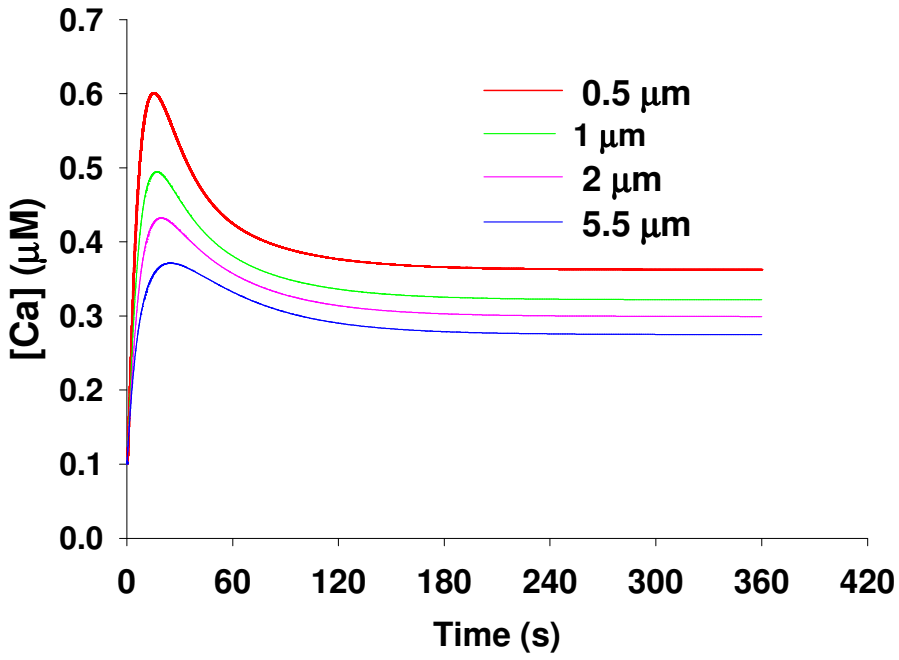

Fig 4.7. Effect of ER localization on calcium signaling. A: Spatial map of intracellular calcium concentration in modeling cell after 30 seconds CCE entry. The ER membrane is 500nm from the portion of cell membrane where CCE channels reside B: The profiles of calcium

transients positioned 10nm underneath the membrane in the caveolae microdomain. Different profiles correspond to different location of ER. ER membrane is 0.5, 1, 2, 5.5 μm underneath the cell membrane respectively. Proximity of the ER to the plasma membrane enhances the peak $[Ca]_m$ by reducing the space available for diffusion.

CHAPTER 5

Conclusion and Future Work

5.1 Summary of Principle Findings

This thesis helps advance our understanding of the calcium and nitric oxide signaling and their interacting mechanisms in endothelial cells in response to shear stress and vasoactive agonist ATP by a combination of experiments and computational simulation.

While the heterogeneity of the endothelium from different tissues is well recognized, the microheterogeneity of endothelial cells within a monolayer represents an emerging area of interest. The calcium response to shear stress in cultured aortic endothelial cells has been the subject of intense study in the past decade and the typical response to the initiation of shear stress is a rapid mobilization of intracellular calcium in a dose-dependent fashion (13, 120). However, little has been done to investigate whether the nature of the response or the mechanisms of mechanotransduction are similar in microvascular cells. The presented in vitro study investigated spatially and temporally heterogeneous calcium changes within cultured monolayers of rat adrenomedullary endothelial cells. To our knowledge, these are the first in vitro experiments to capture the complex dynamics of cell-to-cell signaling observed in vivo and in isolated tissue preparations. The control over the experimental conditions afforded by our in vitro model have allowed us to determine the mechanisms of the heterogeneous cell activation and signal transmission to neighboring cells. We show that the initiation and spread of intracellular calcium increases are mediated by the shear stress-induced release of ATP, and that the extent of cell-cell communication is limited by the balance of diffusive and convective mass transport. Furthermore, we show for the first time, that the magnitude and temporal characteristics of individual cells are different from those of large vessel endothelial cells. The observed response represents a novel mechanism for modulating the response of the

microvascular endothelium. Though cells continue to have isolated transients, the responses are more frequent at the beginning of the flow period. The strength of the response of the endothelium may be determined by the number and frequency of responding groups rather than the magnitude of the signal within individual cells.

eNOS is constitutively expressed in most endothelial cells, and has been characterized that its activation is dependent on an increase in $[Ca^{2+}]_i$ and the binding of Ca^{2+}/CaM to the enzyme. A linear correlation between the magnitude of the free calcium concentration and NO production has been demonstrated in isolated eNOS(20). In endothelial cells, the chelation of calcium or CaM antagonists treatment abolished the agonists like acetycholine and bradykinin induced endothelium-dependent relaxation(23, 89). However, eNOS can be activated by certain stimuli without a sustained increase in $[Ca^{2+}]_i$ being necessary and one of the most important of these stimuli is fluid shear stress(4, 89). These contradictory findings together with the lack of quantitative study on relationship between calcium and NO in ECs establish a need for a comprehensive study. We performed experimental study to characterize the interplay between $[Ca^{2+}]_i$ and endothelial nitric oxide synthase (eNOS) activity in BAECs. To quantitatively study the experimental observation, we developed a 2-D model of transport-limited intracellular calcium signaling in endothelial cells to evaluate the effects of spatial colocalization of eNOS and capacitive calcium entry (CCE) channels in caveolae on eNOS activiation in response to shear stress and ATP. Our mathematical model provides insights into a number of salient functional features that arise in the context of transport limited calcium signaling. The model predicts that spatial segregation of calcium channels in endothelial cells can create microdomains where calcium concentration differs significantly from the spatial average calcium concentration. Our results also suggest a novel mechanism by which the well-known flow-induced elongation of ECs can affect their behavior. By increasing the spatial segregation of the caveolar signaling domains, the effect of the transport-limited

calcium signaling specificity is enhanced. The simulations indicate for elongated ECs, the cells can keep the spatial average calcium concentration low, however maintain high calcium concentration in caveolae domain. Our simulation significantly advances our understanding of how the Ca^{2+} channel cluster and the cell geometry facilitates the development of Ca^{2+} microdomains. Ca^{2+} microdomains enable calcium, a ubiquitous mediator, to selectively activate different signaling pathways.

5.2 Future Work

Many interesting projects can be developed based on the present work. Specially, the following issues can be addressed;

5.2.1 Endothelial heterogeneity

Our data suggest that the spatial and temporal characteristics of the microvascular response to flow are different from large vessel ECs. We also showed that the heterogeneity, in part, due to differences in the expression of P_2Y_2 receptors. One of the important reasons for evaluating the P_2Y_2 receptors in our paper is that the IP_3 response to ATP appears to be mediated exclusively by P_2Y_2 in the endothelial cells from adrenal medulla(1). However, our immunostaining data for P_2Y_2 is suggestive; it is possible that heterogeneous expression of other receptor sub-types contribute in whole or in part to the observed heterogeneity of the calcium response. We observed similarly heterogeneous responses to bradykinin stimulation, but in a different subset of cells compared to ATP stimulation (Fig. 2.14). Thus, it seems possible, even likely, that there is heterogeneity in other purinergic receptors or other G-protein related receptors. siRNA approaches in BAECs and RAMECs would directly demonstrate the levels and activation of the P_2Y_2 receptor is responsible for regulating shear induced calcium increases.

In present work, our experiments provided evidence that ATP is released from RAMECs during shear stress and mediated calcium response. However, we did not show how the ATP was released. Although we demonstrated the heterogeneity, in part, was due to the differences in the purinergic expression, we cannot preclude the ATP release is heterogeneous as well. The real-time bioluminescence imaging of the ATP release from cells as described by Arcuino et al..(3) can provide us both the spatial and temporal information about the ATP release and give a direct link between ATP release and calcium response.

Heterogeneous calcium responses in microvascular endothelial cells have been reported in vivo and in isolated vessels. Spontaneous calcium waves have been observed in lung capillary endothelium(135, 136). The waves originated from some “pacemaker” cells which mostly located at vessel branch points. It is likely that the cells with high expression of purinergic receptor have specific localization in the vessel network and function as “pacemaker” to serve a role in coordinating the microvascular response to meet the perfusion requirements of the tissue or control the localized permeability in microvessels in response to localized transport requirement. The characterization of different purinergic expression levels in the vessel network especially at different branching generations of different vessel sizes will advance our understanding of the heterogeneous pattern of calcium response and cell-cell communication in microcirculation.

5.2.2 Caveolin-1 paradox

eNOS is a dually acylated protein that targets to caveolae of endothelial cells. Caveolae and caveolin-1 are influencing eNOS signaling, but the effects are not yet fully understood. The present study as well as other people’s studies demonstrates that localization of eNOS to caveolae is essential for eNOS activation. The spatial segregation and cluster of CCE channels help create sharp gradients in calcium concentration in caveolae domains, which facilitate

agonist-evoked eNOS activity. Peterson et al. found that cholesterol treatment increased eNOS localization to membrane as well as caveolin-1 expression, which enhanced NO production. Mislocalization of eNOS in the cytoplasm by oxLDL treatment, cholesterol depletion, interaction with NOSIP (eNOS interacting protein) or acylation deficient mutation reduces the basal and stimulated NO production(14, 28, 35, 60, 116). Caveolin-1 is the major structure protein for caveolae assembly and itself positively or negatively regulates cell signaling via direct or indirect protein-protein interaction with resident proteins in the caveolae(53). Interestingly, the interaction between eNOS and caveolin-1 scaffolding domain strongly reduces eNOS activity because caveolin-1 interferes with the binding of calmodulin to eNOS. In cultured ECs, high level of LDL treatment increased the eNOS and caveolin-1 in the membrane, as well as their association, which renders the inactivity of eNOS. Cav-1 null mice lack plasmalemmal caveolae, but are still viable, and the eNOS activity is up-regulated; Ach-stimulated relaxation, NO-dependent microvascular leakage is enhanced, not reduced(38, 110). Caveolae seem to have two apparently paradoxical tasks in eNOS activity: facilitation of agonist-evoked stimulation and tonic repression of basic activity by structure protein caveolin-1 and the controversies remained to be cleared away. These data lead to propose the so-called “caveolae paradox”(40). In Fischer rat thyroid cells lacking caveolins/caveolae, eNOS can still target to cholesterol-rich lipid raft domains of the plasma membrane and is functionally active to produce basal and ionophore stimulated NO(121). Since ionophore elevates $[Ca^{2+}]_i$ by facilitating uniform, non-localized transmembrane calcium influxes, ionophore stimulated NO production does not give any information about the subcellular localization and functional consequence of the other molecules , such as G protein-coupled receptors, CCE channel proteins, CAT-1, which interact and facilitate eNOS activity in cells lacking cvaeolin-1. Whether changes in caveolin-1 affect eNOS localization, interactions with other molecules remained to be determined. iRNA mediated down-regulation of caveolin-1 in

endothleial cells, or cell lines derived from caveolin-deficient mice can provide a useful experimental system to explore the role of caveolin-1 in the eNOS activity and delineate the interactions among signaling proteins as modulated by caveolin-1.

5.2.3 Extension of cell-scale model:

The limitation of the present model has been discussed in Chapter 4. Besides we can further improve the model to include the IP_3 and CIF diffusion, we can also develop vessel model incorporating the cell-scale model. The key features of the cell-scale model are shown diagrammatically below in Fig. 5.1. and include 1) shear stress dependent ATP release, transport and subsequent autocrine stimulation of intracellular calcium; 2) Calcium-induced ATP release forming a positive feedback loop; 3) Capacitive calcium entry (CCE) due to depletion of ER calcium; 4) Calcium-dependent eNOS stimulation and NO release; 5) NO transport in the vessel and 6) Negative feedback of NO concentration on calcium and NO production. The concentrations of ATP and NO at the cell surface will depend on diffusive and convective mass transport.

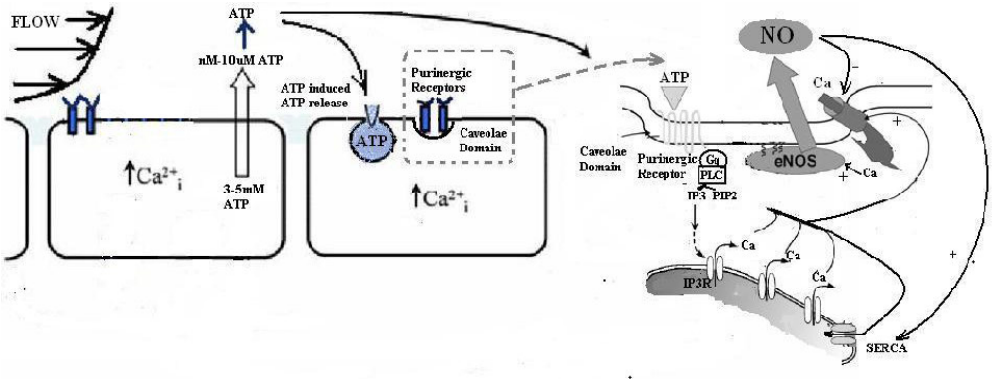

Fig. 5.1. Diagrammatic representation of the features of the cell-scale model (portion adapted from Shaul PW (118).

Model for wall shear stress and ATP concentration:

The velocity profile within blood vessel is given by the parabolic Poiseuille flow solution

$$v = v_{\max} \times (1 - (r / r_0)^2) \qquad (5.1)$$

where v_{max} is the maximum velocity at the centerline (r=0), and r_0 is the radius of blood vessel.

The shear stress to which the endothelial cells are exposed can be determined from the profile as

$$\tau_w = \mu \frac{\partial v}{\partial r}\Big|_{r=r0} = 2\mu v_{\max} / r_0 \qquad (5.2)$$

At endothelial layer, ATP is released and hydrolyzed:

$$D_{ATP}\left[\frac{1}{r}\frac{\partial}{\partial r}(r\frac{\partial C_{ATP}}{\partial r}) + \frac{\partial^2 C_{ATP}}{\partial z^2}\right] = \frac{V_{\max,ATP} C_{ATP}}{K_{m,ATP} + C_{ATP}} - R_{ATP}(\tau_w) \qquad (5.3)$$

where D_{ATP} is the diffusion coefficient for ATP in the blood, V_{max}, ATP is the maximum enzyme reaction velocity for ATP hydrolysis by ecto-ATPase, K_m, ATP is the Michaelis constant for the enzyme. R_{ATP} is the flow-induced ATP release which can be expressed as a linear or nonlinear function of shear stress.

Diffusion and convection of ATP:

$$\mathrm{D}_{\mathrm{ATP}}\left[\frac{1}{\mathrm{r}}\frac{\partial}{\partial \mathrm{r}}(\mathrm{r}\frac{\partial \mathrm{C}_{\mathrm{ATP}}}{\partial \mathrm{r}}) + \frac{\partial^2 \mathrm{C}_{\mathrm{ATP}}}{\partial \mathrm{z}^2}\right] = v\frac{\partial(\mathrm{C}_{\mathrm{ATP}})}{\partial \mathrm{z}} \qquad (5.4)$$

Boundary conditions:

$$\frac{\partial C_{ATP}}{\partial r} = 0 \quad \text{at (z=0 and r=r0)}$$

$$D_{ATP} \left.\frac{\partial C_{ATP}}{\partial r}\right|_{r=r_{0i}^{-}} = D_{ATP} \left.\frac{\partial C_{ATP}}{\partial r}\right|_{r=r_{0}^{+}} \qquad (5.5)$$

We and others have shown that for both large vessel and microvascular endothelial cells, shear stress causes the release of ATP which then stimulates the intracellular release of calcium from the endoplasmic reticulum. ATP induced intracellular calcium signaling can be modeled by lumped-parameter type system of ordinary differential equations(34, 130). In the present studies, we showed that calcium concentration in the neighborhood of the caveolae (where active eNOS resides) can be a factor of 2 or 3 greater than the average cytoplasmic calcium concentration owing to the collocalization of the CCE channel in the caveolae. This cell-scale spatial variation in calcium concentration will provide a scaling parameter that depends on cell geometry and links average cell calcium concentration, which can be validated experimentally, with the predicted concentration at the caveolae to be used for the calcium-dependent eNOS activation.

Ca-NO relationship and NO feedback. Within the physiological range of calcium concentration (0.1-5 μM), the eNOS activity increases linearly with Ca concentration (20).

The NO production rate R_{NO} can be expressed as:

$$R_{NO}([Ca]_i) = R_{\max}\left(\frac{[Ca]_i}{1uM}\right) \qquad (5.6)$$

where $[Ca]_i$ is the localized calcium concentration and $R_{\max}$ is the NO production rate at 1 μM calcium concentration.

NO itself has been reported to produce negative feedback on intracellular calcium concentration and NO production (123). We will incorporate this feedback mechanism into our model. Since the concentration of NO depends on the diffusion and convection in the perfusing medium, its effects on NO production can only be properly simulated by including the extracellular mass transport of NO as have done been described in our group's studies(26). Furthermore, since in vivo, scavenging of NO in blood by reaction with hemoglobin is expected to lower the availability of NO dramatically compared to an in vitro flow experiment without hemoglobin, these simulations are critical for proper interpretation of the in vitro data and transfer of that data to the model of the in vivo response. NO production in the endothelial cells is under autoregulatory control, via the cGMP-dependent inhibition of CCE and acceleration of Ca^{2+} sequestration into the ER (36). We can incorporate NO feedback by modifying the J_{SERCA} and J_{CCE} to be NO dependent as follows:

$$J_{SERCA} = \frac{v_{\max,SERCA}([NO])\,[Ca^{2+}]_i^{nSERCA}}{[Ca^{2+}]_i^{nSERCA} + K_{1/2,SERCA}^{nSERCA}([NO])} \qquad (5.7)$$

$$J_{CCE} = v_{soc}([NO])[CIF]_{cyt}([Ca^{2+}]_{ex} - [Ca^{2+}]_i) \qquad (5.8)$$

$v_{\max,SERCA}([NO])$ and $v_{soc}([NO])$ are functions of NO concentration and are expressed as $v_{\max,SERCA}([NO])$ and $v_{soc}([NO])$ respectively.

NO also decreases eNOS expression, disrupts caveolae signaling by distancing elements of the cascade. These, however, are long time scale events, and will not be included in our proposed project.

REFERENCE

1. **Allsup DJ and Boarder MR.** Comparison of P2 purinergic receptors of aortic endothelial cells with those of adrenal medulla: evidence for heterogeneity of receptor subtype and of inositol phosphate response. *Molecular Pharmacology* 38: 84-91, 1990.

2. **Ando J, Ohtsuka A, Korenaga R, Sakuma I, and Kamiya A.** Flow-induced calcium transients and release of endothelium-derived relaxing factor in cultured vascular endothelial cells. *Front Med Biol Eng* 5: 17-21, 1993.

3. **Arcuino G, Lin J, Takano T, Liu C, Jiang L, Gao Q, Kang J, and Nedergarrd M.** Intercellular Calcium signaling mediated by point-burst release of ATP. *PNAS* 99: 9840-9845, 2002.

4. **Ayajiki K, Kindermann M, Hecker M, Fleming I, and Busse R.** Intracellular pH and tyrosine phosphorylation but not calcium determine shear stress-induced nitric oxide production in native endothelial cells. *Circ Res* 78: 750-758, 1996.

5. **Baker HL, Errington RJ, Davies SC, and Campbell AK.** A Mathematical Model Predicts that Calreticulin Interacts with the Endoplasmic Reticulum Ca2+-ATPase. *Biophysical Journal* 82: 582-590, 2002.

6. **Ballermann BJ, Darkik A, Eng E and Liu A.** Shear stress and the endothelium. *Kidney International* 54: 100-108, 1998.

7. **Barakat AI, Lever EV, Pappone PA and Davies PF.** A Flow-Activated Chloride-Selective Membrane Current in Vascular Endothelial Cells. *Circ Res* 820-828, 1999.

8. **Barbee KA, Davies PF, and Lal R.** Shear stress-induced reorganization of the surface topography of living endothelial cells imaged by atomic force microscopy. *Circ Res* 74: 163-171, 1994.

9. **Barbee KA, Mundel T, Lal R, and Davies PF.** Sub-Cellular Distribution of Shear Stress at the Surface of Flow-Aligned and Nonaligned Endothelial Monolayers. *Am J Physiol* 268: H1765-H1772, 1995.

10. **Berkels R, Suerhoff S, Roesen R, and Klaus W.** Nitric oixde causes a cGMP-independent intracellular calcium rise in porcine endothelial cells - paradox? *Microvascular Research*: 38-44, 2000.

11. **Berridge MJ and Dupont G.** Spatial and temporal signalling by calcium. *Curr Opin Cell Biol,* 6: 267-274, 1994.

12. **Blackman BR, Barbee KA, and Thibault LE.** In vitro cell shearing device to investigate the dynamic response of cells in a controlled hydrodynamic environment. *Annals of Biomedical Engineering* 28: 363-372, 2000.

13. **Blackman BR, Thibault LE, and Barbee KA.** Selective Modulation of Endothelial Cell [Ca2+]i Response to Flow by the Onset Rate of Shear Stress. *Journal of Biomechanical Engineering* 122: 274-282, 2000b.

14. **Blair A, Shaul PW, Yuhanna IS, Conrad PA, and Smart EJ.** Oxidized low density lipoprotein displaces endothelial nitric oxide synthase (eNOS) from plasmalemmal caveolae and impairs eNOS activation. *J Biol Chem* 274: 32512-32519, 1999.

15. **Bodin P, Bailey D and Burnstock G.** Increased flow-induced ATP release from isolated vascular endothelial but not smooth muscle cells. *Br J Pharmacol* 103: 1203-1205., 1991.

16. **Bodin P and Burnstock G.** ATP-stimulated release of ATP by human endothelial cells. *J Cardiovasc Pharmacol* 27: 872-875, 1996.

17. **Bodin P and Burnstock G.** Evidence that release of adenosine of triphosphate from endothelial cells during increased shear stress is vesicular. *Journal of Cardiovascular Pharmacology* 38: 900-908, 2001.

18. **Boo YC and Jo H.** Flow-dependent regulation of endothelial nitric oxide synthase: role of protein kinases. *Am J Physiol Cell Physiol* 285: C499-C508, 2003.

19. **Boo YC, Sorescu GP, Bauer PM, Fulton D, Kemp BE, Harrison DG, Sessa WC, and Jo H.** Phosphrylationh of eNOS at Ser^{635} stimulates NO production in a Ca^{2+}-independent manner (Abstract). *FASEB J* 17: A805, 2003.

20. **Bredt DS and Snyder SH.** Isolation of nitric oixde synthetase, a calmodulin-requiring enzyme. *Proc Natl Acad Sci USA,* 87: 682-685, 1990.

21. **Buerk DG.** Can we model nitric oxide biotransport? A survey of mathematical models for a simple diatomic molecule with surprisingly complex biological activities. *Annu Rev Biomed Eng* 3: 109-143, 2001.

22. **Bulotta S, Cerullo A, Barsacchi R, De Plama C, Rotiroti D, Clementi E, and Borgese N.** Endothelial nitric oxide synthase is segregated from caveolin-1 and localizes to the leading edge of migrating cells. *Exp Cell Res,* 312: 877-889, 2006.

23. **Busse R and Mulsch A.** Calcium-dependent nitric oxide synthesis in endothelial cytosol is mediated by calmodulin. *FEBS Lett* 265: 133-136, 1990.

24. **Chen J, Wang Y, Wang Y, Nakajima T, Iwasawa KH, Sunamoto M, Choi D, Yoshida Y, Sakaki Y, and Toyoka T.** Autocrine action and its underlying mechanism of nitric oxide on intracellular Ca2+ homeostasis in vascular endothelial cells. *Jouranl of BIological Chemistry*: 28739-28749, 2000.

25. **Chen P and Wu KK.** Structural elements contribute to the calcium/calmodulin dependence on enzyme activation in human endothelial nitric-oxide synthase. *J Biol Chem* 278: 52392-52400, 2003.

26. **Chen X, Jaron D, Barbee KA, and Buerk DG.** The influence of radial RBC distribution, blood velocity profiles, and glycocalyx on coupled NO/O_2 transport. *J Appl Physiol*, 2005.

27. **Chi JT, Chang HY, Haraldsen G, Jahnsen FL, Troyanskaya OG, Chang DS, Wang Z, Rockson SG, Van de Rijn M, Botstein D, and Brown PO.** Endothelial cell diversity revealed by global expression profiling. *Proc Natl Acad Sci USA* 100: 10623-10628, 2003.

28. **Church JE and Fulton D.** Differences in eNOS activity because of subcellular localization are dictated by phosphorylation state rather than the local calcium environment. *J Biol Chem* 281: 1477-1488, 2006.

29. **Collins DM, Mccullough WT, and Ellsworth ML.** Conducted vascular responses: Communication across the capillary bed. Microvascular Research. 56: 43-53, 1998.

30. **Communi D, Raspe E, Pirotton S, and Boeynaems JM.** Coexpression of P2Y and P2U receptors on aortic endothelial cells. *Circulation Research* 76: 191-196, 1995.

31. **Cornhill JF, Levesque MJ, Herderick EE, Nerem RM, Kilman JW, and Vasko JS.** Quantitative study of the rabbit aortic endothelium using vascular casts. Atherosclerosis. *Atherosclerosis* 35: 321-337, 1980.

32. **Davies PF.** Flow-mediated endothelial mechanotransduction. *Physiological Reviews* 75: 519-560, 1995.

33. **Davies PF, Mundel T, and Barbee KA.** A mechanism for heterogeneous endothelial responses to flow in vivo and in vitro. *J Biomechanics* 28: 1553-1560, 1995.

34. **De Young GW and Keizer J.** A single-pool inositol 1,4,5- truogisogate-receotir-based model for agonist-stimulated oscillations in Ca2+ concentration. *Proc Natl Acad Sic* 89: 9895-9899, 1992.

35. **Dedio J, Konig P, Wohlfart P, Schroeder C, Kummer W, and Muller-Esterl W.** NOSIP, a novel modulator of endothelial nitric oixde synthase activity. *FASEB J* 15: 79-89, 2001.

36. **Dedkova E and Blatter LA.** Nitric Oxide Inhibits Capacitative Ca^{2+} entry and enhances endoplasmic reticulum Ca^{2+} uptake in bovine vascular endothelial cells. *Journal of Physiology* 539: 77-91, 2002.

37. **Dora KA.** Intercellular Ca2+signaling: the artery wall. *Cell&Developmental biology* 12: 27-35, 2001.

38. **Drab M, Verkade P, Elger M, Kasper M, Lauterbach B, Menne J, Lindschau C, Mende F, Luft FCS, A., Haller H, and Kurzchalia TV.** Loss of caveolae, vascular dysfunction, and pulmonary defects in caveolin-1 gene-distrupted mice. *Science* 293: 2449-2452, 2001.

39. **Dull RO and Davies PF.** Flow modulation of agonist (ATP)-response (Ca2+) coupling in vascular endothelial cell. *Am J Physiol(cell physiol)* 261: H149-H154, 1991.

40. **Feron O and Kelly RA.** The caveolar paradox: suppressing, inducing, and terminating eNOS signaling. *Circ Res* 88: 129-131, 2001.

41. **Fisher AB, Chien S, Barakat AI, and Nerem RM.** Endothelial cellular response to altered shear stress. *Am J Physiol Lung Cell Mol Physiol* 281: 529-533, 2001.

42. **Fleming I and Busse R.** Molecular mechanisms involved in the regulation of the endothelial nitric oxide synthase. *Am J Physiol Regul Integr Comp Physiol* 284: R1-R12, 2003.

43. **Fleming I and Busse R.** Signal transduction of eNOS activation. *Cardiovascular Research* 43: 532-541, 1999.

44. **Florian JA, Kosky JR, Ainslie K, Pang Z, Dull RO and Tarbell JM**. Heparan sulfate proteoglycan is a mechanosensor on endothelial cells. *Circulation Research* 93: e136-e142, 2003.

45. **Forstermann U, Pollock JS, Schmidt HH, Heller MM and Murad F.** Calmodulin-dependent endothelium-derived relaxing factor/nitric oxide synthase activity is present in the particulate and cytosolic fractions of bovine aortic endothelial cells. *Proc Natl Acad Sci USA,* 88: 1788-1792, 1991.

46. **Fulton D, Babbitt R, Zoellner S, Fontana J, Acevedo L, MeCabe TJ, Iwakiri Y, and Sessa WC.** Targeting of Endothelial Nitric-Oxide Synthase to the Cytoplasmic Face of the Golgi Complex or Plasma Membrane Regulates Akt Versus Calcium-dependent Mechanisms for Nitric Oxide Release. *The Jouranl of Biological Chemistry* 279: 30349-30357, 2004.

47. **Fulton D, Gratton J, and Sessa WC.** Post-translational control of endothelial nitric oxide synthase: why isn't calcium/calmodulin enough? *The journal of phyamacology and experimental therapeutics* 299: 818-824, 2001.

48. **Furchgott RF and Jothianandan D.** Endothelium-Dependent and –Independent Vasodilation

Involving Cyclic-Gmp – Relaxation Induced by Nitric-Oxide, Carbon Monoxide, and Light. *Blood Vessels* 28: 52-61, 1991.

49. **Galli C, Meucci O, Scorziello A, Werge TM, Calissano P, and Schettini G.** Apoptosis in cerebellar granule cells is blocked by high KCL, forskolin and IGF-1 through distinct mechanisms of action: the involvement of intracellular calcium and RNA synthesis. *J Neurosci* 15: 1172-1179, 1995.

50. **Garcia-Cardena G, Oh P, Liu J, Schnitzer JE, and Sessa WC.** Targeting of nitric oxide synthase to endothelial cell caveolae via palmitoylation: implications for nitric oxide signalling. *Proc Natl Acad Sci USA,* 93: 6448-6453, 1996.

51. **Garland CJ, Plane F, Kemp BK, and Cocks TM.** Endothelium-dependent hyperpolarization: a role in the control of vascular tone. *Trends Pharmacol Sci* 16: 23-30, 1995.

52. **Govers R and Rabelink TJ.** Cellular regulation of endothleial nitric oxide synthase. *Am J Physiol Renal Physiol* 280: F193-F206, 2001.

53. **Gratton J, Bernatchez P, and Sessa WC.** Caveolae and caveolins in the cardiovascular system. *Circ Res* 94: 1408-1417, 2004.

54. **Gunter TE and Pfeiffer DR.** Mechanisms by which mitochondria transport calcium. *Am J Physiol* 258: C755-786, 1990.

55. **Holda JR, Klishin A, Sedova M, Huser J, and Blatter LA.** Capacitative calcium Entry. *News Physiol Sci* 13: 157-163, 1998.

56. **Isshiki M, Ando J, Korenaga R, Kogo H, Fujimoto T, Fujita T, and kamiya A.** Endothelial Ca2+ waves preferentially orginate at specific loci in caveolin-rich cell edges. *Proceedings of the National Academy of Science of the United States of America*: 5009-5014, 1998.

57. **Isshiki M, Ando J, Yamamoto K, Fujita T, Ying Y, and Anderson RG.** Sites of Ca2+ wave initiation move with caveolae to the trailing edge of migrating cells. *J Cell Sci* 115: 475-484, 2002.

58. **Isshiki M, Mutoh A, and Fujita T.** Subcortical Ca2+ Waves Sneaking Under the Plasma Membrane in Endothelial Cells. *Circ Res* 95: e11-e21, 2004.

59. **Isshiki M, Ying Y, Fujita T, and Anderson RG.** A Molecular Sensor Detects Signal Transduction from Caveolae in Living Cells. *J Biol Chem* 77: 43389-43398, 2002.

60. **Jagnandan D, Sessa WC, and Fulton D.** Intracellular location regulates calcium-calmodulin-dependent activation of organelle-restricted eNOS. *Am J physiol Heart Circ Physiol* 289: 1024-1033, 2005.

61. **Jagnandan D Sessa WC, and Fulton D.** Intracellular location regulated calcium-calmodulin-dependent activation of organelle-restricted eNOS. *Am J physiol Heart Circ Physiol* 289: 1024-1033, 2005.

62. **Jiang Y, Klein MG, and Schneider MF.** Numercial simulaiton of Ca^{2+} "sparks" in skeletal muscle. *Biophysical Journal* 77: 2333-2357, 1999.

63. **John K and Barakat AI.** Modulation of ATP/ADP concentration at the endothelial surface by shear stress: effect of flow-induced ATP release. *Annals of Biomedical Engineering* 29: 740-751, 2001.

64. **Kavdia M and Popel AS.** Venular Endothelial Derived NO can affect paired arteriole: A computational model. *Am J physiol Heart Circ Physiol*: Epub ahead of print, 2005.

65. **Kimura C, Oike M, Ohnaka K, Nose Y, and Ito Y.** Constitutive nitric oxide production in bovine aortic and brain microvascular endothelial cells: a comparative study. *J Physiol* 554: 721-730, 2004.

66. **Kits KS, De.Vileger TA, Kooi BW, and Mansvelder HD.** Diffusion barriers limits the effect of mobile calcium buffers on exocytosis of large dense cored vesicles. *Biophysical Journal* 76: 1693-1705, 1999.

67. **Kojima H, Hirata Y, Kudo Y, Kikuchi K, and Nagano T.** Visualisation of oxygen-concentration-dependent production of nitric oxide in rat hippocampal slices during aglycaemia. *J Neurochem* 76: 1404-1410, 2001.

68. **Kojima H, Urano Y, Kikuchi K, Higuchi T, Hirata Y, and Nagano T.** Fluorescent indicators for imaging nitric oxide production. *Angew Chem Int Ed* 38: 3209-3212, 1999.

69. **Korenaga R, Ando J, Ohtsuka A, Sakuma I, Yang W, Toyo-oka T, and Kamiya A.** Close correlation between cytoplasmic Ca^{2+} levels and release of an endothelium-derived relaxing factor from cultured endotelial cells. *Cell Struct Funct* 18: 95-104, 1993.

70. **Kuchan MJ and Frangos JA.** Role of calcium and calmodulin in flow-induced nitric oxide production in endothelial cells. *Am J Physiol* 266: C628-C636, 1994.

71. **Kwan H, Leung PC, Huang Y and Yao X.** Depletion of intracellular Ca2+ stores sensitizes the flow-induced Ca2+ influx in rat endothelial cells. *Circulation research* 92: 286-292, 2003.

72. **Laughlin MH, Turk JR, Schrage WG, Woodman CR, and Price EM.** Influence of coronary artery diameter on eNOS protein content. *Am J Physiol Heart Circ Physiol* 284: 1307-1312, 2002.

73. **Li YJ, Haga JH, and Chien S.** Molecular basis of the effects of shear stress on vascular endothelial cells. *Journal of BIomechanics* 38: 1949-1971, 2005.

74. **Lin S, Fagan KA, Li K, Shaul PW, Cooper DMF, and Rodman DM.** Sustained Endothelial Nitric-oxide Synthase Activated Requires Capacitative Ca^{2+} Entry. *The Jouranl of Biological Chemistry* 275: 17979-17985, 2000.

75. **Linder L, Kiowski W, Buhler FR, and Luscher TF.** Indirect evidence for release of endothelium-derived relaxing factor in human forearm circulation in vivo: blunted response in essential hypertension. *Circulation* 81: 1762-1767, 1990.

76. **Liu C, Mather S, Huang Y, Garland CJ and Yao X.** Extracellular ATP facilitates flow-induced vasodilation in rat small mesenteric arteries. *Am J physiol Heart Circ Physiol* 286: H1688-H1169, 2004.

77. **Lockwich TP, Liu X, Singh BB, Jadlowiec J, Weiland S, and Ambudkar IS.** Assembly of Trp1 in a Signaling Complex Associated with Caveolin-Scaffolding Lipid Raft Domains. *The Jouranl of Biological Chemistry* 275: 11934-11942, 2000.

78. **Lungu AO, Jin ZG, Yamawaki H, Tanimoto T, Wong C, and Berk BC.** Cyclosporin A inhibits flow-mediated activation of endothelial nitric-oxide synthase by altering cholesterol content in caveolae. *J Biol Chem* 278: 48794-48800, 2004.

79. **Lytton J, Westlin M, Burk SE, Shull GE, and MacLennan DH.** Functional comparisons between isoforms of the sarcoplasmic or endoplasmic reticulum family of calcium pumps. *J Biol Chem* 267: 14483-14489, 1992.

80. **Majno G and Palade GE.** Studies on inflammation: I. The effect of histamine and serotonin on vascular permeability: an electron microscopic study. *J Biophys Biochem Cytol* 11: 571-601, 1961.

81. **Manolopoulos VG, Liu J, Unsworth BR and Lelkes PI.** Adenylyl cyclase isoforms are differentially expressed in primary cultures of endothelial cells and whole tissue homogenates from various rat tissues. *Biochem Biophys Res Commun* 208, 1995.

82. **Marshall J, Dolan BM, Garcia EP, Sathe S, Tang X, Mao Z, and Blair LAC.** Calcium Channel and NMDA Receptor Activities Differentially Regulate Nuclear C/EBPβ Levels to Control Neuronal Survival. *Neuron* 39: 625-639, 2003.

83. **Massion PB, Feron O, Dessy C, and Balligand JL.** Nitric oxide and cardiac function: ten years after, and continuing. *Circ Res* 93: 388-398, 2003.

84. **Mateo J, Miras-Portugal MT, and Castro E.** Co-existence of P2Y and PPADS-insensitive P2U-purinoreceptors in endothelial cells from adrenal medulla. *Br J Pharmacol* 119: 1223-1232, 1996.

85. **McCullough WT, Collins DM and Ellsworth ML.** Arteriolar response to extracellular ATP in striated muscle. *Am J physiol Heart Circ Physiol* 272: 1886-1891, 1997.

86. **Mcknight TR and Curry FE.** Mechanisms of heterogeneous endothelial cytoplasmic calcium increases in venular microvessels. *Microcirculation* 9: 537-550, 2002.

87. **Merritt JE MS, Davies MP and Welwyn KE.** Use of fluo-3 to measure cytosolic Ca^{2+} in platelets and neutrophils, loading cells with the dye, calibration of traces, measurements in the presence of plasma, and buffereing of cytosolic ca^{2+}. *Biochem J* 269: 513-519, 1990.

88. **Motte S, Pirotton S and Boeynaems JM.** Heterogeneity of ATP receptors in aortic endothelial cell. Involvement of P2y and P2u receptors in inositol phosphate response. *Circ Res* 72: 505-510, 1993.

89. **Muller JM, Davis MJ, Kuo L, and Chilian WM.** Changes in coronary endothelial cell Ca^{2+} concentration during shear stress- and agonist-induced vasodilation. *Am J physiol Heart Circ Physiol* 276: H1706-H1714, 1999.

90. **Nakao M OK, Fujisawa S and Iijima T.** Mechanical stress-induced Ca^{2+} entry and Cl^- current in cultured human aortic endothelial cells. *Am J Physiol Cell Physiol* 276: C238-C249, 1999.

91. **Naraghi M, Muller TH, and Neher E.** Two-Dimensional determination of the cellular Ca2+ Binding in Bovine Chromaffin Cells. *Biophysical Journal* 75: 1635-1647, 1998.

92. **Nash MS, Young KW, Challiss RA and Nahorski SR.** Intracellular signaling: Receptor-specific messenger oscillations. *Nature* 413: 381-382, 2001.

93. **Nelson MT, Cheng H, Rubart M, Santana LF, Bonev AD, Knot HJ, and Lederer WJ.** Relaxation of arterial smooth muscle by calcium sparks. *Science* 270: 633-637, 1995.

94. **Nilius B and Droogmans G.** Ion Channels and Their Functional Role in Vascular Endothelium. *Physiological Reviews* 81: 1415-1459, 2001.

95. **Nollert MU, Eskin SG, and McIntire LV.** Shear stress increases inositol trisphosphate levels in human endothelial cells. *Biochem Biophys Res Commun*: 281-287, 1990.

96. **Nowycky MC and Pinter MJ.** Time courses of calicum and calcium bound buffers following calcium influx in a model cell. *Biophysical Journal* 64: 77-91, 1993.

97. **Okuda M, Takahashi MS, J., Murry CE, Traub O, Kawakatsu H, and Berk BC.** Shear Stress Stimulation of p130cas Tyrosine Phosphorylation Requires Calcium-dependent c-Src Activation. *J Biol*

Chem 274: 26803-26809, 1999.

98. **Olesen SP, Clapham DE, and Davies PF.** Haemodynamic shear stress activates a K+ current in vascular endothelial cells. *Nature* 331: 168-170, 1988.

99. **Ontkean M, Gay R, and Greenberg B.** Diminished endothelium-derived relaxing factor activity in an experimental model of chronic heart failure. *Circ Res* 69: 1088-1096, 1991.

100. **Pagakis SN, Curry FE.** Imaging of Ca2+ transients in endothelial cells of single perfused capillaries: correlation of peak [Ca2+]i with sites of macromolecule leakage. *Microcirculation* 1: 213-230, 1994.

101. **Parekh AB and Putney JW Jr.** Store-Operated Calcium Channels. *Physiological Reviews* 2005: 757-810, 2005.

102. **Park H, Go YM, Darji R, Choi JW, Lisanti MP, Maland MC, and Jo H.** Caveolin-1 regulates shear stress-dependent activation of extracellular signal-regulated kinase. *Am J Physiol Heart Circ Physiol* 178: H1285-H1293, 2000.

103. **Pocock TM, Williams B, Curry FE and Bates DO.** VEGF and ATP act by different mechanisms to increase microvascular permeability and endothelial [Ca2+]i. *Am J Physiol Heart Circ Physiol* 279: H1625-H1643, 2000.

104. **Popescu LM.** Conceptual model of the excitation-contraction coupling in smooth muscle: the possible role of the surface micro-vesicles. *Studia Biophysica* 44: 141-153, 1974.

105. **Prasad AR, Logan SA, Nerem RM, Schwartz CJ, and Sprague EA.** Flow-related responses of intracellular inositol phosphate levels in cultured aortic endothelial cells. *Circ Res*: 827-836, 1993.

106. **Purkiss JR, Wilkinson GF, Boarder MR.** Evidence for a nucleotide receptor on adrenal medullary endothelial cells linked to phospholipase C and phospholipase D. *Br J Pharmacol* 108: 1031-1037, 1993.

107. **Putney JW Jr, Broad LM, Braun F, J., Lievremont JP, and Bird GS.** Mechanisms of Capacitative Calcium Entry. *Journal of Cell Science* 114: 2223-2229, 2001.

108. **Qiu E KD, Hu Q, And Ziegelstein RC.** Determinants of shear stress-stimulated endothelial nitric oxide production assessed in real-time by 4,5-Diaminofluorescein fluorescence. *Biochem Biophys Res Commun* 286: 328-335, 2001.

109. **Ralevic V aBG.** Receptors for purines and pyrimidines. *Pharmacol Rev* 50: 413-492, 1998.

110. **Razani B, Engelman JA, Wang XB, Schubert W, Zhang XL, Marks CB, Macaluso F, Russel RG, Li M, Pestell RG, Di Vizio D, Hou H, Kenitz B, Lagaud G, Christ GJ, Edelmann W, and Lisanti MP.** Caveolin-1 null mice are viable but show evidence of hyperproliferative and vascular abnormalities. *J Biol Chem* 276: 38121-38138, 2001.

111. **Rizzo V, Morton C, Depaola N, Schnitzer JE, and Davies PF.** Recruitment of endothelial caveolae into mechanotransduction pathways by flow conditioning in vitro. *Am J Physiol Heart Circ Physiol* 285: 1720-1729, 2003.

112. **Rizzuto R, Pinton P, Brini M, Chiesa A, Filippin L, and Pozzan T.** Mitochondria as Biosensors of Calcium Microdomains. *Cell Calcium* 26: 193-199, 1999.

113. **Sala F and Hernandez-Cruz A.** Calcium diffusion modelling in a spherical neuron: relevance of

buffering properties. *Biophysical Journal* 57: 313-324, 1990.

114. **Duza T and Sarelius IH.** Localized transient increase in endothelial cell Ca^{2+} in arterioles in situ: implications for coordination of vascular function. *Am J Physiol Heart Circ Physiol* 286: H2322-H2331, 2004.

115. **Sedova M and Blatter LA.** Dynamic regulation of [Ca2+]i by plasma membrane Ca2+-ATPase and Na+=Ca2+ exchange during capacitative Ca2+ entry in bovine vascular endothelial cells. *Cell Calcium* 25: 333-343, 1999.

116. **Sessa WC, Barber CM, and Lynch KR.** Mutation of N-myristoylation site converts endothelial cell nitric oxide synthase from a membrane to cytosolic protein. *Circ Res* 72: 921-924, 1993.

117. **Sessa WC, Harrison JK, Barber CM, Zeng D, Durieux ME, D'Angelo DD, Lynch KR, and Peach MJ.** Molecular cloning and expression of endothelial nitric oixde synthase is necessary for the efficient synthesis of nitric oxide. *J Biol Chem* 267: 15274-15276, 1992.

118. **Shaul PW.** Regulation of Endothelial Nitric Oxide Synthase: Location, Locaiton, Location. *Annu Rev Physiol* 64: 749-774, 2002.

119. **Shaul PW and Anderson RG.** Role of plasmalemmal caveolae in signal transduction. *Am J Physiol Lung Cell Mol Physiol* 275: 1843-1851, 1998.

120. **Shen J, Luscinskas FW, Connolly A.,Dewey CF Jr, Gimbrone MA Jr.** Fluid shear stress modulates cytosolic free calcium calcium in vascular endothelial cells. *Am J Physiol* 262: C384-C390, 1992.

121. **Sowa G, Pypaert M, and Sessa WC.** Distinction between signaling mechanisms in lipid rafts vs. caveolae. *Proc Natl Acad Sci USA*: 14072-14077, 2001.

122. **Stan RV.** Structure and function of endothlial caveolae. *Microsc Res Tech* 57: 350-364, 2002.

123. **Takeuchi K, Watanabe H, Tran Q, Ozeki M, Sumi D, Hayashi T, Iguchi A, Ignarro LJ, Ohashi K, and Hayashi H.** Nitric Oxide: Inhibitory Effects on Endothelial Cell Calcium Signaling, Postaglandin, I2 production and nitric oxide synthase expression. *Cardiovascular Research* 62: 194-201, 2004.

124. **Taylor CW.** Controlling Calcium Entry. *Cell* 111: 767-769, 2002.

125. **Tran QK, Ohashi K, and Watanabe H.** Calcium Signalling in Endothelial Cells. *Cardiovascular Research* 48: 13-22, 2000.

126. **Tsai AG, Acero C, Nance P, Cabrales P, Frangos JA, Buerk DG, and Intaglietta M.** Elevated plasma viscosity in extreme hemodilution increases perivascular nitric oxide concentration and microvascular perfusion. *Am J Physiol Heart Circ Physiol* 288: H1730-H1739, 2005.

127. **Tymianski M, Charlton MP, Carlen PL, and Tator CH.** Source specificity of early calcium neurotoxicity in cultured embryonic spinal neurons. *The journal of neuronscience* 13: 2085-2104, 1993.

128. **Ungvari Z, Csiszar A, and Koller A.** Increases in endothelial Ca2+ activate KCa channels and elicit EDHF-type arteriolar dilation via gap junctions. *Am J Physiol Heart Circ Physicol* 282: H1760-H1767, 2002.

129. **Ungvari Z, Sun D, Huang A, Kaley G, and Koller A.** Role of endothelial [Ca2+]i in activation of eNOS in pressurized arterioles by agonists and wall shear stress. *Am J Physiol Heart Circ Physiol* 281:

H606-H612, 2001.

130. **Wiesner TF, Berk BC, and Nerem RC.** A mathematical model of cytosolic calcium dynamics in human umbilical vein endothleial cells. *Am J Physiol* 270: C1556-1569, 1996.

131. **Yamada E.** The fine structure of the gall bladder epithelium of the mouse. *J Biophys Biochem Cytol*: 445-458, 1955.

132. **Yamamoto K, Korenaga R, Kamiya A and Ando J.** Fluid shear stress activates Ca2+ influx into human endothelial cells via P2X4 purinoceptors. *Circulation Research* 87: 385-391, 2000.

133. **Yamamoto K, Sokabe T, Ohura N, Nakatsuka H, Kamiya A and Ando J.** Endogeneously released ATP mediates shear stress-induced Ca2+ influx into pulmonary artery endothelial cells. *Am J physiol Heart Circ Physiol* 285: H793-H803, 2003.

134. **Ye JF, Zheng XX, and Xu LX.** Real-time detection of nitric oxide in cultured rat aortic endothelial cells induced by shear stress. *Acta Biochimical et Biophysica Sinica* 35: 296-300, 2002.

135. **Yegutkin G, Bodin P, and Burnstock G.** Effect of shear stress on the release of soluble ecto-enzytems ATPase and 5'-nucleotidase along with endogenous ATP from vascular endothelial cells. *British J of Pharmacoloty* 129: 921-926, 2000.

136. **Ying X, Minamiya Y, Fu C, and Bhattacharya J.** Ca2+ waves in lung capillary endothelium. *Circ Res* 79: 898-908, 1996.

137. **Ying X, Minamiya Y, Fu C and Bhattacharya J.** Ca2+ waves in the lung capillary endothelium. *Circ Res* 79: 898-908, 1996.

138. **Yu J, Bergaya S, Murata T, Alp IF, Bauer MP, Lin MI, Drab M, Kurzchalia TV, Stan RV, and Sessa WC.** Direct evidence for the role of caveolin-1 and caveolae in mechanotransduction and remodeling of blood vessels. *The Jouranl of Clinical Investigation* 116: 1284-1291, 2006.

139. **Zhang X.** Real Time And In Vivo Monitoring of Nitric Oxide By Electrochemical Sensors-From Dream To Reality. *Frontiers in Bioscience* 9: 3434-3446, 2004.

140. **Zhu X and Birnbaumer L.** Calcium Channels Formed by Mammalian Trp Homologues. *News in Physiological Sciences* 13: 211-218, 1998.

VITA

Dihui Hong

Education

Ph.D. in Biomedical Engineering Drexel University, Philadelphia, PA, 2007
M.S. in Biomedical Engineering, Zhejiang University, Hangzhou, China, 2003
B.S. in Biomedical Engineering, Zhejiang University, Hangzhou, China, 2000

Research Experience

Lab of Cellular Biomechanics & Lab of Cardiovascular Engineering, Drexel University
Research Assistant, 2003-present

Lab of Quantitative Physiology, Cell Physiology Group, Zhejiang University
Research Assistant, 2000-2003

Lab of Quantitative Physiology, Circulation Group, Zhejiang University
Research Assistant, 1997-2000

Teaching Experience

School of biomedical engineering, science and health systems, Drexel University, Philadelphia. PA

Undergraduate course: Engineering principles of living systems I, II: Instructed and prepared lab courses, graded homework and exam. 2005-2007

Selected publications

Hong, D., Jaron, D., Buerk, D. G., Barbee, K. A., Analysis of Transport limited calcium signaling in spatially segregated cellular caveolae domains (Submitted)

Hong, D., Jaron, D., Buerk, D. G., Barbee, K. A., Heterogeneous response of microvascular endothelial cells to shear stress. Am J Physiol Heart Circ Physiol, 290: H2498-2508, 2006.

Hong, D., Ning, G., Zhao,T., Zhang M., and Zheng X., Method of normal estimation based on approximation for visualization. Journal of Electronic Imaging, 12(3), 470-477, 2003.

Hong, D., Ning, G., Zhao,T., Ye J., and Zheng X., A novel method of normal estimation for visualization of medical images, Space Medicine & Medical Engineering, 16(3), 157-161, 2003.

Yang Y., Ning G., Kutor J., Hong D., Zhang M., Zheng X., Nitric oxide spatial distribution in single cultured hippocampus neurons: investigation by projection of reconstructed 3-D image and visualization technique, Cell Biol Int. 28 (8-9): 577-83, 2004.

Zheng X., Ning G., Hong D., Zhang M., Nitric oxide imaging in neurons using confocal microscopy, Methods Mol Biol. 279:69-80, 2004.

Zhang M., Ning G., Hong D., Yang Y., Kutor J., Zheng X., The influence of oxygen-glucose deprivation on nitric oxide and intracellular Ca2+ in cultured hippocampal neurons. Acta Biochimica et Biophysica Sina, 35(6): 561-566, 2003.

Zhang M., Ning G., Shou C., Lu Y., Hong D., Zheng X., Inhibitory effect of jujuboside A on glutamate-mediated excitatory signal pathway in hippocampus. Planta Med, 69(8):692-5, 2003.

Selected Honors / Awards

- 2003-2007, Calhoun Fellowship
- 2003, Graduated with Highest Honor
- 2001, Guang Hua Fellowship
- 1996-2003, Outstanding Student Scholarship, Distinguished Student Honor
- 2000, Excellent undergraduates dissertation, Zhejiang University; Graduate with Honor.